Targeting and Modeling the Biomechanical Environment of the Pulmonary Vasculature to Study Pulmonary Arterial Hypertension

By

Reid William D'Amico

Dissertation

Submitted to the Faculty of the

Graduate School of Vanderbilt University

in partial fulfillment of the requirements

for the degree of

DOCTOR OF PHILOSOPHY

in

Biomedical Engineering

August 10, 2018

Nashville, Tennessee

Approved:

James D. West, Ph.D.

W. David Merryman, Ph.D.

Leon Bellan, Ph.D.

Ethan Lippmann, Ph.D.

Joshua Fessel, M.D., Ph.D.

This work is dedicated to my mother, my father, my brother, and my grandmothers. You are my biggest cheerleaders and advocates. You are my foundation. You are the teachers of hard work, dreaming big, and pushing through life's many obstacles. I love you all with my whole heart.

To my best friends, experience-sharers, and supporters: Kelly Draehn, Haley Mendoza-Romero, Brittney Parker, Nicholas Rotti, Jason Seigel, and Ananya Zutshi. For being my companions in growth and adventure. For being my allies in self-discovery. For being my helpers when the weight of cystic fibrosis brought me down. You give me ineffable happiness.

To my high school Chemistry and Physics teacher, Tina Webb-Browning. You introduced me to the difficulty and beauty of science. You introduced me to the skills needed to succeed in research. Thank you for lighting the spark.

ACKNOWLEDGEMENTS

I would first like to acknowledge my colleagues and co-authors for their immeasurable intellectual contributions to the work completed in my time at Vanderbilt. Thank you to Christy Moore for teaching me the procedures used on mice to study pulmonary disease, Thomas Blackwell for sharing expertise with cell culture and molecular biology, Shannon Faley for guiding me through the development of my model, Evan Brittain for introducing me to the field, tools, and analysis of clinical research, and Santhi Gladson, Sheila Shay, Ha-na Shim, Leon Bellan, Joshua Fessel, Joanna Prosser, Courtney Copeland, Anna Hemnes, John Newman, Brian O'Grady, Stephen Halliday, Tufik Assad, Quinn Wells, Eric Faber-Eger, and Rebecca Levinson.

I would like to give a special thank you to my other lab members: Emily Hornsby, Erica Carrier, Megha Talati, Toshio Suzuki, Michelle Clifton, Thong Luong, Julio Fuentes, Peter Chen, Niki Fortune, and Anandharajan Rathinasabapathy. Thank you for making my time in the lab memorable and enjoyable.

I would like to acknowledge the support, dedication, and guidance of my thesis mentors: Joshua Fessel, Leon Bellan, Ethan Lippmann, and David Merryman. Thank you all for your special role in guiding me professionally and scientifically. Lastly, I would like to give a special acknowledgement to my advisor, James West. I thank you for your tremendous mentorship and investment in my personal development and in my career advancement as a scientist, engineer, and advocate.

Lastly I would like to thank the National Institutes of Health, the American Heart Association, and the National Science Foundation for the funding of this work. I am

especially grateful to be a recipient of the National Science Foundation Graduate Research Fellowship. To those at the Foundation, thank you for believing in me and facilitating the development of many of my skills as a scientist.

TABLE OF CONTENTS

Page

LIST OF TABLES

LIST OF FIGURES

GLOSSARY OF TERMS AND ABBREVIATIONS

2D	Two Dimensional
3D	Three Dimensional
6MWD	Six Minute Walk Distance
AJ	Adherens Junctions
ANGII	Angiotensin II
ANOVA	Analysis of Variance
ATP	Adenosine Triphosphate
BioVU	Vanderbilt DNA Repository
BMP	Bone Morphogenetic Protein
Bmpr2	Bone Morphogenetic Protein Receptor 2
C-GMP	Cyclic Guanosine Monophosphate
CAS	Crk-Associated Substrate, also known as p130
CAV	Caveolin-1
CFL1	Cofilin 1
CHD	Congenital Heart Defect
CTD	Connective Tissue Disease
DelX4	BMPR2 Mutant Mouse Genotype
DMSO	Dimethyl Sulfoxide
DYNLT1	Dynein Light Chain Tctex-Type 1
EC	Endothelial Cell
ECM	Extracellular Matrix
EDHF	Endothelium Derived Hyperpolarizing Factor
eNOS	Endothelial Nitric Oxide Synthase
HFpEF	Heart Failure with Preserved Ejection Fraction
HIV	Human Immunodeficiency Virus
IACUC	The Institute of Animal Care and Use Committee
IPAH	Idiopathic Pulmonary Arterial Hypertension
GO	Gene Ontology
LIMK1	LIM Domain Kinase 1
MPMVEC	Murine Pulmonary Microvascular Endothelial Cell
mtDNA	Mitochondrial DNA
MTG	Microbial Transglutaminase
NO	Nitric Oxide
NRF1	Nuclear Respiratory Factor 1

NRF2	Nuclear Respiratory Factor 2
OHE	Hydroxylation of Estradiol
OXPHOS	Oxidative Phosphorylation
PAH	Pulmonary Arterial Hypertension
PBS	Phosphate Buffered Saline
PDMS	Polydimethylsiloxane
PH	Pulmonary Hypertension
PPARA	Peroxisome Proliferator Activated Receptor Alpha
PPARD	Peroxisome Proliferator Activated Receptor Alpha
PPARGC1A	PPARG Coactivator 1 Alpha
R899X	Rho-family GTPase
RAC	Rac Family Small GTPase 1
RHC	Right Heart Catheterization
Rho	Rho-family GTPase
RTK	Receptor Tyrosine Kinase
RV	Right Ventricle
RVSP	Right Ventricular Systolic Pressure
SD	Synthetic Derivative
SFK	Src Family Kinase
SMC	Smooth Muscle Cell
SRC	Proto-oncogene tyrosine-protein kinase
TFAM	Transcription Factor A Mitochondria
TJ	Tight Junction
VE	Vascular Endothelial
VUMC	Vanderbilt University Medical Center
WHO	World Health Organization
WT	Wild-type
ZO	Zonula Occludens

CHAPTER 1: PROJECT MOTIVATION

A Brief Introduction to Pulmonary Arterial Hypertension

Pulmonary arterial hypertension (PAH) is a progressive illness of the pulmonary microvascular that eventually results in right ventricular (RV) heart failure and death. Pulmonary hypertension (PH) is a disease characterized by a mean pulmonary arterial pressure greater than 25 mmHg.[1] PH was initially classified as either primary pulmonary hypertension (no identifiable cause) or secondary pulmonary hypertension if an identifiable cause was present. As the understanding of disease physiology progressed, additional etiologies of PH have been defined. The World Health Organization (WHO) has currently classified PH into five groups based upon etiology and mechanism, as seen in **Table 1.1**. Group 1 PH (in blue) or PAH consists of idiopathic PAH (IPAH), heritable PAH, and PAH due to diseases that lead to the localized damage of the small pulmonary resistance arterioles.[2,3] These damages can be caused by drugs and toxins, connective tissue diseases (CTD), HIV infection, portal hypertension, and congenital heart disease (CHD).[2] Despite advances in treatments, three year survival rates are poor and many patients in end-stage disease undergo heart and lung transplants.[4-7] The strongest heritable risk factor for development of PAH is the presence of a mutation in the type 2 receptor for the bone morphogenetic protein (BMP) pathway (BMPR2), present in the large majority of familial cases. Penetrance is incomplete in both mouse models and humans with BMPR2-associated PAH, with the risk of developing overt disease about 20–25%.[8]

Group	Subtypes
Group 1: Pulmonary Arterial Hypertension	Idiopathic
	Drug Induced
	Other Conditions (HIV, CTD, Congenital, etc)
	Heriditary
	Persistent PH of the newborn
Group 1'	Pulmonary veno-occlusive disease
Group 2: PH Due to Left Ventricular Dysfunction	Systolic
	Diastolic
	Valvular
Group 3: PH Due to Lung Diseases and or Hypoxia	Chronic obstructive pulmonary disease
	Other pulmonary diseases (mixed resitrctive and obstructive)
	Sleep-disordered breathing
	Alveolar Hypoventilation Disorders
	Chronic high altitude exposure
	Developental Abnormalities
Group 4: Chronic Thromboembolic	
Group 5: Miscellaneous	Hematologic disorders
	Systemic disorders
	Metabolic disorders
	Other

Table 1.1: Dana Point classification of pulmonary hypertension. Pulmonary hypertension is grouped into five different functional categories and further stratified by etiology. Pulmonary arterial hypertension (Group 1) is shown in blue.

However, the mechanism underlying BMPR2 and the development of PAH is not well understood.[9] The structural deformity seen in the mutated BMPR2 protein is known to play a role in PAH. In heritable BMPR2 mutations, the c-terminus of the protein is truncated. This results in the up-regulation of phosphorylation of proteins responsible for maintenance of cellular mechanisms like growth, cytoskeletal maintenance, and cell division. A key protein, SRC, binds to the cytoplasmic tail of BMPR2, and a BMPR2 mutation leads to increased SRC phosphorylation and downstream activity with relation to PAH.[10-12] The relationship between SRC and PAH has been studied intensely, but the pathologic role that SRC plays in PAH is not well understood. It has been shown

that reducing the increased phosphorylation of SRC does not prevent heritable PAH. This finding emboldens how the aberrant localization and trafficking of this protein may play a greater role in disease progression.[13]

Other less common genetic mutations associated with PAH are largely found in genes responsible for cytoskeletal origination and mechanical management of the vessel's extracellular matrix (ECM). While BMPR2 is not a directly related to the cytoskeletal architecture, the global relationship between cytoskeletal defects and PAH underscores how the downstream cytoskeletal and endothelial consequences related to defects in the BMPR2 pathway could be targets for disease-treating therapies.[14]

The current therapies used to treat PAH were originally developed to treat other conditions. None of these medications are disease modifying and do not address the underlying vessel stiffening and vascular dysfunction.[15] For example, the impact of two cancer-targeting SRC phosphorylation inhibiting drugs, saracatinib and dasatinib, have been tested for their ability to prevent heritable PAH. While the direct inhibition of SRC phosphorylation failed to prevent BMPR2 associated PAH, other SRC pathway targets have been shown to ameliorate hallmarks of disease, and may serve as potential novel therapies.[13]

Instead, most current therapies offer temporary improvement in symptoms through vasodilation. The lack of therapies in PAH can be attributed to a lack of understanding of the molecular and cellular pathogenesis. PAH is a disease defined by aberrant mechanical parameters. High pressures, pulsatile flow, and varying shear stresses all likely play a role in the development of the disease. Unfortunately, current 2D cell culture fails to introduce this physical environment resulting in models that aren't

biomimetic of the physical environment of the tissue. Animal models present a valuable opportunity to study PAH, but are limited by dissimilarities to humans in disease progression.[16] Because of these shortcomings, the field has worked to develop a next generation approach to study PAH. The introduction of an artificial vessel containing the correct mechanical and chemical cues could serve as an opportunity to study the disease in a more physiologically relevant way to humans, and advance treatments and the understanding of PAH.

Motivation

Pulmonary arterial hypertension is a progressive disease with no effective therapies. Difficulty studying the microvessels in the lung is a likely contributor to poor outcome and limited treatments that address underlying disease. The translation from traditional 2D to 3D cell culture is an important step towards more biomimetic tissue models. However, current 3D methods that embed cells within a stagnant matrix only serve to study the effect of the extracellular environment on cellular function and development. The incorporation of tunable microfluidics introduces a valuable tool to study the effect of hemodynamics on tissue function. Advances in biology, tissue modeling, microfluidics, and microfabrication have led to the development of many vascular models, but to date, no model accurately captures all aspects of the human vasculature. A novel pulmonary vascular platform has the potential to incorporate many of the mechanical and chemical stimuli seen in the lung's vessels. The tunability and ease of imaging of a hydrogel-based platform introduces the opportunity to study PAH in ways that cannot be currently performed in vitro or in vivo.

Preliminary studies in a pulmonary vasculature cell culture platform suggests that artificial vessels within the platform can be endothelialized and exposed to biomimetic pressure and flow for up to seven days. Artificial endothelialized vessels enable us to study the influence of flow and pressure on cellular arrangement and vascular dysfunction. No previous studies have incorporated the correct shear and pressures seen in the pulmonary vasculature. Constructing such a device would advance the field by enabling us to study PAH in ways currently unavailable in in vivo and in vitro models. It was believed that a novel cell culture model could reproduce and elucidate key

endothelial dysfunction and genetic expression findings seen in PAH. Clinical validation using Vanderbilt's large-scale DNA repository, BioVU, could be used for genetic linkages and clinical outcomes to validate the recapitulation of PAH and correlate in vitro to in vivo findings.

Project Aims

PAH is a deadly illness with few treatment options for clinical management. We targeted one of the key proteins likely related to endothelial dysfunction, SRC, by inhibiting its up-regulated phosphorylation seen in BMPR2-associated PAH. We sought to **1a)** reduce the elevated right ventricular systolic pressures seen in BMPR2 mutant mice and also **1b)** reduce the increased number of muscularized vessels seen in PAH lungs. After targeting SRC failed to reduce pressures and the number of vessels, we transitioned to create a more physiologically accurate approach to study PAH. Current laboratory practice limits how we can study PAH. Animal models fail to recapitulate human-like PAH and 2D cell culture neglects to introduce key mechanical stimuli seen in the body. PAH is known to localize in the small resistance level vessels in the lung. These vessels are exposed to high shear and pulsatile flow that become more extreme as the disease progresses. The inability to incorporate this important mechanical environment in previous models may have contributed to our lack of effective therapies to treat PAH. Engineering a tunable 3D cell culture platform that mimics many of the mechanical parameters seen in the lung vasculature is critical to advance the field.

We sought to **2a)** develop an artificial arteriole platform that can incorporate physiological pressure and flow seen in the pulmonary vasculature. The model was designed to be easily adjusted to change pulse rates, shear, pressure, and stiffness of the matrix. The tunability and imaging capabilities designed into the platform presented an opportunity to study PAH in ways that can not be studied in vitro or in vivo.

Specifically, we studied how the influence of physiological pressure and shear stress influence **2b)** genetic expression, **2c)** cellular morphology, and **2d)** permeability

of endothelial cells in the wild type (WT) and Bmpr2^{R899X} pulmonary microvasculature. The ability to study these genotypic and phenotypic abnormalities at the intersection of controllable pressures and flow in PAH has remained elusive in current PAH models.

Preliminary work validated that a pulmonary vascular platform was feasible to construct. Artificial endothelium were shown to form confluent monolayers within the channels and remained endothelialized in pulsatile flow for up to a week.

In traditional 2D cell culture, the BMPR2 mutation is known to lead to differences in gene expression in Bmpr2^{R899X} endothelial cells compared to WT endothelial cells. The RNA Seq was designed to **2b.1)** correlate findings between previous 2D gene expression studies and our new model, and to **2b.2**) elucidate new expression changes in Bmpr2^{R899X} and WT endothelial cells cultured within the artificial arteriole. The model also was designed to advance our understanding of endothelial dysfunction by visualizing two key manifestations: morphological response to flow and barrier function. Specifically, the artificial arteriole was imaged **2c)** to visualize cellular elongation and alignment in response to shear and pressure within the artificial endothelium, and **2d)** to study the permeabilities of mutant and WT endothelium to verify that the increased permeability of the Bmpr2^{R899X} endothelium could be recapitulated within the artificial arteriole.

Lastly, we surveyed Vanderbilt's large-scale de-identified medical record system and DNA repository to explore potential associations between genetic variations in the oxidative phosphorylation (OXPHOS) pathway and survival outcomes, RV health, and exercise capacity in PAH.

We specifically sought to investigate a possible association between genetic variants in the OXPHOS pathway and **3a)** increased right ventricular function, **3b)** preserved six-minute walk capacity, and **3c)** increased survival outcomes in PAH patients. Associations between the OXPHOS pathway and elite athletic status is known, and further bolsters our hypothesis that this pathways may be associated with patient RV function, exercise capacity, and longevity. Discovering associations within this pathway could lead to new avenues of therapeutic intervention. We anticipated using data from this study to further validate the findings in our artificial arteriole by bridging RNA Seq findings to genetic findings in the patient cohort.

CHAPTER 2: BACKGROUND

BMPR2 Protein Interaction

Within the past two decades, substantial evidence has been accumulated to understand the complex protein interaction and signaling nature of BMPR2. In 2003 the LIM Motif-containing Kinase, LIMK1, was shown to interact with WT BMPR2 and this interaction was shown to reduce LIMK1's activity. In the mutant BMPR2 conditions seen in LIMK1, the interaction between LIMK1 and BMPR2 was shown to be reduced, and thus increased the activity of LIMK1.[17] The primary phosphorylation target of LIMK1 is the actin regulating protein (CFL1). The increased activity of LIMK1 was found to increase the activity of CFL1 in the lung of Bmpr2^{R899X,} with functional consequences that promote the pulmonary hypertension phenotype.[18]

Dynein Light Chain Tctex-Type 1(DYNLT1) is known to be co-localized, bind, and be phosphorylated by WT BMPR2.[19] Because of the mutation in the mutant BMPR2 protein, similar disruptions are seen in DYNLT1 as with LIMK1. DYNLT1 interacts with proteins that regulate mitochondrial permeability, and the Rho/RAC pathway.[20,21] This results in profound defects in energy metabolism in both patients and BMPR2 mouse models.[22] Because of the increasing recognition of the importance of the metabolic dysfunction in PAH, DYNLT1 has been noted as a target of high interest for therapeutic intervention.[18]

SRC is also known to interact with BMPR2 and lead to downstream consequences related to cytoskeletal assembly in architecture such as caveolin (through interactions with caveolin-1 (CAV1)) and in focal adhesion assembly.[18] Because of this regulated cytoskeletal phenotype associated with SRC interaction with

mutant BMPR2, it has been the target of therapeutic intervention. SRC therapeutics that inhibit its phosphorylation have been developed to treat cancers, but the impact of directly inhibiting SRC were only recently studied.[23,24] Previous groups have probed other targets in the SRC pathway and found success in preventing the development of heritable PAH.[13] However, these studies suggest that the increased phosphorylation of SRC due to BMPR2 mutations not only augments downstream activity, but deregulated trafficking and localization are also noted in BMPR2 mutant cells from mice.[13]

A summary of these deregulated protein interactions in mutated BMPR2 cells can be seen in **Figure 2.1**.

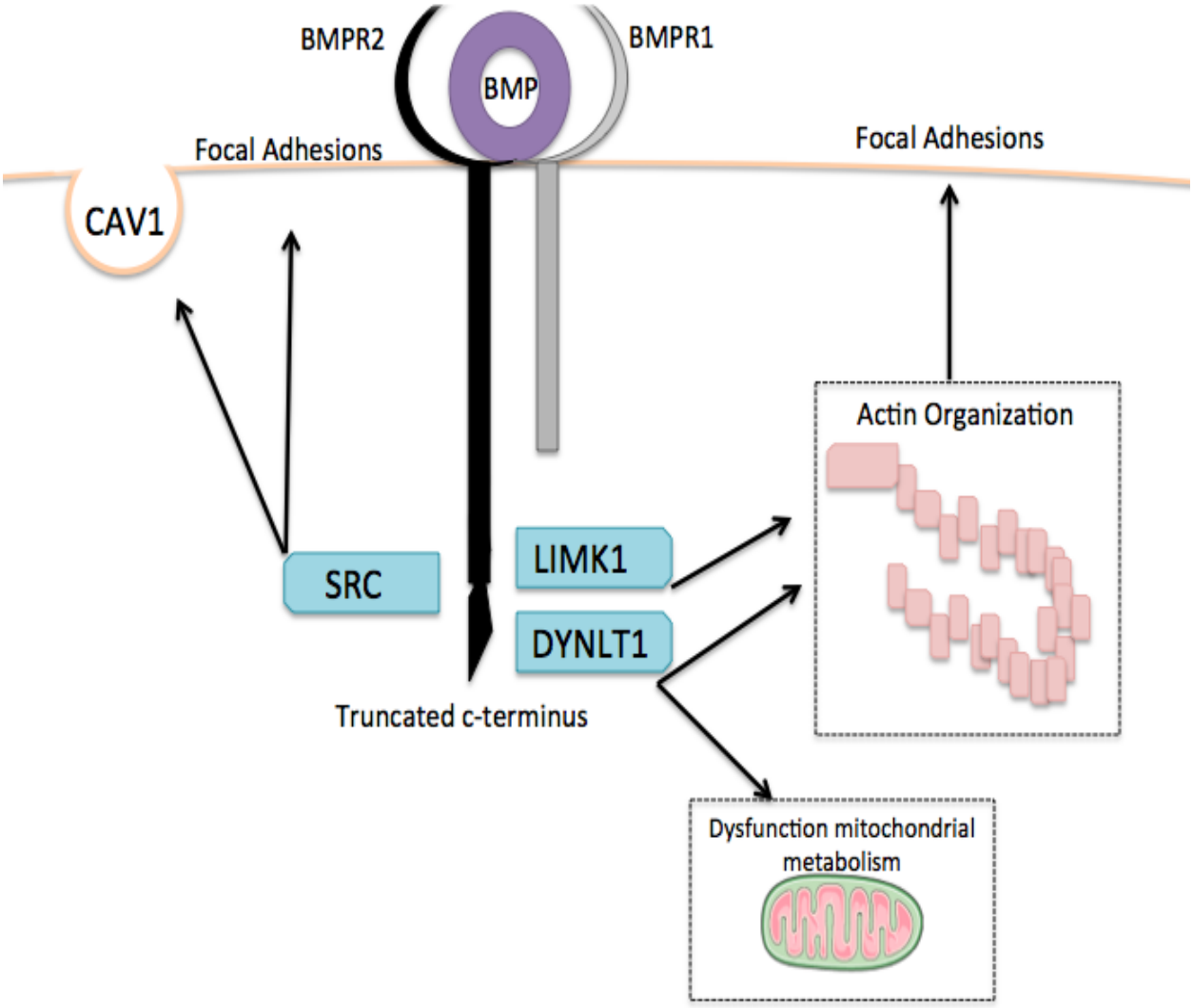

Figure 2.1 BMPR2 signaling mechanisms with relevance to PAH. Signaling through the truncated c-terminus of the Type 2 receptor regulates SRC, LIMK1, and DYNLT1 (light blue). These three combined deregulated proteins result in altered regulation in mitochondrial metabolism, actin organization (series of light pink squares), caveoli, and focal adhesions. Adapted from [18].

PAH and the Vascular Endothelium

A dysfunctional vascular endothelium plays a critical role in the development of many vascular pathologies, including PAH**.** Studying the underlying biology and mechanobiology of the endothelium and its regulation at the cellular and molecular level are fundamental to elucidating new therapies to treat vascular diseases like PAH. However, two-dimensional cell culture techniques are still widely used in a laboratory practice. With these current techniques, cells are often grown on a rigid, flat substrate and are submerged under a stagnant nutrient-rich media. The ability to recapitulate more realistic mechanical and chemical environments would create an opportunity to probe into many of the underlying causes of vascular dysfunction and failure.

Over the last several years, recognition of the importance of the extracellular and mechanical environment has increased. The next generation cell culture paradigm of growing cells in complex 3D structures has revolutionized the way we can model and study diseases in vitro. In particular, a great amount of effort has been placed into modeling the blood vessels in the body. While no model can perfectly model the complexity of the human vasculature, different models can be used to study specific areas of vascular function. For example, models have been used to study angiogenesis, transport across barriers, the effect of shear stress, and hemodynamics.[25-31] By successfully tuning vascular models to study specific research questions, compounding variables that are encountered in vivo can be controlled or eliminated from the experiment. However, several limitations still exist in this field. Many organ-on-a chip models use substrates that are much stiffer than the natural environment of the cell, such as glass or polydimethylsiloxane (PDMS). Other models have failed to incorporate

other key features like cylindrical vessel geometries, physiologically relevant shear stresses, and pressures. The field's current inability to study cellular and molecular phenomenon over a period of days also limits the number of pathogenic and scientific questions that can be asked.

Endothelial Cells and Modeled Mechanical Stimuli

Vascular endothelial cells (ECs) form a monolayer that covers the vascular lumen. The endothelium is dynamic and regulates a host of physiological function like tone, permeability, and thromboresistance as seen in **Figure 2.2**. Because of this complex environment, ECs are able to respond to biochemical and mechanical forces by changing cellular, molecular, and gene expression levels through mechanotransduction pathways. The release of effector molecules regulates EC physiological function and also regulates neighboring cells like smooth muscle cells (SMCs), platelets, and leukocytes.[32]

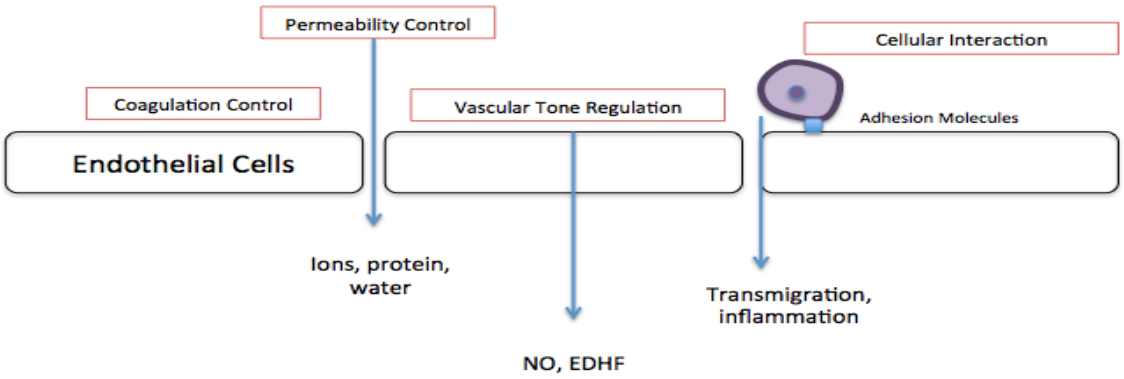

Figure 2.2: Endothelial function. Endothelial cells possess a variety of key functions used to regulate the endothelium. These range from the use of NO and EDHF to regulate vascular tone, regulation of vascular permeability, immune cell recruitment, and thromboresistance. Adapted from [35].

One of the key vasoactive molecules involved in the regulation of ECs is nitric oxide (NO). NO is derived from L-arginine through the action of endothelial NO synthase (eNOS). Through the aid of cofactors such as tetrahydrobiopterin, NO can

diffuse through the endothelium and interact with the vascular SMCs. This process activates guanylate cyclase and results in the cyclic guanosine monophosphate (c-GMP) modulated vasodilation of the vessels.[32] Similarly, the endothelium can also mediate vascular tone by increasing potassium conductance that results in the depolarization of SMCs by the production of endothelial derived hyperpolarization factor (EDHF).[33] The interplay among these mechanisms are key to maintaining vascular homeostasis. However, the disruption of any of these key mechanisms can lead to vascular failure, or specifically the dysfunction of the endothelium.[35] Altered regulation of endothelial cell function can lead to a number of downstream consequences including increased vascular leak.[35]

Vascular ECs cover the luminal surface of the blood vessel and serve as the barrier between the blood and the surrounding tissues. Ions and water-soluble solutes are known to diffuse across the endothelial barrier by means of paracellular pathways through intercellular gaps. Immune cells are also known to migrate across the endothelium through paracellular pathways.[36] Studying vascular dysfunction and permeability has limitations in our current in vivo and in vitro models. In animal studies, it is difficult to observe tissue and organ-level permeability unless the tissue is removed, and while studying barrier function in vitro is easier, most models often fail to capture much of the biomimetic mechanical and chemical environments seen in vivo. Artificial vessel models serve to create a next generation approach to studying these phenomena at the intersection of in vitro and in vivo models. Due to their naturally transparent appearance, artificial vessels present an opportunity for rapid and simple imaging of changes that can occur after an endothelium is exposed to a stimulus.

There are a number of protein interactions that control the cell-cell barrier by regulating the permeability of solutes and immune cells.[37] These protein complexes, known as junctions, are divided into two classifications: tight junctions (TJ) and adherens junctions (AJ). These junctions comprise transmembrane proteins that associate with cytoplasmic proteins that link the actin and cytoskeleton of neighboring cells **(Figure 2.3).**

Vascular-endothelial (VE) cadherin plays a key role in vascular development and integrity.[38,39] As the key AJ protein, VE-cadherin has been shown to be indispensable for the formation and regulation of cell-cell junctions in ECs. VE-cadherin binds with itself to form the junction between cells. Inside the cell, VE-cadherin binds with β-catenin, which binds with α-catenin.

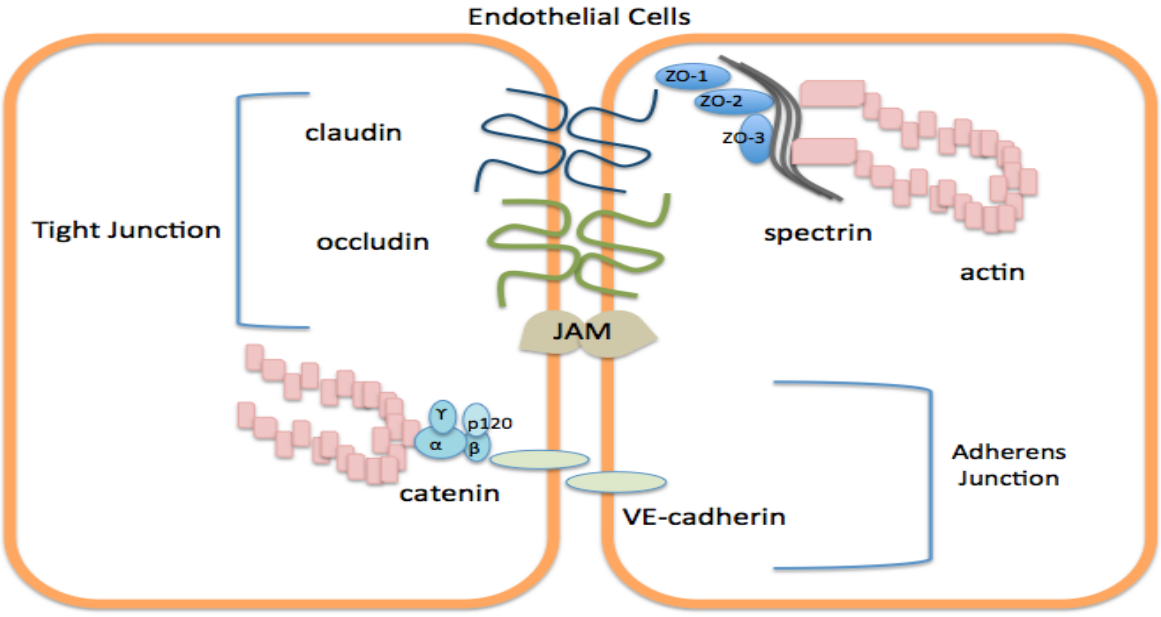

Figure 2.3: Molecular cell-to-cell junctions in endothelial cells. Tight junctions and adherens junctions are used to regulate the paracellular space between neighboring cells. Adapted from [35].

Collectively, this chain of interaction is associated with the cell's actin and cytoskeleton. VE-cadherin is known to be dynamic and can be altered and reorganized under different conditions. For example, VE-cadherin is known to re-localize under hypoxic conditions, and also known to perish when exposed to hydrogen peroxide in cell culture.[40-43] Because VE-cadherin is able to respond to a variety of situations, it makes it a potential marker to study endothelial dysfunction under a variety of conditions.

In TJs, claudins are linked to the actin and cytoskeleton of the cell through zonula occludens (ZO) ZO1, ZO2, and ZO3. While claudins make up a family of 24 members in humans, claudin-1, claudin-3, claudin-5, claudin-12, and claudin-15 are specifically expressed in human endothelial cells.[44-47] When claudin-5 is knocked out in a mouse model, the size-selected blood brain barrier is disrupted.[48] When claudin-1 is knocked out in cultured human endothelial cells, there is a significant increase in the permeability through the TJs indicating that claudin-1 plays a critical role in the regulation of permeability in non-neural tissues.[49] Many of these proteins represent potential cytoskeletal targets that can be studied in an artificial vessel.

Mechanical stresses associated with hemodynamic forces such as shear stress and pressure stimulate EC signaling. Chronic changes in these forces caused by hypertension and metabolic disorders can induce endothelial dysfunction and vascular failure. Microtubules are one of the main EC cytoskeletal fibers that regulate key functions that contribute to vascular integrity.[50] Microtubules polymerize with β -tubulin and α-tubulin and serves as a major component of the cellular cytoskeleton. Microtubules control EC cell shape, cell adhesion, mitosis, angiogenesis, intracellular

movement of vesicles, and are involved in wound endothelialization.[51] Their naturally unstable state allows for dynamic recycling and regulation of the cytoskeletal environment.[52-54] Many of these findings suggest the direct role that extracellular stimuli play on the regulatory mechanisms of ECs.

Studies have revealed a possible link between mechanical forces, microtubule formation, and vascular disease. Previous reports have shown that mechanical stretch increases reactive oxygen species generation and alters cytoskeletal regulation of ECs.[55-58] It has also been reported that mechanical forces like shear stress alter the vascular renin angiotensin system; specifically, cyclical stress has been reported to release angiotensin II (ANGII) in human ECs.[59] It has been shown that ANGII and cyclical mechanical stretch is linked to microtubule deacetylation in human ECs. This synergistic response may partly be attributed to endothelial dysfunction in vascular disease.[60]

However, despite knowing that mechanical stimuli like shear, pressure, and ECM stiffness affect cytoskeletal arrangement and vascular dysfunction, traditional use of 2D cell culture is often used to study disease. The use of 3D vascular models to study endothelium within a cylindrical tube have been studied in multiple contexts including angiogenesis, tumor biology, and the feasibility of 3D printed biomaterials.[61-65] The fabrication cost is cheap and rapid, and introduces the opportunity to study vascular diseases in a more physiologically relevant way.

Modeled Endothelial Response to Flow

The impact of laminar flow on endothelial gene expression has begun to provide framework for understanding vascular remodeling, responses to changing hemodynamics, to the development of disease.[66] The investigation of the specific genes differentially regulated in varying-flow environments may lead to future therapies in PAH. Previous studies have shown that genes responsible for cell growth, cell migration, gene expression regulation, nitric oxide synthesis, prostanoid synthesis, ECM, and vasoconstrictor regulation play a critical role in vascular homeostasis.[66]

Endothelial cells are able to mechanosense unidirectional shear stress and induce morphological and biochemical changes in response.[67] Pulsatile flow is present in both and arteries and the veins and leads the reorganization of the endothelial cytoskeleton and focal adhesions when compared to unidirectional flow.[68,69] Since PAH is localized in the smaller resistance level vessels in the lung, it is important to capture this pulsatile flow. By only introducing unidirectional shear stress, vascular models fail to capture vessels other than capillaries, which are known to have constant flow.[70]

Ultimately, tissue engineered vascular platforms introduce the ability to image and study diseases in a physiologically tunable way. Understanding the interplay of mechanical and biological parameters make artificial vessel platforms a key next generation approach to study PAH. However, no current model exists that replicates the pulmonary vasculature. Specifically, no cell culture model captures the complex physical environment seen in the resistance level vessels in the lung.

Clinical Cohort of PAH Patients

BioVU is Vanderbilt University Medical Center's (VUMC) large-scale DNA repository, totaling more than 225,000 samples.[71] The registry is compiled by using discarded blood from patients taken during routing clinical testing procedures. The patients are informed and give consent that they will be anonymously donating blood that has been linked to their medical record through and encryption process. The Synthetic Derivative (SD) is VUMC's de-identified electronic medical record that can be linked to a patient' DNA. Using both BioVU and the SD, insightful experiments can be designed that investigate clinical questions.

To interrogate a certain disease, a clinical cohort must be compiled from the SD and manually verified by a human in order to confirm appropriate status. A cohort of patients with PAH was extracted from the SD and matched with corresponding DNA in BioVU. First, contender patients must have undergone right heart catheterization (RHC) in order to be considered. If the patient had a mean pulmonary artery wedge pressure greater than 25 mmHg, the patient's pulmonary capillary wedge pressure was measured. If the patients wedge pressure was greater than 15 mmHg and the patient was on a PAH specific medication, the patient was characterized as a PAH patient. Whereas, if the patient had a normal RHC less than 25 mmHg, a wedge pressure less than 15 mmHg, and an ejection fraction greater than 55%, the patient was categorized as a control. Patients were excluded from analysis if 1) they had a normal mean pulmonary artery pressure with either a wedge pressure above 15 mmHg or an ejection fraction less than 55% or 2) the patient had a high pulmonary artery pressure and pulmonary wedge pressure greater than 15mmHg and was not on a PAH specific

medication, or 3) the patient had a high pulmonary artery pressure and pulmonary wedge pressure less than 15mmHg but did not have an ejection fraction less than 55%. If patients had a high pulmonary artery pressure and pulmonary wedge pressure less than 15mmHg but had an ejection fraction greater than 55%, they were classified as having heart failure with preserved ejection fraction (HFpEF). This classification scheme can be seen in **Figure 2.4**. All patients' electronic medical records underwent manual review to confirm cohort status. To date, there are 455 manually sorted and confirmed PAH patients in the VUMC PAH cohort.

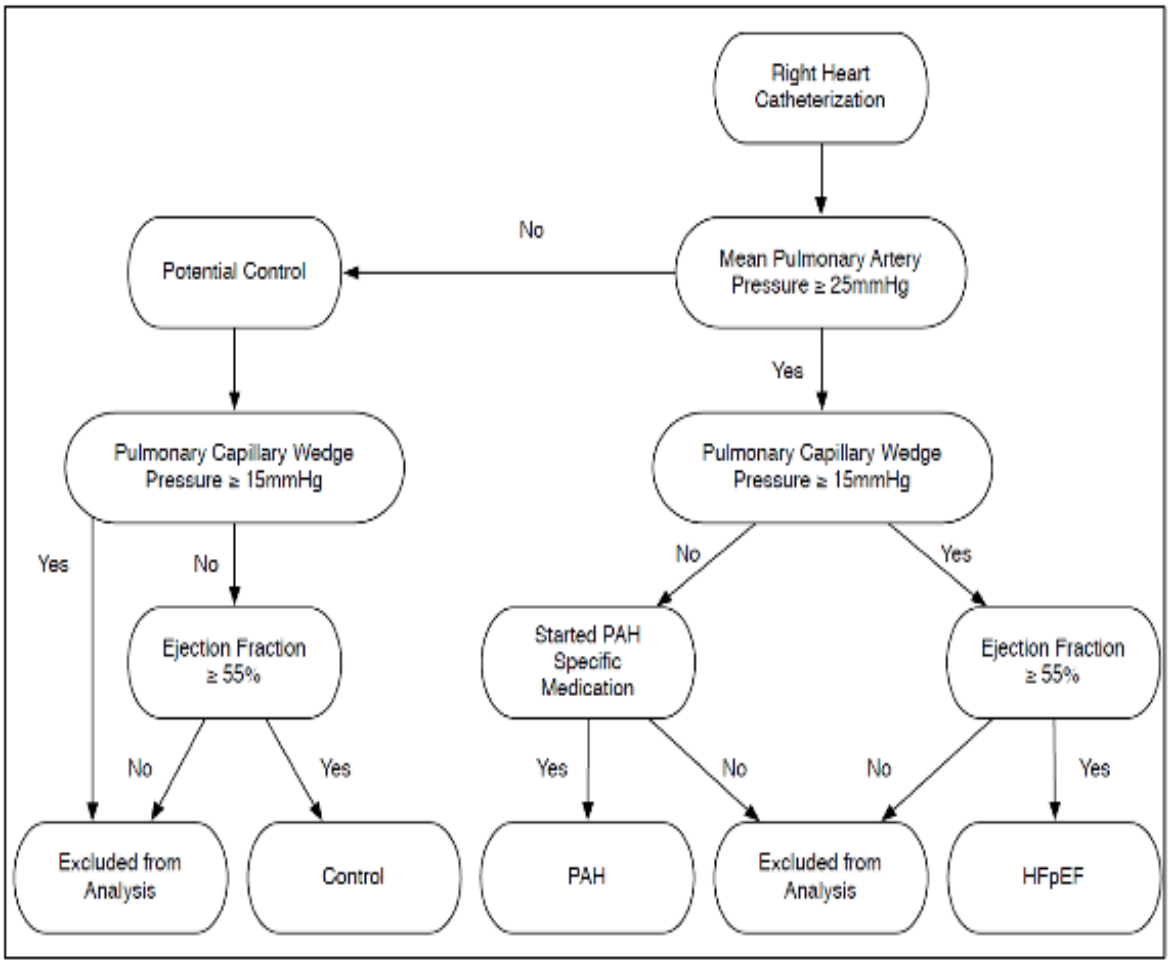

Figure 2.4 Flow chart of PAH and control classification from the Synthetic Derivative. The patients for classification must have undergone a right heart catheterization to be considered for the study. Classification materials included mean pulmonary artery pressures, pulmonary capillary wedge pressure, specific medications, and the ejection fractions. Patients were either classified as having PAH, controls, excluded from analysis or as having heart failure with preserved ejection fraction. All electronic medical records were manually reviewed to confirm cohort.

CHAPTER 3: SARACATINIB AND DASATINIB FAIL TO PREVENT HERITABLE PULMONARY ARTERIAL HYPERTENSION

Text and figures adapted in part from:

Reid W. D'Amico ,Santhi Gladson , Sheila Shay , Courtney Copeland, James D. West. Saracatinib And Dasatinib Fail To Prevent Heritable Pulmonary Arterial Hypertension. Submitted.

Introduction

PAH is a fatal and progressive illness of the pulmonary microvasculature. The insidious remodeling of the small resistance arteries in the lung leads to increased pulmonary vascular resistance, increasing the workload on the heart's right ventricle until it eventually fails.[72,73]

The most studied genetic risk factor for the development of PAH is a mutation in the BMPR2 protein. However, the mechanism underlying BMPR2 and the development of heritable PAH is not well understood.[8-10,74] A structural deformity seen in the mutated cytoplasmic tail in the BMPR2 protein results in a role in a host of deregulated protein pathways in PAH. In heritable BMPR2 mutations, the c-terminus of the protein is shortened. This increases the phosphorylation of many proteins responsible for maintenance of cellular mechanisms like growth, ECM maintenance, and cell division.[10,11] Downstream defects in BMPR2-associated PAH leads to alterations in cell-cell and cell-ECM force transduction, largely contributing to the mechanical pathology seen in the resistance vessels.[1] When studying the abnormal mechanical properties of the small vessels in the lung, it is critical to probe the molecular mediators of ECM

regulation, mechanotransduction, and intercellular force transduction, as many of these proteins could be targeted by therapeutics.[75]

Over recent years, considerable evidence has been accumulated suggesting the involvement of receptor tyrosine kinases (RTK) in the pathogenesis of pulmonary vascular remodeling seen in PAH. SRC Family Kinases (SFKs) are the largest subfamily of non-RTKs consisting of 9 kinases, known as SRC tyrosine kinase or SRC, which share similar structures and function.[76] SFKs play an important role in regulating signals from many RTKs and have evolved many complex regulatory strategies that couple with the cytoplasmic domains of many proteins. This complex regulation by SFKs is what controls many signaling pathways required for DNA synthesis, control of receptor turnover, differentiation, actin cytoskeleton rearrangements, motility, and survival.[77,78] The relationship among SFKs, vascular remodeling, and the pathogenesis of PAH are not well-explored.

In heritable PAH due to BMPR2 mutations, SRC's phosphorylation and downstream activity is increased.[10,11] SRC binds to the cytoplasmic tail of the mutated BMPR2 protein, which is likely a key component in the development of PAH.[12,13] We hypothesized that inhibiting SRC's phosphorylation would prevent its downstream activities and may prevent the development of heritable PAH. To test this hypothesis, we studied the ability of two known molecules that prevent SRC's phosphorylation, saracatinib and dasatibib.[23,24]

Methods

1.Heritable PAH: BMPR2 Mutant Mice

When exposed to doxycycline, Rosa26-Bmpr2^{R899X} mice will express the patient-derived R899X mutation in all tissues. After transgene activation, about 50% of Rosa26-Bmpr2^{R899X} adult mice (10-14 weeks of age) will develop PAH as characterized by right ventricular systolic pressures (RVSP) above normal range.[10] BMPR2 mutant mice were fed a western diet consisting of doxycycline (Bioserv) at 0.2g/kg for 6 weeks. Two weeks after the start of the diet, osmotic pumps (Alzet 1004) containing either dasatinib or saracatinib in 50% DMSO/50% 16α-hydroxyestrone(16-OHE) solution or vehicle with the same DMSO/16OHE formulation were implanted. 16-OHE was used to further drive the disease progression.[80] Dasatinib, saracatinib, or vehicle was delivered at 1 mg/kg/day for the remaining four weeks. After completion, the mice were placed under surgical anesthesia (Avertin) and the RVSP was measured by inserting a catheter into the right heart through the right jugular vein in a closed-chested procedure, as previously described.[79] Ten-second segments of RVSP measurement were extracted from the RVSP waveform, and the maximum RVSP was calculated by measuring the difference between the peak and trough of the wave.

After sacrifice, tissues were collected for further analysis. All surgical procedures were approved by the Vanderbilt institutional animal care and use committee (IACUC).

2. Histology & Western Blots

After RVSP measurement, the lungs were flushed with 5 mL PBS via perfusion through the right ventricle. To remove the blood, a small cut was placed in the left atrium. The lungs were then inflated with 0.8% low melt agarose.

The lungs from mice with or without an activated R899X mutation in the BMPR2 receptor were isolated, embedded with Optimal Cutting Temperature compound, and sectioned after the mice were treated for four weeks with saracatinib, dasatinib, or vehicle.

Lung sections were stained with α smooth muscle actin (αSMA, Sigma) and DAPI. To quantify αSMA positive vessels, an observer blinded to treatment group counted the numbers of fully muscularized vessels per field in 10 random 10x fields in three mice per group. αSMA positive vessels were stratified by diameter (<25um or 50-100um). Vessels were identified with a Nikon Eclipse Ti microscope and were measured along the longest axis. The apexes and edges of the lungs were avoided in histological quantification and observation.

SRC activity was quantified by measuring a known downstream protein activated by SRC, p-CAS and CAS. Antibodies used for Western blots were: p-CAS (Cell Signaling #4015, 1:1000). All phosphorylation proteins were normalized to their respective total protein (i.e. pCAS/CAS).

3. Statistical methods

Statistics were performed using two factor ANOVA (+/- BMPR2 mutation, +/- SRC Inhibitor), with Fisher's exact test t for comparisons between experimental groups. Statistics were performed within R.

Results

1. SRC Phosphorylation Inhibition Fails to Prevent PAH in BMPR2 Mutant Mice

ROSA26-rtTA x TetO7-BMPR2^{R899X} mice express a dominant negative form of BMPR2, the patient-derived R899X mutation when induced by doxycycline. This allows strong suppression of BMPR2 in adult mice while avoiding developmental defects associated with its suppression in development. These ROSA26-BMPR2^{R899X} mice spontaneously develop pulmonary hypertension with reduced penetrance when their transgene is activated for six weeks, associated with multiple molecular abnormalities including increased SRC phosphorylation.

To determine whether inhibition of this SRC activity would prevent pulmonary hypertension, age and sex matched wild type and ROSA26-BMPR2^{R899X} mutant mice were treated with saracatinib and dasatinib for the last four weeks during six weeks of transgene activation. Saracatinib and dasatinib were shown to inhibit the action of downstream targets in the SRC pathways (**Figure 3.1**), indicating proper osmotic delivery through the subcutaneously placed pumps to achieve direct SRC inhibition.

While vehicle-treated mice developed elevated RVSP at about 35% penetrance, mice treated with SRC inhibitors have pressures indistinguishable from the vehicle-treated BMPR2 mutants (**Figure 3.2**).

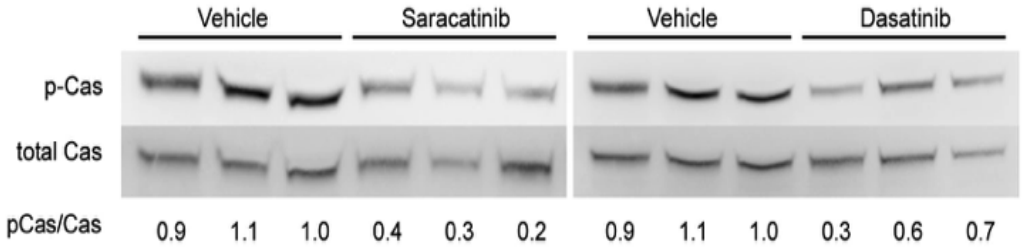

Figure 3.1: Saracatinib and Dasatinib reduce SRC phosphorylation and downstream activity. Western blots from ROSA26-BMPR2^{R899X} mutant lung treated with saracatinib, dasatinib, or vehicle. Mutants have increased phosphorylation of SRC target, CAS. CAS phosphorylation and activity is reduced with saracatinib and dasatinib treatment.

BMPR2 mutant mice have greater RVSP's than WT mice ($p<0.05$) and delivery of saracatinib and dasatinib to mutant mice does not reduce RVSP when compared vehicle treated mutants ($p>0.05$).

Lung sections from ROSA26-BMPR2^{R899X} mutant mice had an increased number of large muscularized vessels when compared to the wild type mice ($p<0.05$) (**Figure 3.3)**. The number of muscularized vessels in the mutant mice was not normalized to the wild type mice by saracatinib and dasatinib treatment ($p>0.05$). The number of fully muscularized vessels is about doubled in all BMPR2 mutant mice, independent of treatment. All vessels were consistently measured along the longest axis and included the border of the masculinized vessels. Fully muscularized vessels were measured and vessels that did not have at least 75% vessel perimeter were excluded from the analysis. The muscles were stratified within Nikon and analyzed within R. All imaging channels were taken manually and overlaid in ImageJ.

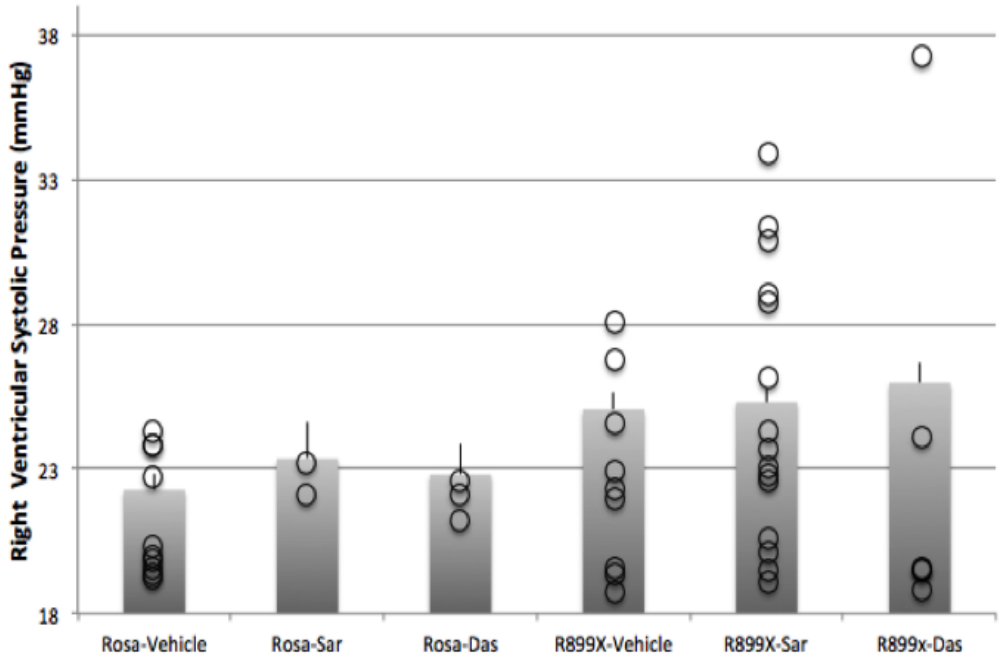

Figure 3.2: Saracatinib and Dasatinib do not lower RVSP in mutant mice. Right ventricular systolic pressures were significantly elevated (p<.001) in ROSA26-BMPR2^{R899X} mutants after six weeks of transgene activation through a western diet consisting of 1g/kg doxycycline. This elevation was not ameliorated through the administration of saracatinib and dasatinib pumps for the final four weeks. The circles represent the individual pressures of the mice and the bars represent the averages of all mice within the group. The error bars are reported as SEM.

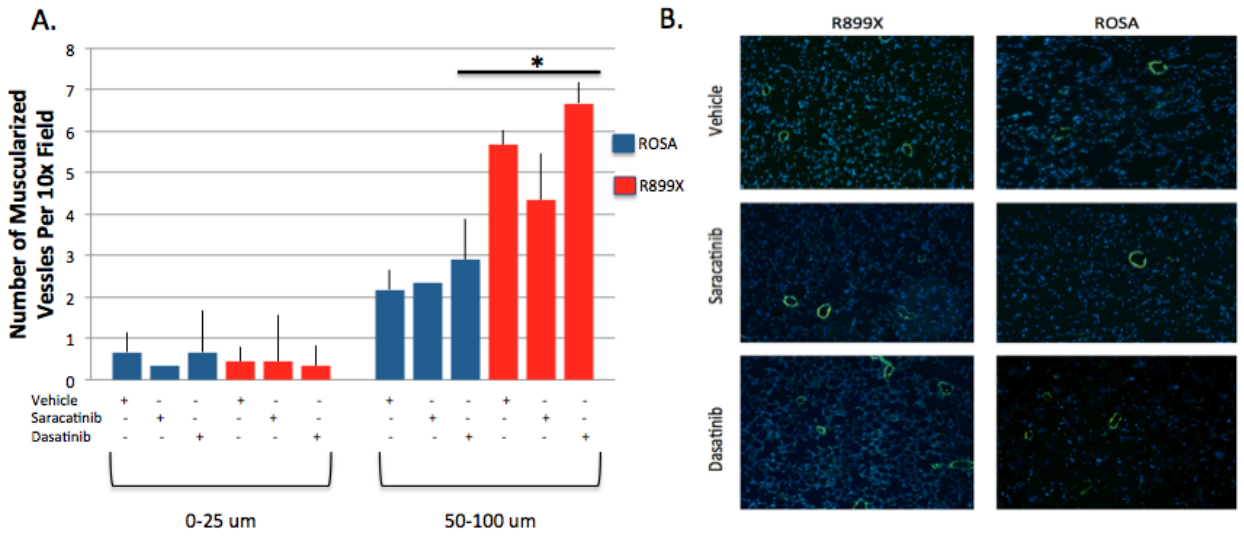

Figure 3.3: Saracatinib and Dasatinib do not reduce large muscularized vessels in mutant mice. **A)** ROSA26-BMPR2^{R899X} mutants and wild type mice have about the same number of small muscularized vessels per field. However, ROSA26-BMPR2^{R899X} mutants have about twice as many fully muscularized large sized vessels (50-100um). Saracatinib and dasatinib administration did not normalize the number of large muscularized vessels in the mutant mice. The error bars are reported as SEM. **B)** Representative images of the ROSA26-BMPR2^{R899X} mutants and wild type mice illustrate indistinguishable changes in muscularized vessels after administration of saracatinib and dasatinib. Images are taken at 10x.

Discussion

These results suggested that saracatinib and dasatinib did not prevent the onset of PAH despite inhibiting the downstream activity of phosphorylated SRC due to the BMPR2 mutation (**Figure 3.1**). Wild type BMPR2's cytoplasmic tail binds with SRC but does not lead to its phosphorylation. The truncated cytoplasmic tail in the mutant BMPR2 protein results in both the increase in phosphorylation and downstream activity of SRC. The administration of saracatinib and dasatinib are known to inhibit SRC's activity.[23,24] Previous studies have shown that antagonizing other proteins in the SRC pathways have resulted in the amelioration of PAH in identical animal models.[13] Here, we show that inhibiting this downstream activity by other therapeutic agents does not prevent the development of PAH.

Western blots confirmed that both saracatinib and dasatinib inhibit as expected, with decreased expression of key proteins downstream of SRC. The animal model also revealed an expected penetrance and development of PAH, as measured through RVSP **(Figure 3.2).** Despite therapeutic intervention, the elevated RVSP in the Rosa26-Bmpr2^{R899X} mutant mice was not lowered. This finding suggested that the inhibition of SRC and its downstream activity do not reduce the elevated pressures that are hallmark of PAH.

Rosa26-Bmpr2^{R899X} mice had about twice the amount of large fully muscularized vessels when compared to the wild type mice **(Figure 3.3)**. The administration of saracatinib and dasatinib failed to normalize the number of vessels. This finding once

again suggests that saracatinib and dasatinib do not prohibit the development of heritable PAH.

Because antagonizing the SRC pathway in PAH saw previous success, further efforts should focus on understanding the complexity of the interaction between SRC and the truncated cytoplasmic tail in the BMPR2 mutation in PAH. It is plausible that the development of PAH may not be due to the phosphorylation or downstream activity associated with SRC's differential regulation. Other studies have shown that SRC trafficking and localization is altered within the mutant cells when compared to the wild type cells.[13] A previous study interrogated the SRC pathway in heritable PAH and found success in preventing the onset of disease.[13] However, a key difference is that this previous study also restricted the aberrant SRC trafficking seen in mutant cells. Therefore, it is possible that the differential trafficking of SRC in heritable PAH plays a significant role in disease development and the inhibition of SRC itself is only part of the strategy that would need to be adopted the treat the disease. SRC is known to be sequestered in its phosphorylated form in PAH, and is thus unable to activate distant targets. This sequestration may be the dominating problem in SRC's role in PAH, and inhibiting SRC's phosphorylation may be the incorrect target to prevent heritable PAH.[13] Interestingly, one of the therapies, dasatinib, is known to cause PAH in humans.[81] This clinical observation further bolsters our belief that inhibiting SRC does not prevent disease, and the localization and trafficking is a more likely player in pathogenesis. Our study indicates that more information is needed to understand the complex role of SRC and the development of PAH. The inhibition and normalization of SRC's

phosphorylation and downstream target activity alone is not sufficient to prevent heritable PAH.

CHAPTER 4: ENGINEERING A PULMONARY VASCULAR PLATFORM TO STUDY PATHOGENIC ENDOTHELIUM IN PAH

Introduction

PAH is a disease characterized by the progressive occlusion of small pulmonary arteries through the proliferation of vascular cells. This leads to an increase in pulmonary vascular resistance, and eventually results in death from right heart failure [1-7]. The heritable form of PAH due to BMPR2 mutations leads to significant alterations in transcriptome-wide expressions in both human lung and cells cultured in flasks [8-10]. Specifically, studies have found that the deregulation of the Ras/Rho GTPase pathway plays a large role in the cytoskeletal defects seen in PAH [8,10-14]. The cytoskeletal defects and endothelial dysfunction are widely observed in PAH patients, and have been linked to BMPR2-associated disease [8]. While it is known that endothelial cells are sensitive and reactive to mechanical forces like shear [15,16], the intersection of BMPR2 associated PAH and mechanical properties of the pulmonary vasculature is still largely unknown.

Investigators have been interested in the effects of mechanical stimuli (e.g. pressure and flow) on the endothelium for decades. Surgical trials in animals in the 1960s showed that alleviating pressure and flow alone largely resolved pulmonary vascular remodeling [17-21]. However, this level of fine control of local vascular mechanics is impractical when studying vascular disease in humans and is incapable of revealing important molecular consequences of pulmonary vascular remodeling. More recently, there has been a growing interest in examining some of these mechanical

factors in the context of pulmonary hypertension, with recent papers investigating the effects of stiffness, flow, and stretch on pulmonary vascular cells [22-24]. There is substantial evidence that changes in the mechanical properties of the pulmonary vasculature are the critical determinants of disease progression. These mechanical stimuli override the effects of initiating events and result in common molecular and physiological pathology by the time disease has become clinically relevant regardless of initial etiology [25-28].

The aberrant gene expression and cytoskeletal architecture in BMPR2 mutant pulmonary endothelial cells may contribute to endothelial dysfunction [8]. This endothelial dysfunction can manifest in a number of ways, including abnormal barrier function, deregulated cytoskeletal assembly, and improper cytoskeletal organization. However, all in vitro studies have examined cells in stagnant dishes and no studies have probed the effect of mechanical stimuli on driving the endothelial dysfunction in PAH. To date, it has not been possible to study the effects of pressure and flow in a relevant 3D model, as none of the earlier platforms used were capable of independently controlling these critical parameters.

To overcome this limitation, we have created a new artificial arteriole cell culture platform that comprises a hydrogel-based extracellular matrix, controlled perfusion system, and fluidic network. Pressures, shear stresses, and pulsatile flow are controlled by a microcontroller-operated system of pumps and channels, and each parameter may be set to a biologically-relevant value. Thus, we are able to mimic, in a 3D cell culture platform, the mechanical stimuli that are seen in the vessels in the lung.

This artificial arteriole platform presents an opportunity to study how oscillatory flow leads to differences in gene expression, morphology, and barrier function in $Bmpr2^{R899X}$ and wild type (WT) murine pulmonary microvascular endothelial cells (MPMVECs) and thus provides more biomimetic environment to study PAH in vitro.

Methods

1. Device Fabrication

In order to study the effects of mechanical stimuli on the vascular endothelium in PAH, a suitable platform was first constructed. The platform was designed to consider multiple different areas of mechanical consideration, such as pressure, flow, shear, and stiffness of the ECM. These factors are likely to play a role in PAH, and therefore would provide an invaluable opportunity to study their contributing effects in a way that hasn't been studied previously.

1.1 Pump and Microcontroller Interface

A simple, affordable DC peristaltic pump (Adafruit Industries New York, New York USA) was used to mimic the pulsatile nature of the heart. An Arduino microcontroller (Arduino Turin, Italy) was used to power and control the pump duty cycle. The Arduino code provided pulses at 1Hz, or the standard human heart rate at 60 beats per minute. A diode was placed across the peristaltic pump to ensure unidirectional flow of current. See the appendix for code used; Figure 4.1 depicts overview of circuit design.

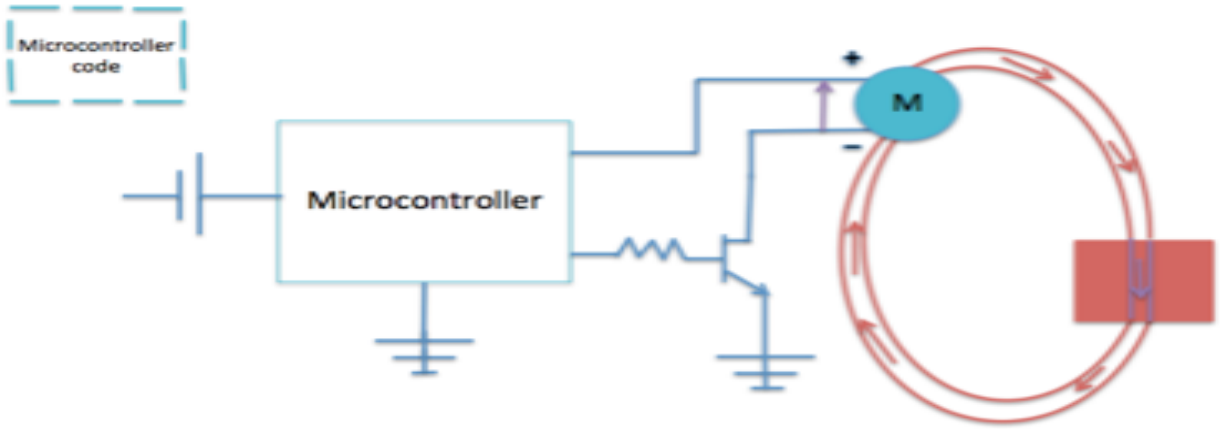

Figure 4.1: Overview schematic of platform circuit and media circulation. A combination of a microcontroller, resistors, diodes, transistors, motors, and conduit tubing were used to construct the pulmonary vascular platform. See appendix for specific parts used.

1.2 Microvessel Fabrication

A transparent PDMS (Sylgard 184, Dow Corning, Midland, MI, mixed at 1:10 ratio) compartment was fabricated to house the artificial pulmonary vessel. This transparent mold was 12.5mm x 12.5 mm with a depth of 7mm. Holes were cut in the PDMS mold approximately 2mm above the surface so that the artificial vessel was close to the surface of the PDMS thereby facilitating high resolution imaging. If the channel were too close to the PDMS mold, anisotropic mechanical effects from the surrounding PDMS or ECM environment could be significant.[113] The ideal height of the fabricated vessel should be about 500um from the surface of the mold. [113] A male 1/16" luer lock was fitted to a hole on one end of the PDMS mold (Cole Parmer, Vernon Hills, IL). A solution of 10% w/v porcine gelatin (Sigma Aldrich, St. Louis, MO USA) was dissolved in EGM2 media containing doxycycline (Lonza, Alpharetta, GA USA). A crosslinking

enzyme, microbial transglutaminase (MTG) (Modernist Pantry, Eliot, ME USA) was dissolved in 10% w/v PBS and mixed at 10% w/v with the gelatin to induce chemical crosslinking.[114]

A 900μm diameter steel rod served as a template to define the diameter of the artificial vessel. The rod was threaded through the PDMS holes and male luer locks, and the MTG and gelatin solution was poured into the PDMS mold at 37°C. Devices were covered and placed in 37°C incubator for twenty minutes. After gelation, the rod was pulled from one side of the gelatin until completely removed. To protect against tearing of the gelatin, the rod can be coated in bovine serum albumin.[122,123] The hollow channels were then coated with 100ug/mL collagen IV (Sigma Aldrich, St. Louis, MO USA) and 100ug/mL fibronectin (Sigma Aldrich, St. Louis, MO USA) for 48 hours before cell seeding. During coating, devices are kept submerged in media. See schematic representation of fabrication process in **Figure 4.2** and an image of the completed device in **Figure 4.3.**

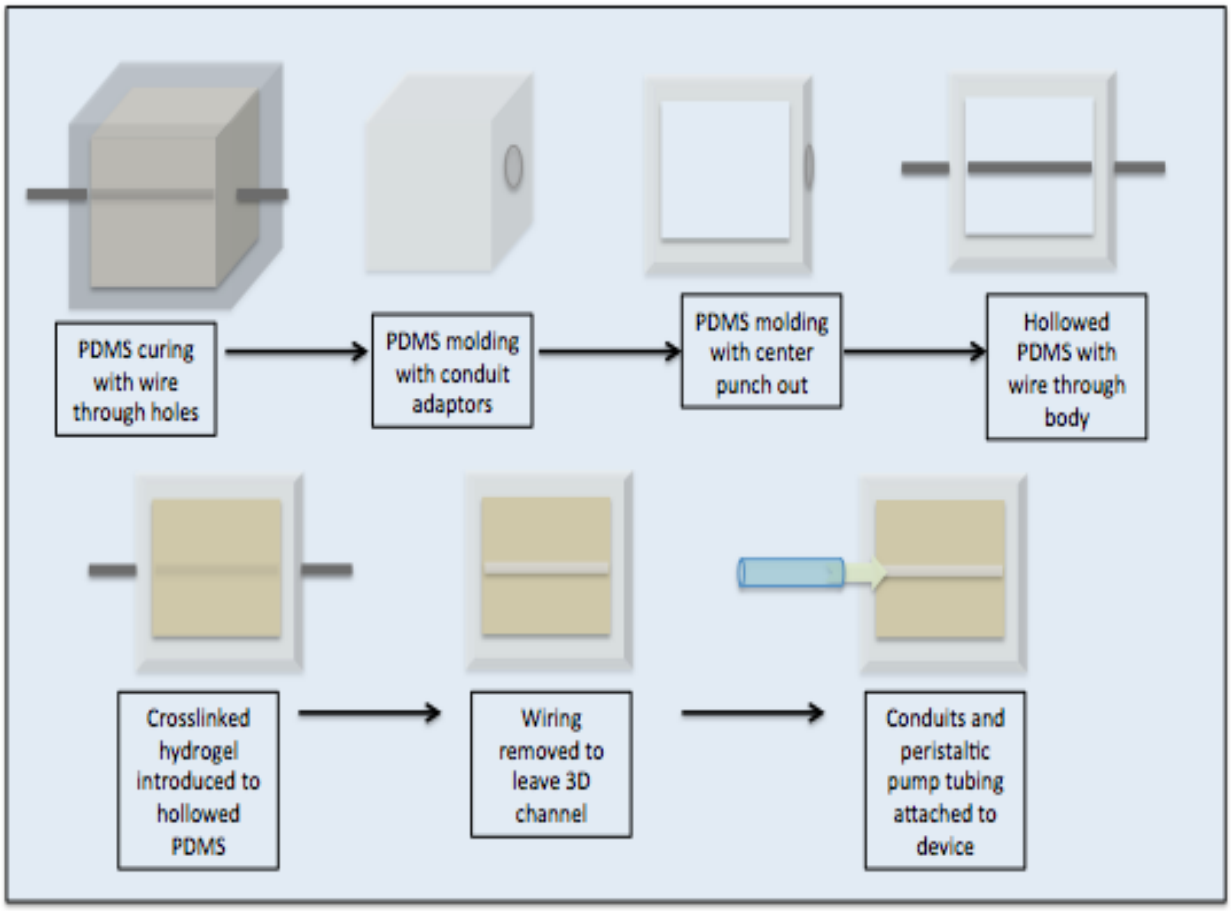

Figure 4.2: Fabrication process for assembly of PDMS molds and hydrogels. PDMS housing was first created through a two-step process including the formation of the walls of the housing then a base for the mold. Channel rods of desired size were threaded through the PDMS housing. Warm gelatin and MTG crosslinking agent were poured into the housing and allowed to solidify until cross-linked. The rods were carefully removed from the PDMS and gelatin leaving a casted vessel of appropriate diameter. Gelatin/PDMS molds were conditioned in media for at least 24 hours before being attached to perfusion system.

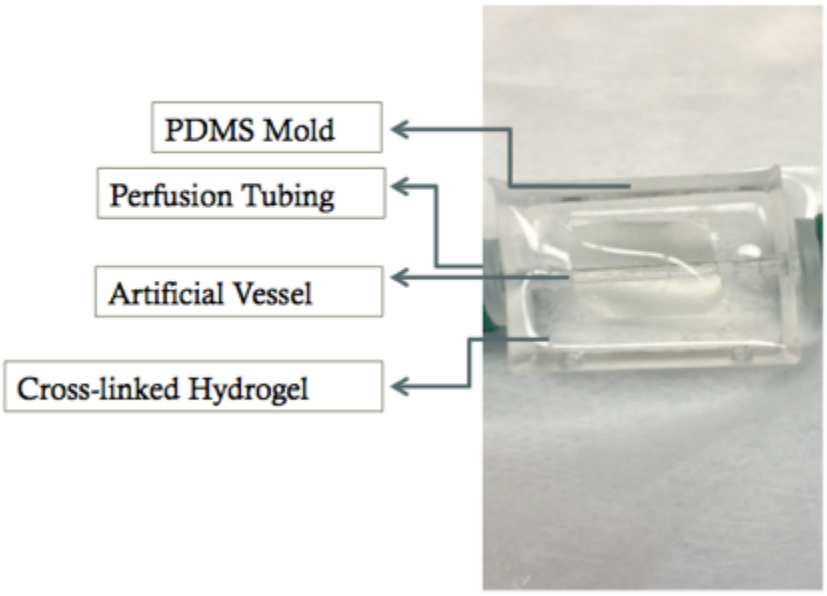

Figure 4.3 Annotation of compartments and parts in the PDMS mold and hydrogel construct. The device was made up of PDMS mold that houses the hydrogel. Within the hydrogel, a channel was casted through the device and connects the barbs and perfusion tubing on each side. The hydrogel has been cross-linked for increased rigidity.

2. Mechanical analysis inside vessel channel

2.1 Calculations

Before fabrication and mechanical testing of pressures inside the artificial channel, Poiseuille's law was used to extract pressures at various lengths and radii from the channel geometry. Poiseuille's law defines the relationship below (Eq1):

$$Eq1: \quad Q = \frac{\Delta P \, \pi \, r^4}{8L\eta}$$

The flow rate is represented by the variable Q, the radius by variable r, the length by variable L, and the viscosity by variable η. From above in Eq1. it is evident that the radius of the vessel can undergo minor changes and have great effects on the flow and the pressure drop within the system. This is discovered to be advantageous from a manufacturing standpoint. Slightly varying the diameter of the casted microvessel would likely serve to capture many of the complex flow, pressure and shear changes expected to be seen in PAH. For example, Eq2. and Eq3. below illustrate the effect that the radius of the channel can have on the shear experienced within the channel.

Eq2. $$\dot{\gamma} = \frac{du}{dr}$$ Eq3. $$\tau = \mu \cdot \frac{du}{dy}$$

Using previously measured peristaltic pump flow rates, and assuming laminar flow, the effects of a 1500um and a 900um channel can be summarized in **Table 4.1** below. After characterizing multiple diameter configurations, a 900μm channel was selected for experimentation. The flow rate during a 100 ms pulse time was measured to be 800uL/s.

	900 um diameter vessel*	1500 um diameter vessel
Shear Stress	98 dyn/cm^2	21 dyn/cm^2
Shear Rate	11,178 s^{-1}	2,400 s^{-1}

Table 4.1: Shear outputs from modeling high and normal shear environments within the artificial vessel. The 900 um channels, marked with an asterisk, was used for experimentation in this chapter due to its ability to reproduce the desired shear within the lung vasculature.

As seen above, the two example vessels above can be used to model two dramatically different situations in the pulmonary vasculature. Unfortunately, the shear stress and shear rate of the resistance levels where PAH is thought to develop have not been thoroughly studied, and are likely vary dramatically. Therefore, a large range in mechanical shear may be necessary to truly study its effect on PMVECs. Estimated shear from more thoroughly studied hemodynamic systems approximate that the above values are physiologically relevant in the lung.[67,124]

2.2 Pressure Measurements

Perhaps one of the most important aspects of the pulmonary vascular platform was its ability to also incorporate pulsatile pressure that is mimetic of the vessels in the lung. Since it is well known that endothelial cells are mechanosensitive, it is imperative to consider the pressure waves experienced in vivo.

To study the pressure waveforms that can be captured within the channel, a pressure sensitive catheter (Miller Instruments, Houston, TX USA) was introduced into the center of the channel. Vessel diameters ranged from 500 um to 1500 um. Pump

tubing connecting the vessel were also adjusted from 500 um to 3000 um. The ability to tune and adapt the platform for a variety of experiments introduces the possibility to study the effect of pressure on PMVECs cultured within the channel. **Figure 4.4** illustrates the great variability of pressure waves that can be generated by merely tuning vessel and tubing diameter of the platform. The simplicity and cheap cost of adjusting the platform makes it highly desirable to study the effects of pulsatility on endothelium. Specifically for PAH, the platform provides a unique opportunity to incorporate high pressure oscillatory flow to see its impact on pathogenesis and disease.

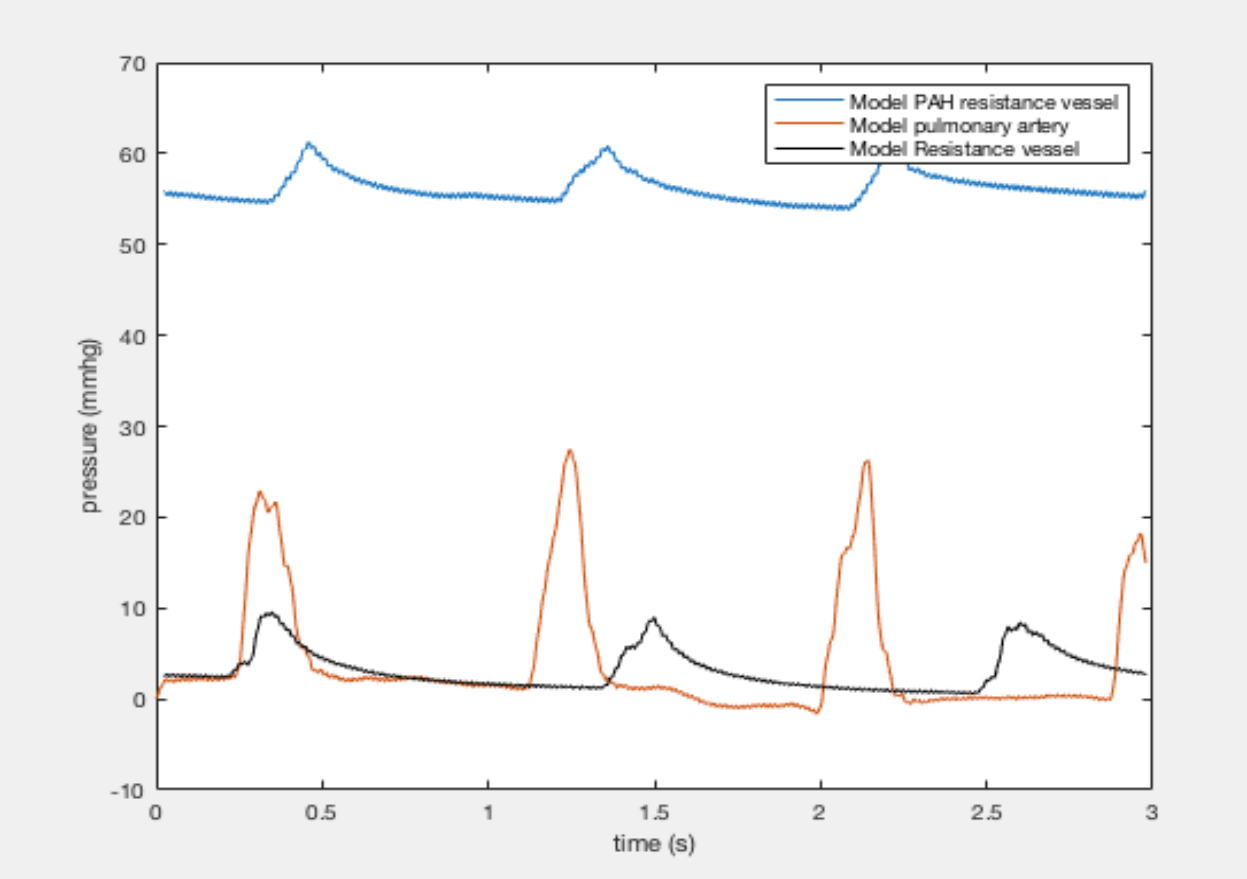

Figure 4.4: Representative waveforms observed in channel. Adjusting geometries of the channel and the perfusion tubing led to drastic changes in pressure waveforms in the channel. Pressures representing the pulmonary artery were created using a channel diameter of 1200 um, with inflow and outflow tubing geometry of 3000 um and 500 um, respectively. Pressures representing the PAH were created using a channel diameter of 500 um, with inflow and outflow tubing a geometry of 3000 um and 3000 um, respectively. Pressures representing the non-PAH were created using a channel diameter of 3000 um, with inflow and outflow tubing geometry of 3000 um and 500 um, respectively.

3. Experiment Preparations

3.1 Bmpr2^{R899X} and WT Cells

Bmpr2^{R899X}cells were derived from Immortomouse X Rosa26-rtTA2 X TetO7-Bmpr2^{R899X}. The immortomouse contained a transgenic insertion of the SV40 large T antigen, tsA58, under the control of an interferon inducible promoter.[115] When the cells were grown at 33°C and the interferon is added, the transgene was activated and the cells are immortalized. When the cells are moved to 37°C, the transgene became inert. The immortalized cells proliferate as though they were immortalized at 33°C, but revert to a normal immortal phenotype when cultured at 37°C. The BMPR2 mutation was induced by the addition of doxycycline to the media. The Immorto-BMPR2 mutant pulmonary endothelial cells were harvested from mice as previously described.[116]

3.2 Cell Seeding

Bmpr2^{R899X} and WT cells were seeded at a density of 75,000-cells/ device. The following day, the devices were seeded with another 75,000 cells/device. All cell seeding takes place in the immortalized condition (33°C with appropriate media) with the BMPR2 mutation activated via doxycycline. 24 hours prior to experimentation, conditional immortalization was turned off by moving the cells to a 37°C and removing the interferon.

3.3 Platform Set-up

Two perpendicular holes about 40mm apart were drilled in medium polystyrene round containers (Ted Pella, Redding, CA). Luer lock fittings with lock nuts were inserted into the two drilled holes and secured with nylon panel lock nuts (Cole Parmer, Vernon Hills, IL). The peristaltic pump was connected to the external conduits of the luer

locks. Within the container, one of the luer locks was fitted with a 1.92mm diameter tube (VWR, Randor, PA) approximately 35mm long that sits in the container. The other luer was fitted with the same tubing but with a 1/16” female luer locks fitted to the end. Prior to experimentation, the perfusion setup is submerged in bleach for 24 hours and then 100% ethanol for 48 hours. Immediately before, use, the containers are aspirated of liquid, dried, and rinsed with PBS. The peristaltic pumps are perfused with 100mL of 100% ethanol and then 100mL of PBS immediately before use. The containers are filled with 20 mL of media containing doxycycline (without immortalized conditions) were perfused through the peristaltic pump until no air is left in the tubing. Fully endothelialized channels are attached to the female luer locks within the container. The containers and the channels are placed in the incubator and connected to the preprogrammed circuit and then perfusion was initiated. An example of the completed platform can be seen in **Figure 4.5**.

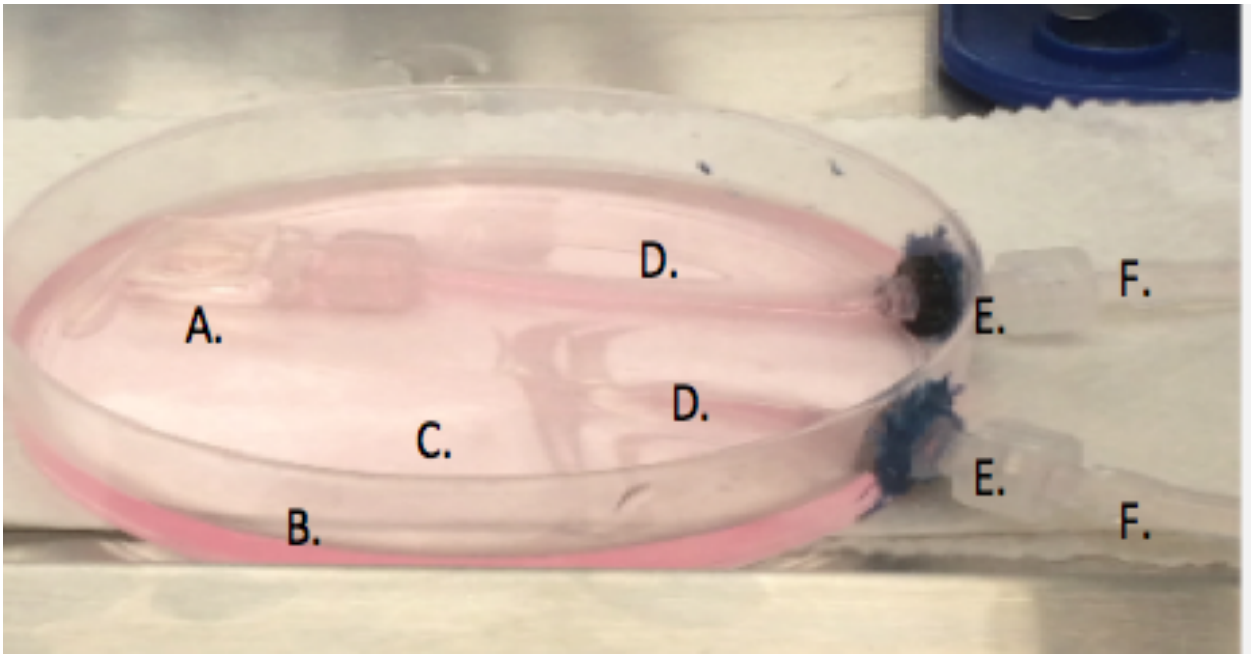

Figure 4.5: Image of platform inside sterile cell culture hood. Image of petri dish showing perfusion tubing, PDMS/hydrogel construct, and assembled platform. A) PDMS/Hydrogel device, B) Petri dish housing, C) Media reservoir, D) In/outflow tubing, E) Adapter conduits adhered to dish, F) Peristaltic pump perfusion tubing. Note: actual device perfusion and experimentation occurs within a 37°C incubator.

3.4 Assessment of Artificial Lumen

24 hours after the second seeding channels were perfused and then seeded channels are assessed for confluent monolayers around the entire cylinder. Channels were stained with calcein AM stain (Life Technologies, Carlsbad, California). A Zeiss LSM 710 Confocal Microscope was used to observe if the channels were confluent. Channels not confluent were disconnected from perfusion and monitored until confluent.

3.5 RNA Sequencing

Channels were perfused for 24 hours. Each array consisted of two channels per condition ($Bmpr2^{R899X}$and WT and perfused or static). RNA-Seq was performed on an

Illumina HiSeq system with a directional mRNA library prep, SR-50, with 30 million reads. RNA aligning was performed with TopHat to verify consensus genome sequence using ultra high-throughput short read aligner Bowtie2. Gene ontology analyses were performed with WebGestalt as previously reported.[117,118]

3.6 Endothelial Alignment

The channels were perfused with media for 0, 1, and 3 hours. Cells were immediately fixed and permeabilized within the channel. Cells were stained with phalloidin and DAPI and imaged with a Zeiss LSM 710 Confocal Microscope. Three devices were imaged per condition and a minimum of three images were taken per device. Alignment was quantified in ImageJ by measuring the cellular length in the direction of flow and the cellular width perpendicular to flow. A ratio of the length to the width was calculated to quantify the elongation of the cell in response to flow.

3.7 Barrier Function

The channels were perfused with media for 0 and 3 hours. Cells were perfused (30uL/min) for 1 hour with FITC-dextran microparticles (5mg/mL, M_w=5,000, Invitrogen, Carlsbad, CA) and imaged every thirty seconds. The fluorescence signal of the permeabilized FITC-dextran was quantified in Image J and Matlab (see code in supplement). Intensity values were manually extracted from ImageJ in order to compensate for unanticipated channel movement. Diffusion coefficients of the gelatin were calculated before experimentation.

3.8 Statistical Analysis

Statistics were performed using a one or two factor ANOVA (+/- BMPR2 mutation and +/- perfusion) with a Fisher's exact post hoc test for comparisons between groups.

P-values less than 0.05 were considered significant, but P values $P<0.1$ were still used in the RNA seq analysis. Statistics were performed in R Studio.

Results

1. Artificial Pulmonary Arteriole Validation

By manipulating the vessel diameter, and conduit tubing diameter and length, we were able to change both the shear stresses and pressure waveforms within the channel. The inner-channel pressure was successfully characterized within the center of the channel by a catheter inserted prior to each flow experiment.

While it was possible to generate several different flow waveforms in the channel using our perfusion system, the waveform that recapitulated the pressures in resistance level vessels in the pulmonary vascular was chosen for experimentation. Devices designed to replicate the pulmonary vasculature generated stable pressure values, with a standard deviation of 0.68 mmHg. The platform chosen had a channel diameter of 900 μm and perfusion conduit tubing with a diameter of 1.5 mm.

The fluidic resistance provided by this channel geometry facilitated the production of an oscillatory pressure wave with a pressure difference of about 9 mmHg that was sustained throughout the course of each experiment **(Figure 4.6).** Poiseuille's law was used to estimate a shear stress of 98 dyn/cm^2. During this flow pulse, the maximum flow rate within the channels was 800 μL/s and the minimum flow rate was 0 μL/s. Our chosen parameters for pressure and flow closely represented the data from initial physiological studies. Previous studies reported arteriole pressures of about 11mmHg.[147] Flow rates for the pulmonary vasculature vary tremendously due to physiological variation in the diameters of the arterioles and capillaries. We chose 800 μL/s because it is within other reported flow rates of 0.6 μL/s and 50,000 μL/s.[148,149]

Endotheliums were formed by seeding the artificial arteriole with a total of 150,000 cells. After seeding, channels were allowed to proliferate until confluency. Channels were then perfused at an oscillatory flow rate of 800μL/s with a pressure of 9 mmHg for one second followed by one second of relaxation (pump off). Seeded channels were imaged to verify that an artificial endothelium remained following 24 hours of oscillatory flow (**Figure 4.6**). In order to be used for experimentation, no notable acellular patches or defects were present in the channels after exposure to flow.

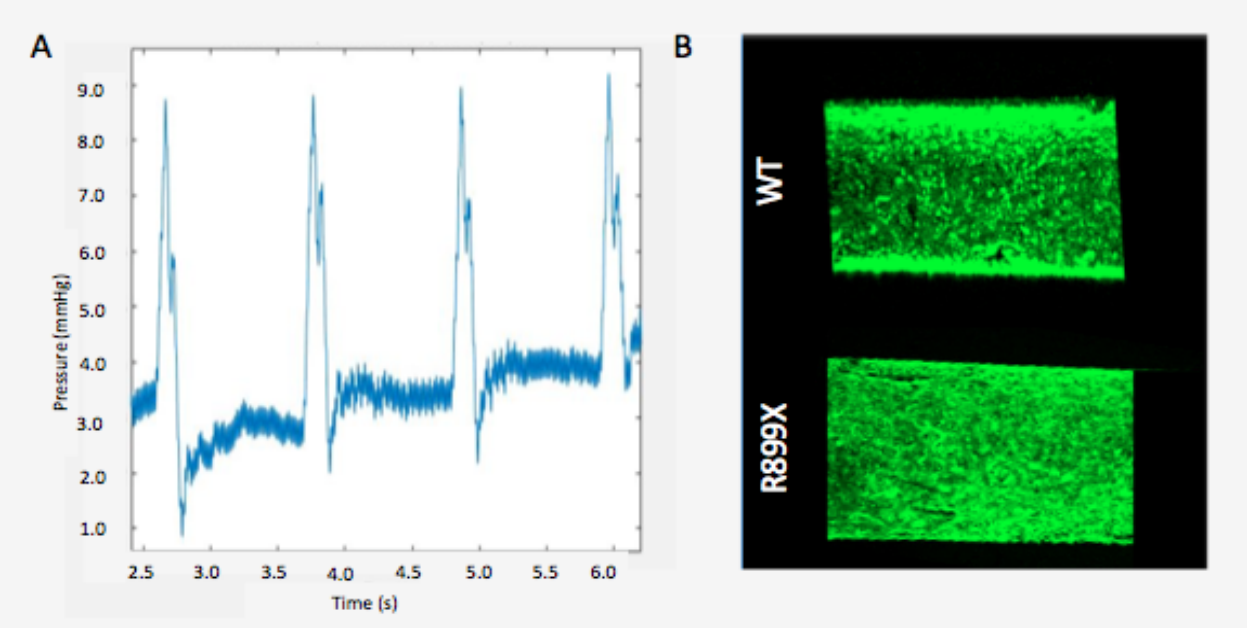

Figure 4.6: Validation of mechanical and cellular properties. **A)** Sample waveform depicting the oscillatory pressure waves observed within the center of the channel. **B).**WT and mutant Bmpr2^{R899X} endothelial cell channels imaged at 5x with fluorescent calcein AM to observe the monolayer formed by the cells. Channels were imaged after perfusion to ensure that the endothelial monolayer remained intact after the flow experiments. Cells were removed from conditional immortalization and the transgene was activated though doxycycline.

2. Oscillatory Flow Drives Genome-wide Changes in WT and Bmpr2^{R899X} Pulmonary Endothelial Cells.

The molecular consequences of oscillatory flow on the Bmpr2^{R899X} mutation were determined after we performed RNA-Seq on an Illumina HiSeq system and measured gene expression of both adult WT and Bmpr2^{R899X} MPMVECs that were control immortalized with transgenes activated. After exposure to flow, the changes in gene expression within the mutant and WT cells as well as between perfusion conditions were dramatic, with 457 genes changed more than 0.4 log times the un-perfused condition.

Gene outcomes after exposure to flow were sorted into either a congruent or incongruent category **(Figure 4.7)**. Congruent genes demonstrated similar directional changes in expression when exposed to flow, but are offset by different magnitudes in expression. A total of 248 genes were sorted into a congruent category. Of these congruent genes, 202 have functional annotation and 131 fell into statistically overrepresented gene ontology biological process groups. **Figure 4.8** illustrates gene ontology groups by significance and number of genes.

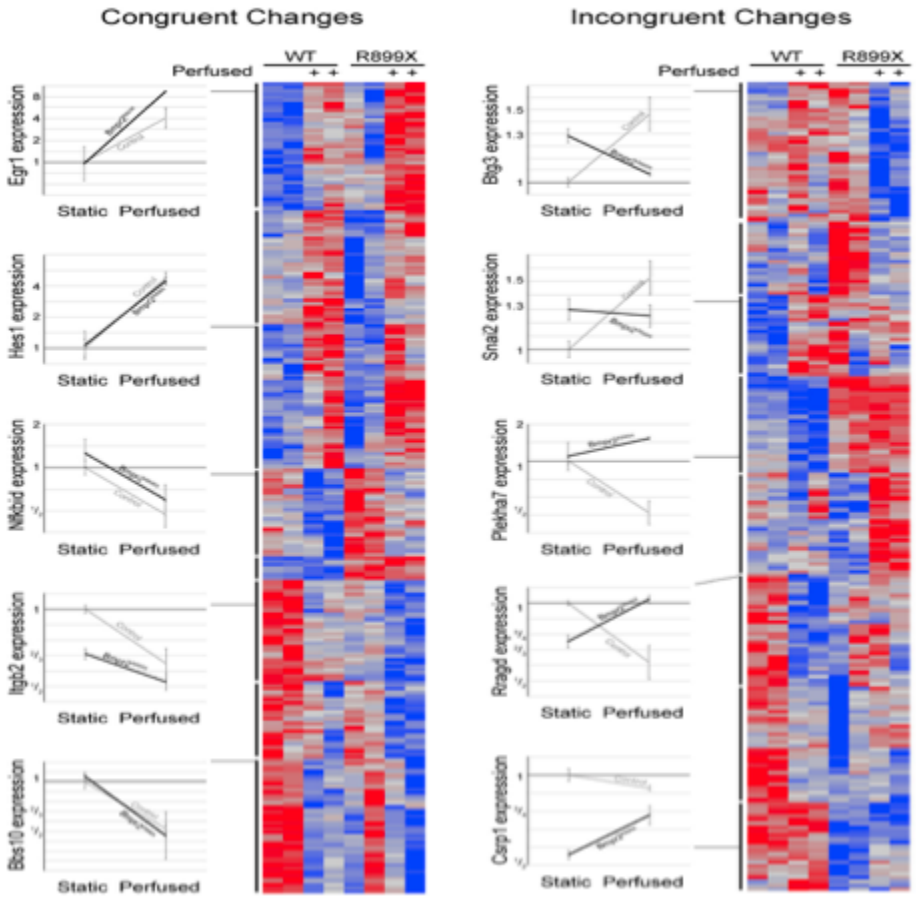

Figure 4.7: Congruent and incongruent heat map depiction of gene expression changes. Heat maps were separated by cell genotype (WT and Bmpr2^{R899X}) with flow (+) or without flow. Representative genes and corresponding expression changes were selected to illustrate change in expression seen within the congruent and incongruent maps. Congruent genes had similar directional changes to flow but were offset by the magnitude of expression. Incongruent genes had opposite directional responses to flow that result in different magnitude changes. The inclusion of flow led to notable gene expression changes in both the R899X and WT endothelial cell. Notable changes in gene expression were seen between the cell's genotype and flow conditions.

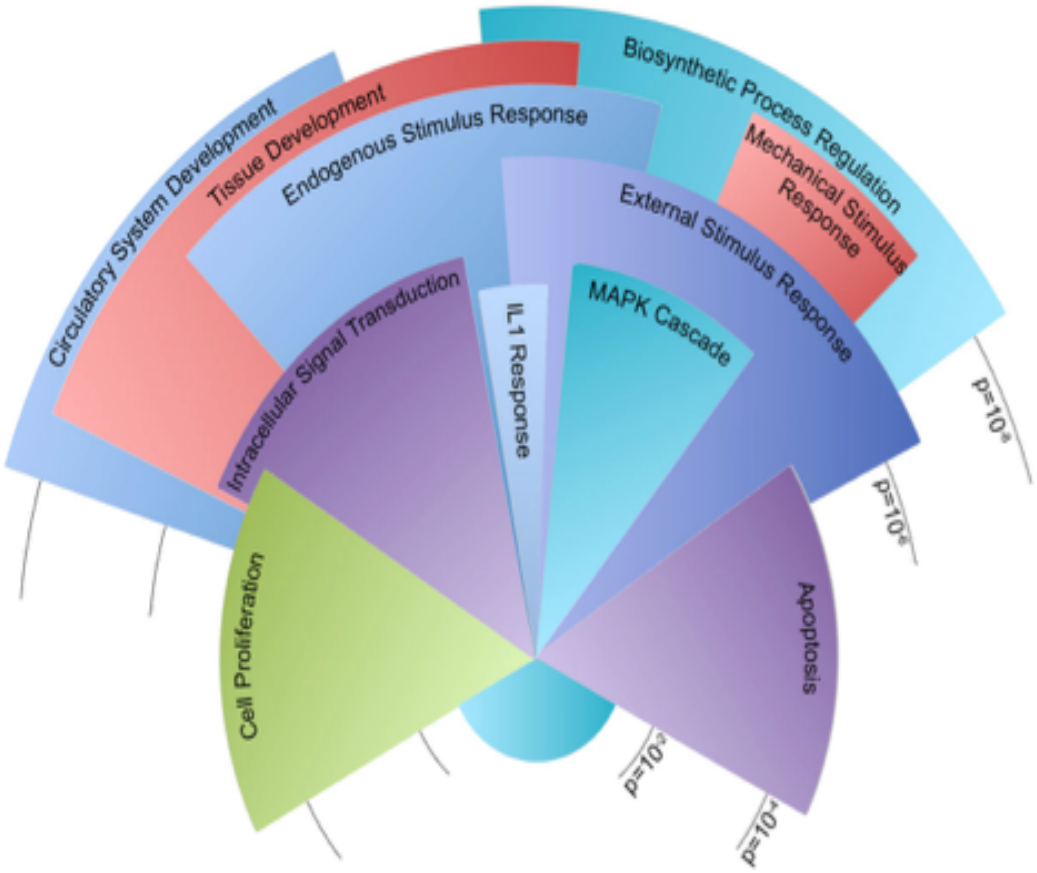

Figure 4.8: Congruent genes dysregulated in Bmpr2^{R899X} endothelial cells after 24 hours of perfusion. Pie chart shows relative number of genes in statistically dysregulated gene ontology groups. Arc length of the gene ontology groups corresponds to the number of genes present in each group. Radius length corresponds to significance, where the longest categories were significantly dysregulated at ~ $P<1x10^{-8}$ and the shortest categories were dysregulated at $P<1x10^{-3}$.

.

The incongruent category is characterized by expression behavior that diverges when the cells are exposed to flow. For example, the introduction of flow may lead to an increase in expression in one group and a decrease in expression in another. A total of 209 genes were sorted into an incongruent category. Of these incongruent genes, 148 have functional annotation and 77 fell into statistically overrepresented gene ontology biological process groups (**Figure 4.9)**.

Within the congruent category, the majority of genes were involved in the development of the circulatory system and other tissues. Other genes corresponded to the regulation of cell proliferation, cell death, and responses to external and mechanical stimuli. Similarly, many incongruent genes were involved in sensing external stimuli and the apoptotic process. Genes involved in cell adhesion were the most notably inconsistent gene ontology group when the congruent category was compared to the incongruent scenario. Both incongruent and congruent genes had ontologies correlating to mechanisms concerning response to external mechanical stimuli. In particular, the differences in cellular adhesion and cytoskeletal architecture were known to be different between $Bmpr2^{R899X}$ and WT cells.

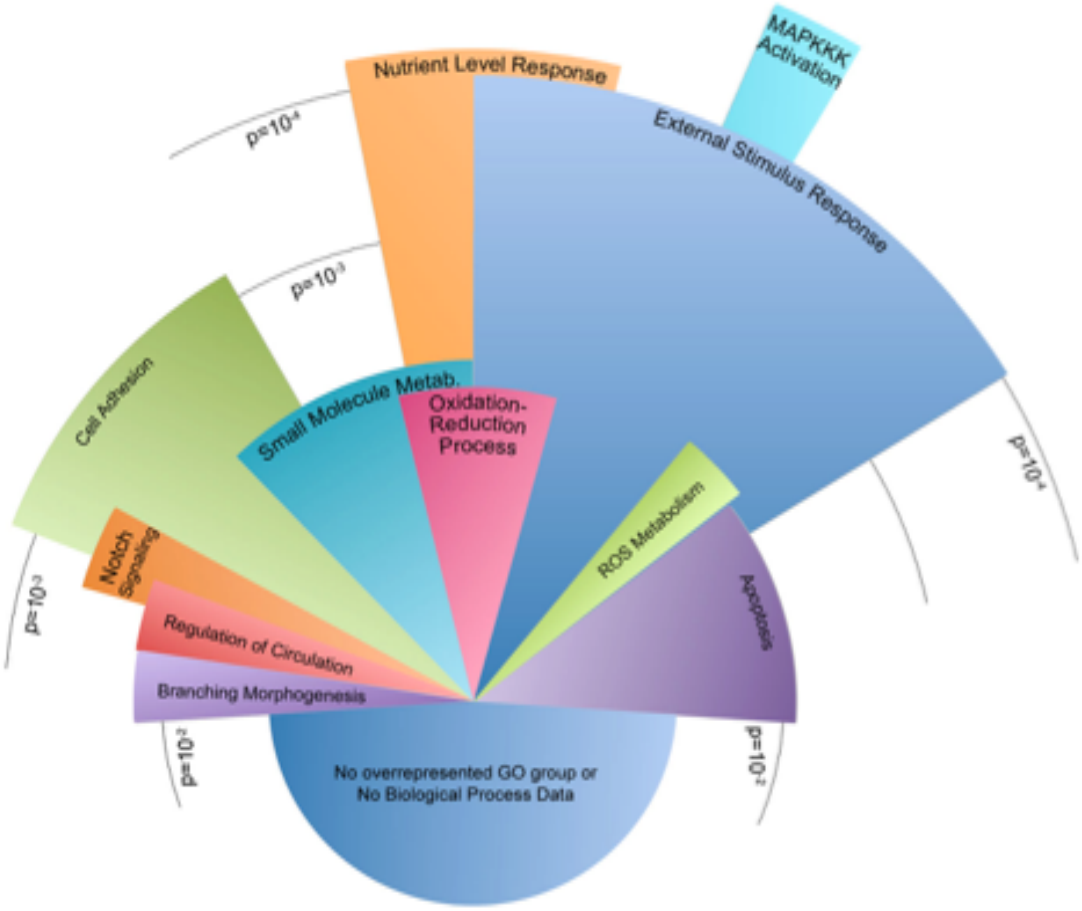

Figure 4.9: Incongruent genes dysregulated in Bmpr2^{R899X} endothelial cells after 24 hours of perfusion. Pie chart shows relative number of genes in statistically dysregulated gene ontology groups. Arc length of the gene ontology groups corresponds to the number of genes present in each group. Radius length corresponds to significance, where the longest categories were significantly dysregulated at ~ $P<1x10^{-5}$ and the shortest categories were dysregulated at $P<1x10^{-2}$.

3. Bmpr2^{R899X}Pulmonary Endothelial Cells Do Not Change Morphology in Response to Flow.

Endothelial monolayers were imaged at three different time points (t=0,1,and 3 hours) to assess morphological response to flow within the artificial arteriole. As seen before, WT cells respond to flow by slowly elongating in the direction of shear.[107-109] Conversely, the mutant Bmpr2^{R899X} did not respond to flow and did not elongate after 3 hours of exposure to perfusion (**Figure 4.10**).

This difference in alignment between Bmpr2^{R899X} and WT was drastic after 3 hours of perfusion ($p<1.0e^{-5}$). WT cells responded to flow within an hour while the mutant cells showed no sign of elongation at 1 hour ($P<1.0e^{-4}$). Before perfusion, both the WT and Bmpr2^{R899X}cells had nearly indistinguishable cell morphologies ($P>0.05$), with a similar alignment ratio of about 1.1 (measured by the ratio of cell's length in the flow direction divided by the length perpendicular to flow). The difference in morphology magnifies the role that cellular adhesion and cytoskeletal genes may play in the mutant and WT when exposed to flow.

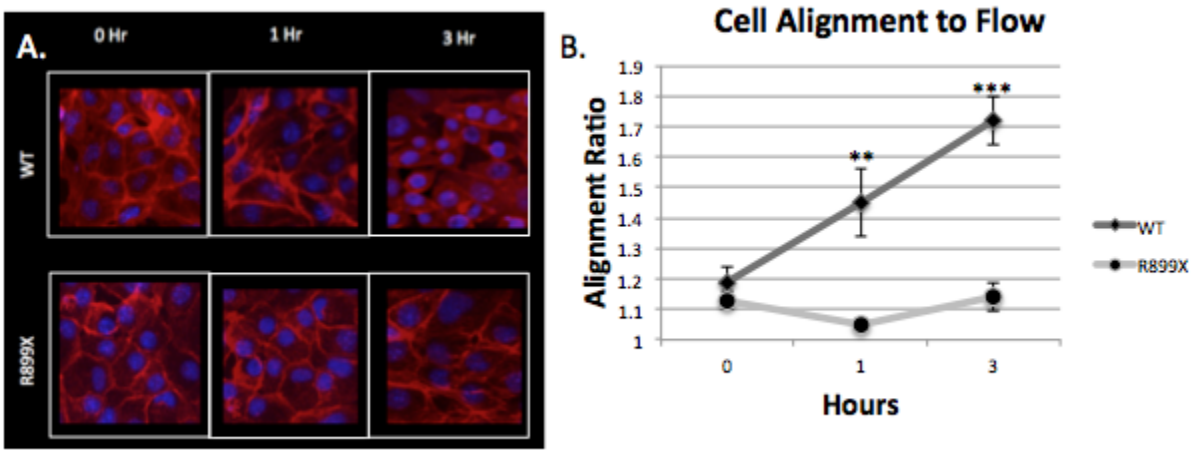

Figure 4.10: Bmpr2^{R899X}endothelial cells do not align in the direction of flow. A) Morphological differences were seen in the WT cells as the amount of perfusion time increases, whereas the Bmpr2^{R899X}cells did not show evidence of elongation. Images were taken at 20x B) Without perfusion, both Bmpr2^{R899X}and WT endothelial cells showed no difference in cell morphology and alignment ratio ($P>0.05$). After 1 hour of perfusion, the WT cells started to align, but the Bmpr2^{R899X} cells showed no evidence of aligning in the direction of flow ($P<1.0e^{-4}$). The WT cells continued to elongate and increase their alignment ratio while the Bmpr2^{R899X} cells maintained a nearly constant alignment ratio ($P<1.0e^{-5}$).

4. Bmpr2^{R899X} Pulmonary Endothelial Cells Demonstrate Significant Barrier Dysfunction In-Vitro.

Channels and gels were imaged following either perfusion (t=3hrs) or static conditions (t=0hrs) to assess the barrier function of the endotheliums in the Bmpr2^{R899X} and the WT endothelial channels. The WT endothelial cells maintained barrier integrity when perfused with 10k FITC dextran in both perfused and static conditions with permeabilities of $1.65e^{-7}$and $5.93e^{-8}$cm/s, respectively. There was no significant difference between perfused and static WT channels ($P>0.05$). As depicted in **Figure 11.A**, little FITC dextran was seen leaking out of the WT channel and into the hydrogel.

Unlike the WT experiments, the Bmpr2^{R899X} endothelialized channels exhibited more FITC dextran leakage in both the perfusion and static conditions, with permeabilities of 1.51e^{-6}and 3.00e^{-6} cm/s respectively. This increased permeability can also be seen in **Figure 11.A**. Similarly to the WT channels, Bmpr2^{R899X} channels had no significant differences in permeability in static or perfusion conditions ($P>0.05$). A control channel without any endothelium had a greater amount of leakage than all seeded channels, regardless of the mutation. The control channel seen in **Figure 11.B** has been outlined in order to see where it is located, since the fluorescence from the FITC dextran diffusion obfuscates the channel boundary. In both the perfusion and the static conditions, the WT channels were always less permeable than the Bmpr2^{R899X} channels, with $P<0.05$ for both static and perfusion conditions (**Figure 11.C)**.

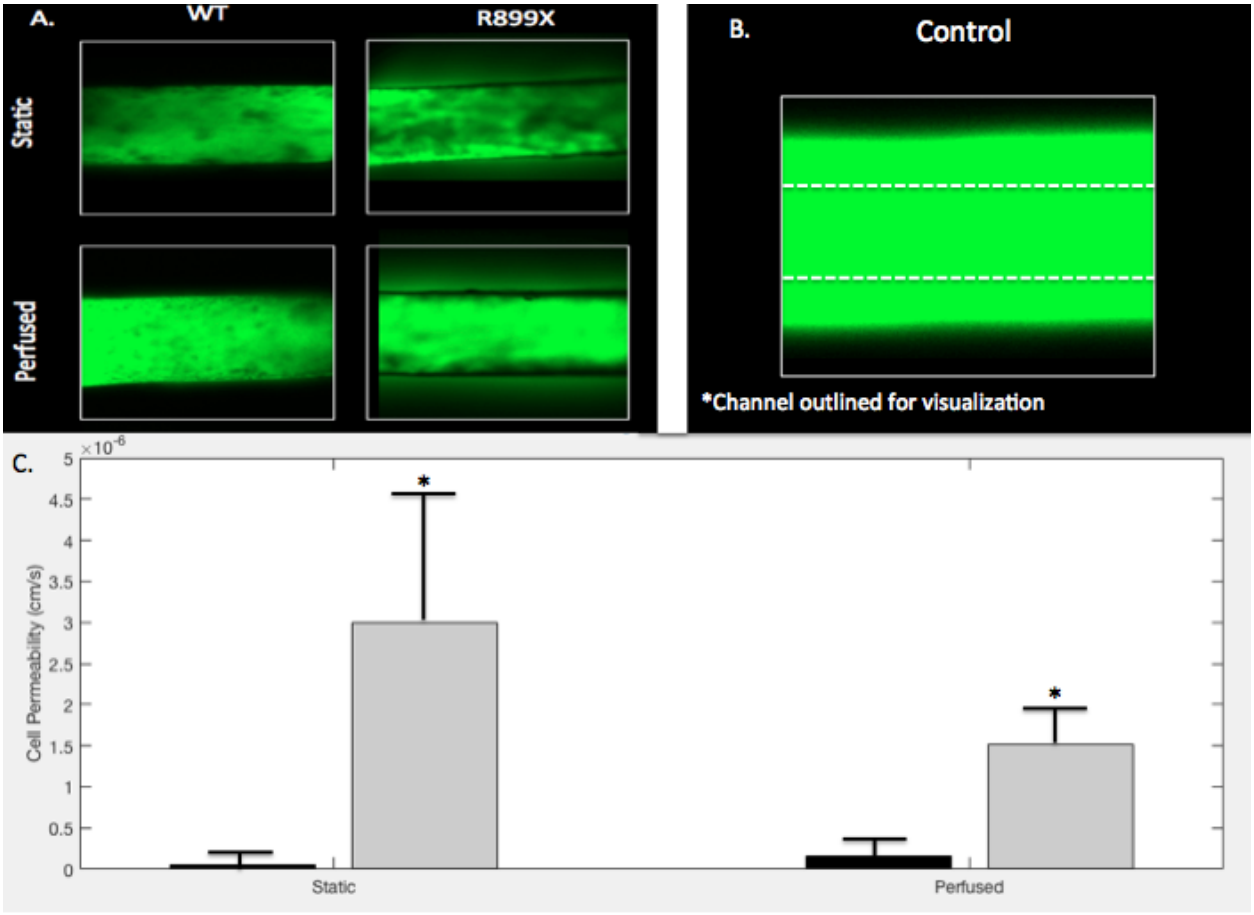

Figure 4.11: **Bmpr2^{R899X} MPVESCs have increased permeability compared to WT cells under perfusion and static conditions.** A) Static and perfused WT and Bmpr2^{R899X} channels were imaged at 5x following one hour perfusion with FITC dextran. B) A control channel without cells was perfused with FITC dextran for comparison. Because of excessive fluorescence due to high permeability, the outline of the channel was added. C. Permeabilities of the WT and Bmpr2^{R899X} are plotted under both conditions to visualize magnitude differences in permeability between genotype. No statistical difference was seen between perfusion and static conditions in all genotypes ($P>0.05$); however WT and Bmpr2^{R899X} channels had significantly different permeabilities under both static and perfusion conditions ($P<0.05$).

Discussion

Several groups have used microfluidic systems to model vascular shear to study the responses of endothelial cells to mechanical stimuli.[68,119-121] Our model expanded on the initial characterization of the endothelial cells and flow by developing a more physiological relevant environment to study pulmonary vascular disease. In our design phase, we sought to incorporate tunable parameters like shear stress, matrix stiffness, pressure, and oscillatory flow so that a wider range of biological questions could be asked due to the customizable parameters of the artificial arteriole.

Before experimentation, all devices and platforms were tested for mechanical and cellular consistency before data collection (**Figure 4.6).** RNA-Seq from WT and $Bmpr2^{R899X}$ MPMVECs cultured under static and perfusion conditions demonstrated that many central pathways relevant to PAH etiology were altered in the mutant cells when exposed to flow (**Figure 4.7)**. These findings were stratified into two categories: congruent or incongruent gene expression changes. In the congruent gene expression category, the majority of genes were involved in the development of the circulatory system and other tissues **(Figure 4.8)**. The majority of significant genes discovered were in the congruent gene category. In most cases, the $Bmpr2^{R899X}$ cells demonstrated a greater level of gene expression when compared to the WT cells. The $Bmpr2^{R899X}$ cells tended to over respond to many key molecular pathways, but the response mirrored the up or down regulation patterns seen in the WT cells.

Gene expression in the incongruent category showed differing gene expression changes to many gene ontologies, but most notably to genes regulating the cytoskeleton and response to external stimuli **(Figure 4.9)**. In many instances, WT cells

had up or down gene expression pathways in response to flow, but the mutant Bmpr2^{R899X} cells would often have a contradictory response. However, the deregulated cytoskeleton pathways have been observed before.[10] The BMPR2 protein is known to directly interact with many proteins relevant to the cytoskeleton.[10,12,17,19] The induction of mechanical stress (e.g. oscillatory pressure and flow) further exacerbated an already deregulated endothelial profile.

Evidence of an altered response to flow and pressure was first observed in the Bmpr2^{R899X}cell's morphology when the channels were first perfused (**Figure 4.10)**. Endothelial cells were known to respond to flow, but the aberrant alignment of the Bmpr2^{R899X} cells may be correlated to the deregulated cytoskeletal and mechanical response pathway.[107-109] The inability of the Bmpr2^{R899X} mutant cells to adapt to flow conditions may explain many of the endothelial defects known to take place in PAH.[110-112]

Endothelial dysfunction and permeability issues are a known hallmark of Bmpr2^{R899X} PAH.[10] Previous studies have observed that perfusion of Evan's Blue through the pulmonary vasculature of Bmpr2^{R899X} mice results in observable leakage that is much higher than in control mice.[10] To recapitulate this behavior in our platform, we tested the permeability of Bmpr2^{R899X} and WT endothelial MPVECs cultured in our channels. Channels either experienced no flow or were perfused for 3 hours to replicate the longest time point seen in the alignment study. After cells were exposed to oscillatory flow and perfused with dextran, intensity values were taken within the channel, within the gelatin, and within the region dextran perfused into the hydrogel. Permeability values were calculated for the Bmpr2^{R899X} and WT cells in both perfused and static

conditions. **Figure 4.11** illustrates how the WT cells maintain a greater barrier to 10k dextran in both perfusion and static conditions when compared to the $Bmpr2^{R899X}$ cells ($P<0.05$). The $Bmpr2^{R899X}$ cells are more permeable to both the WT cells in both the static and perfused condition, with the perfused condition not increasing the rate of permeability. The lack of significant differences in permeability under flow suggests that the pathologic barrier function in PAH may be independent of physiological pressure or flow.

The increased permeability of the $Bmpr2^{R899X}$ cells has been previously observed in vivo, but this is the first time similar increased permeability (as well as lack of cellular alignment) has been demonstrated in a 3D hydrogel culture model. No studies have looked at the impact of PAH's heritable $Bmpr2^{R899X}$ mutation and its changes in flow environments. These findings demonstrate how mechanical parameters often neglected in 2D cell culture yield important information needed to understand the pathology of PAH.

Due to the artificial arteriole's successes in modeling PAH, future studies should strive to use the model's customizability to generate new disease environments. For example, future experiments could incorporate other hierarchal tissues and cells in the blood vessel to model dynamic tissue signaling. Manipulation of the circulating media could also be exploited by adjusting media chemistry or adding circulating cells to model other disease phenomena like inflammation.

Manipulating disease severity inside the artificial arteriole is an important next step. Given the mechanical sensitivity of the endothelium, the viscosity of the circulating fluid, the geometry of the channel, as well as the stiffness of the surrounding hydrogel will

likely have an effect of the gene expression and endothelial function. Studying increased levels pressure and shear stress may elucidate how the genetic and phenotypic environment may be altered as PAH advances. As PAH progresses, vessels occlude and shear stress increases along with pressure. The development of PAH likely alters the endothelium. Adjusting the artificial arteriole's geometry presents an opportunity to examine the effect of flow conditions associated with disease severity of PAH on the diseased endothelium. In addition, much of the chemical environment seen in blood is also neglected when using media to perfuse the endothelium. Striving to incorporate a more realistic hemodynamic chemical and mechanical environment are also needed to create a more realistic model system of the pulmonary vasculature.

CHAPTER 5: GENETIC VARIATION OF OXIDATIVE PHOSPHORYLATION GENES ASSOCIATE WITH RIGHT VENTRICULAR FUNCTION IN PATIENTS WITH PULMONARY ARTERIAL HYPERTENSION

Introduction

Mitochondrial aerobic ATP generation by the oxidative phosphorylation system (OXPHOS) is a key energy process for exercise. It is well-regarded that one of the main determinants contributing to someone's athleticism and endurance status is the oxidative potential of their mitochondria.[125,126] As such, there is thought to be a strong connection between genes that regulate the OXPHOS or mitochondrial DNA (mtDNA) and outcomes of elite athletic performance.[127-142] Several of these studies have analyzed the possible association among genetic variants in the OXPHOS pathway, including: PPARD, PPARGC1A, NRF, PPARA, and TFAM. This pathway can be seen in **Figure 5.1**. Genes in this pathway are known to interact with mitochondrial biogenesis, mtDNA replication, ATP production through the OXPHOS system, or enhanced lipid oxidation under an exercise stimulus.

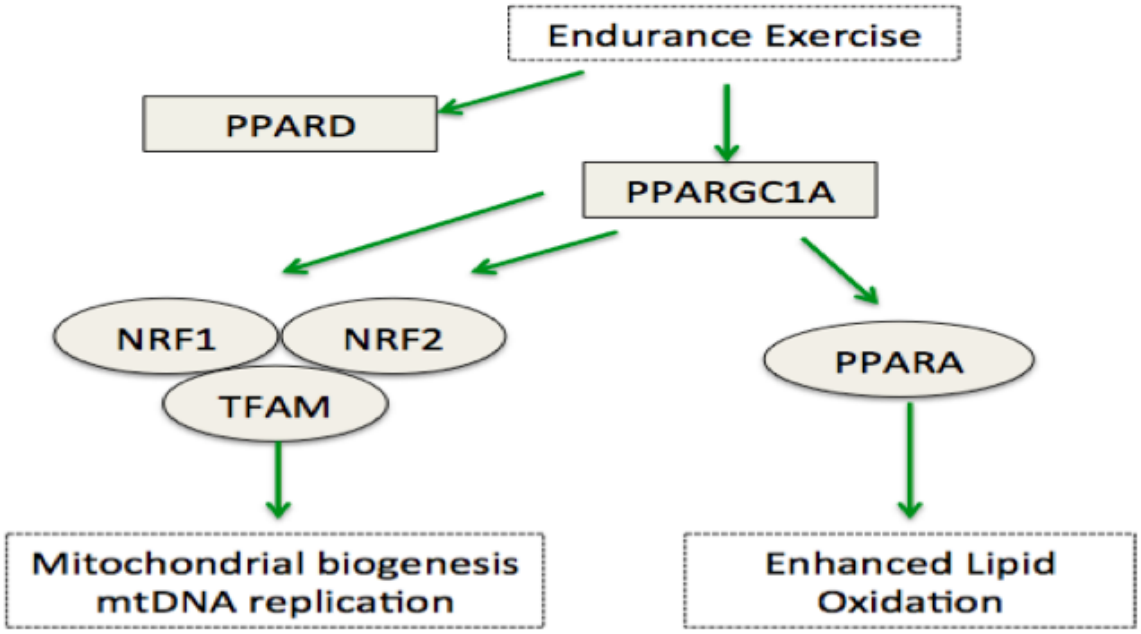

Figure 5.1: Mechanisms of genes that regulate the OXPHOS pathway that associate to endurance status. PPARD, PPARGC1A, NRF, PPARA, and TFAM as well as mtDNA are all known to help regulate the OXPHOS pathway. The introduction of endurance exercise on the body up-regulates each of the genes seen above in the ovals. This activated pathway causes increased lipid oxidation as well as mitochondrial biogenesis and mtDNA replication.

Previous studies have analyzed polymorphisms in each other the genes in **Figure 5.1** and found potential correlations to elite endurance status. Two NRF1 polymorphisms (rs2402970 and rs6949152) were shown to be associated with training responsiveness and endurance capacity.[143] Similarly polymorphisms in NRF2, rs7181866, rs12594956, and rs8031031 were found at higher frequencies in elite endurance athletes when compared to a control population.[130,132] Parallel findings from other external stimuli are also speculated to also play a role in endurance and mitochondrial regulation. For example, a study suggested that ROS and PPARGC1A

may be key modulators in exercise-induced remodeling of the mitochondrial population.[144]

Correlations between mtDNA specific genes have also been explored. Because of a lack of histone protection in mtDNA, mutations occur at a higher rate. These mutilation characteristics are formed into population specific lineages called haplogroups. Studies have found correlations between haplogroups and that may influence endurance.[136-142]

PAH is a disease characterized by elevated pulmonary pressures that eventually result in right heart failure and patient death. Two clinical metrics used to assess disease progression in PAH are right heart catheterization and six-minute walk. Right heart catheterization is used to survey the health of the right heart by qualifying its shape and function; whereas the six-minute walk can be used to see how far a patient can walk in six minutes in order to assess exercise capacity. We believe that these collective measurements can be used to evaluate a PAH patient's exercise capacity and potential longevity. It is traditionally observed that worsening right ventricular health and decreasing six-minute walk distances are indications of worsening health and potential death.

We hypothesized that genetic variations in the nuclear DNA involved in regulating the OXPHOS pathway as well as mtDNA haplogroups are associated with preserved right ventricular function, preserved six-minute walk capacity as well as increased survival outcomes. We surveyed Vanderbilt's large-scale de-identified medical record system, the SD, and accessed Vanderbilt's DNA repository, BioVU, to explore this potential association. Elucidating the role that polymorphisms and mtDNA

play in the OXPHOS pathway in PAH patients may underscore the importance of this pathway in PAH and may be used to validate findings of our artificial arteriole.

Methods

1. Cohort Validation and Data Extraction

The Synthetic Derivative database at Vanderbilt was queried for all patients who underwent right heart catheterization between 1998-2014. All selected patients met hemodynamic criteria for PAH. Electronic medical records (EMR) were manually reviewed to confirm a clinical diagnosis of PAH. This analysis included all subjects meeting a clinical diagnosis of PAH with existing genotyping on the Multiethnic Genotyping Array platform in Vanderbilt's EMR-linked bio-repository, BioVU. The cohort was stratified by race, and Caucasian subjects were used going forward. The demographic background of the Caucasian cohort is summarized in **Table 5.1**.

	n(%)
Age	
0-25	2 (2%)
25-50	44 (40%)
50 or greater	63 (58%)
Gender	
Female	82 (75%)
Race	
White	109 (100%)
Etiology	
Heritable	8 (7%)
Idiopathic	56 (52%)
Congenital	5 (5%)
HIV	1 (1%)
Connective Tissue Disease	21 (19%)
Portopulonary	14 (13%)
Drug Induced	3 (3%)

Table 5.1 Demographic information of Caucasian PAH population at Vanderbilt University.

Within the medical record, the longitudinal RV function was extracted and findings were graded on a semi-quantitative basis before stratifying for improvement or no improvement. The six-minute walk distance (6MWD) closest to the first RV assessment and at the most recent RV assessment was also extracted from the EMR. An improvement in 6MWD was defined as an increase in of 30 meters or greater.

2. Cohort Genotyping Analysis

The patients with existing genotyping of seven genes in the OXPHOS pathway were analyzed to see if single nucleotide polymorphisms (SNPs) in these genes were associated with improved exercise capacity or preserved RV function via a Fisher's Exact Test. The summary of genetic variants tested can be seen in **Table 5.2**. Kaplan-Meier survival curves were generated and analyzed using a log-rank test of the seven genes in the OXPHOS pathway as well as with mitochondrial haplogroups.

Genetic Variant	RV Function P-value	6MWD P-value
TFAM		
rs1049432	0.69	0.25
PPARD		
rs2016520	0.52	0.18
PPARGC1A		
rs8192678	0.14	0.14
PPARA		
rs4253778	0.05	0.81
NRF1		
rs6949152	0.3	0.27
NRF2		
rs7181866	0.17	0.33

Table 5.2 Fisher's Exact Test correlation RV function, 6MWD, and selected SNPs in the OXPHOS pathway.

Results

Of the medical records examined, 109 Caucasian PAH patients (75% female, age 50±13 years) were extracted and confirmed with existing genotyping data. **Table 5.1** illustrates the demographics of the cohort. The median time interval between echoes was 2279 days (IQR 609-2495).

The variant in PPARA (rs4253778) was nearly associated with improved longitudinal RV function over the course of a patient's medical record (p=0.05). Because of the cohort size, we were under-power to detect differences in clinical and survival endpoints. The Kaplan-Meier Survival Analysis for (rs4253778) revealed a non-significant association in increased patient survival (p=0.17) (**Fig2.A**). No other SNPs in of the nuclear genes in the OXPHOS pathway demonstrated significant correlations to right heart health as well as 6MWD. There were also no other statistically significant correlations to improved survival outcomes. A Kaplan-Meier Survival Analysis Curve for Haplogroup H may be associated with worsened survival ($p<0.05$) (**Fig 2.B**). No other haplogroups were associated with survival outcomes.

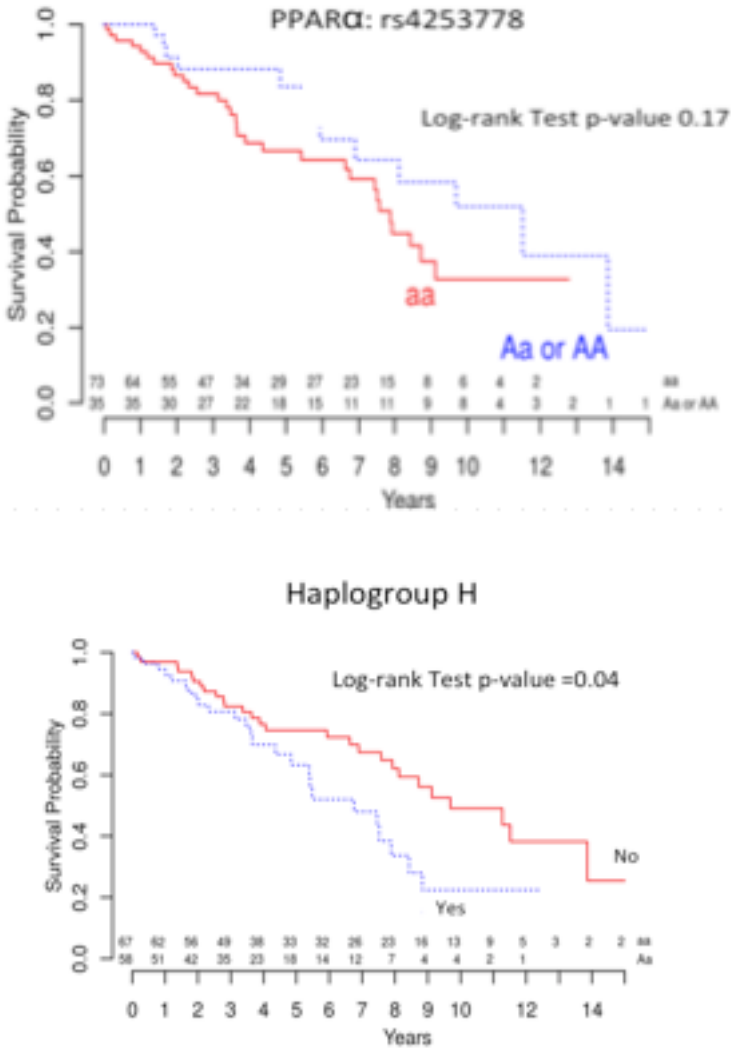

Figure 5.2 Kaplan-Meier Survival Plots of Findings for genes in the OXPHOS pathway as well as mtDNA. A) Survival plot for PPARA showed no significant association between rs4253778 and survival outcomes and PAH patients despite a near significant association found with rs4253778 and preserved right heart health. B) Haplogroup H was found to be associated with worsened survival outcomes in the PAH cohort.

After running a Fisher's Exact Test, there was a possible association found between haplogroup J and improved RV function (OR=4.78, p=0.056). 57% of subjects with haplogroup J demonstrated improved longitudinal RV function compared to 21% in

other haplogroups. While haplogroup H was found to be associated with worsened survival outcomes, there was no association found between haplogroup H and RV function or 6MWD.

No genetic associations were found among the genetic variants tested and 6MWD. Similarly, no associations were found among mitochondrial haplogroups and 6MWD.

Discussion

The genes studied for an association in longevity, RV function, and 6MWD were associated with increased exercise capacity in healthy adults.[145] This association leads to increased biological plausibility for using clinical endurance metrics to find associations between diagnostic values and disease outcomes. Genetic association in OXPHOS genes may be associated with improved RV function and survival in patients with PAH. A Fisher's Exact Test revealed that a certain SNP in PPARA may be associated with RV function in a cohort of PAH patients at Vanderbilt University. PPARA is a transcription factor that is associated with enhanced lipid oxidation.[145] Activated PPARA promotes the up-regulation of genes that are responsible for management of fatty acids as well as peroxisomal and fall acid oxidation in the mitochondria.[146] It is plausible that PPARA's interplay within the lipid oxidation and the OXPHOS pathway may be associated with improved RV health in PAH patients. When PPARA was examined with respect to longevity in patients, no significant findings were found (**Figure 5.2a)**.

Interestingly, one of the findings from the RNA Seq of the pulmonary vascular platform identified a gene that directly interacts with PPARA. Cbp/P300 Interacting Transactivator With Glu/Asp Rich Carboxy-Terminal Domain 2 (CITED2) stimulates the proliferation of PPARA transcriptional activation. As seen in **Figure 5.3**, the induction of flow stimulates greater gene expression of CITED2 in the mutant cell lines versus the WT cells. It is possible that this elevated expression of CITED2 leads to many of the pathological metabolic activity seen in PAH. It is unknown whether the SNP found to be associated with RV function is a loss of function or gain of function mutation. More

studies need to be done in order to identify that causation of the associate SNP. However, this genetic connection between the in vitro pulmonary platform and clinical associations strengthen the potential utility of more advanced cell culture techniques. The ability to bolster findings in clinical research through basic sciences has been a precedent for drug development and disease characterization for years. Bridging human clinical data and our in vitro model data is critically important to validate the potential accuracy of the device. Without the introduction of flow, CITED2, and other deregulated genetic variants would not have been found, thus indicating the platform's utility. Although, repetition and further experiment design are needed, the platform provided evidence to pursue a new avenues of PAH research through replicating a finding concerning PPARA.

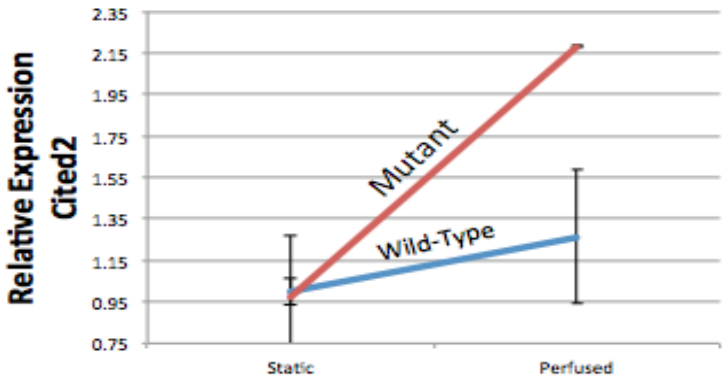

Figure 5.3 CITED2 gene expression of mutant and WT endothelial cells exposed to flow. The introduction of perfusion increases the gene expression of CITED2 by about two times the expression levels of WT cells.

Haplogroup J is potentially associated with improved RV function in our PAH cohort (p=0.056), but had no corresponding association with 6MWD or longevity. Haplogroup J has been found to occur at higher frequencies in sprinters, according to one study.[137] Haplogroup H, however, was found to be associated with worsened survival outcomes (p=0.04), as seen in **Figure 5.2b**. To our knowledge, haplogroup H has not been associated with either non-elite or elite endurance statuses.

Validation in larger, external cohorts are required for this study. Unfortunately, it is difficult to acquire large cohorts of patients with rare diseases like PAH. The small sample sizes and reduced power require replication in other patient populations. In order to do this, validation will need to occur in patient cohorts at other medical centers. However, it is important to recognize how next generation in vitro models may be able to help address this problem. While these kinds of systems will never obviate the need to validate and replicate in other clinical cohorts, they can help inform experimental decisions.

CHAPTER 6: IMPACT AND FUTURE DIRECTIONS

Summary of Impact and Limitations

In chapter 3, we illustrated that the inhibition of SRC phosphorylation did not reduce the increased pressures and increased large vessel muscularization seen in our BMPR2 mutant mouse model. In chapter 4, we engineered a model of the pulmonary vasculature to advance our current gold standard in vitro cellular models. This model was used to discover gene expression differences in $Bmpr2^{R899X}$ and WT MPMVECs when the cells were either exposed to flow or left in static conditions within the engineered platform. This model also elucidated the lack of elongation and morphological changes of $Bmpr2^{R899X}$ cells when exposed to flow for three hours. The platform also recapitulated the increased endothelial leak that is known to occur in BMPR2 animal models. In chapter 5, we hypothesized that genes that associated elite endurance status may be linked to increased longevity, RV function, or 6MWD. We discovered potential associations between a SNP in the OXPHOS pathway (within the gene PPARA) and increased RV function, and a possible association between Haplogroup J and increased RV function, and an association between Haplogroup H and decreased longevity in patients with PAH. No associations were found in any OXPHOS genes or haplogroups and 6MWD. A gene found in the RNA Seq performed in chapter 4 was found to be directly related to the gene, PPARA, the gene found to possibly be associated with increased RV function in chapter 5.

RVSP data from RHC in mice from chapter 3 showed that saracatinib and dasatinib did not reduce the RVSPs in mutant mice with BMPR2-associated PAH. Similarly, saracatinib and dasatinib intervention did not normalize the number of large

muscularized vessels in the sectioned mouse lung. SRC is known to have greater activity in PAH due to increased phosphorylation from a mutated c-terminus in the BMPR2 protein.[8-10,74] SRC's increased phosphorylation is known to lead to a number of downstream consequences in PAH, with deregulated cytoskeleton properties being the most highlighted.[10] The inability to prevent heritable PAH via the inhibition of SRC phosphorylation hints at the need to further explore SRC's irregular trafficking and sequestration. This aberrant activity in PAH is speculated to be related to disease progression, since previous studies that have corrected SRC's phosphorylation, trafficking, and sequestration, have prevented heritable PAH in mouse models.[13] A limitation in our study design was our lack of probing how saracatinib and dasatinib affect SRC's sequestration and trafficking. Future studies should place greater attention to these phenomena.

It is well known that many clinical trials fail to get medications, treatments, and devices from the laboratory to the patient. It is possible that the lack of efficiency can be attributed to the way that we study disease in the lab. In chapter 1, we discuss how standard 2D cell culture modeling is sometimes an inappropriate way to study disease and tissues. Pulmonary vessels are no exception, as the tissues in this system are exposed to various mechanical stimuli that are not seen in a cell culture flask or dish. We know that cells from tissues have differential responses when exposed to stimuli like shear, pressure, and flow when compared to cells cultured in dishes. Including these mechanical parameters in in vitro experiments, like the platform engineered in chapter 4, may lead to more human-like disease models. Including more realistic disease environment may lead to more efficient pipelines for therapeutic development. However,

a general limitation of the field will be the inability to model the whole tissue with all relevant cells types.

Our pulmonary vascular platform was able to elucidate many of the genes that have deregulated expression levels when the MPMVECs were exposed to flow. These findings both replicated similar trends seen in other mouse studies, and also uncovered a host of pathways relevant to PAH etiology that change in the mutant cells compared to the WT cells.[10] A number of BMPR2 mutant cells consistently over expressed genes when compared to the WT endothelial cells under flow. This overexpression was especially notable in the majority of genes found within the congruent gene expression category. Within the incongruent category, we saw that many cytoskeletal and mechanical sensing genes fell within this category. We know that deregulated cytoskeletal architectures occurs in PAH, but this was the first time we observed that flow led to a number of exacerbated responses.[10] This indicates that the inclusion of parameters like shear and pressure can yield more information not seen in standard cell culture 3D models. Even in the platform's first experimental iteration, several discoveries were made. Further tweaking these parameters may lead to more realistic disease severities or conditions.

The model also inadvertently led to the novel observation that the $Bmpr2^{R899X}$ cells did not align in the direction of flow. Endothelial cells are expected to elongate in the direction of flow, but the lack of alignment seen in the mutant cells should be studied further.[107-109] It is possible that a clue to this abnormal morphology may be found in the incongruent gene expression result seen in the RNA Seq. The deregulated genes found

in this category could results in a host of phenotypes that cause the cells to not respond to the stimulus of flow.

The final experiment in chapter 4 studied the permeability seen in the artificial endothelium. Validating engineered models of disease is a crucial way to confirm device utility and appropriate recapitulation. $Bmpr2^{R899X}$ endothelial cells are known for their leaky phenotype in vivo.[10] This phenotype was replicated in the model with the $Bmpr2^{R899X}$ demonstrating permeability about a magnitude more permeable than the WT cells. The ability to incorporate realistic permeability in an artificial model presents several opportunities to monitor, understand, and treat the endothelial dysfunction seen in several pulmonary vascular diseases. The matrix stiffness and composition may be a limitation of this experiment. Future work should strive to create a more biomimetic ECM found within the lung vasculature if more realistic permeabilities are to be found.

Chapter 5 served to use clinical human data from a PAH patient cohort at Vanderbilt University Medical Center to uncover associations that may elucidate the importance of the OXPHOS pathway in PAH. The possible associations found between nuclear genes in the OXPHOS pathway and mitochondrial haplogroups illustrate the possibility that this pathway may be relevant to disease outcomes in PAH. The ability to continue to grow the cohort presents an opportunity for this to be an ongoing study. A SNP in PPARA was found to be associated with improved RV function. Interestingly, a finding from the RNA Seq in chapter 4 revealed an incongruent gene, CITED2, which is directly related to the regulation of PPARA in both mice and humans. This possible connection between clinical data and the data extracted from the platform may serve two purposes: 1) It can underscore the importance of the SNP in PPARA and PAH and

2) it may show how the translation from simple cell culture to more complex models can lead to findindings that can aid clinical research.

Future Directions

Further studies examining the underlying pathology and mechanism of SRC would be helpful to understand its true role in pathology and PAH. It is clear that SRC's activity is up-regulated, but merely reducing this activity does not prevent the development of PAH. It is advised to explore options to inhibit the abnormal SRC trafficking and sequestration known to occur.

It is also possible that these studies can be performed within the pulmonary vascular platform. We have shown that two BMPR2 mutant cells lines (R899X and DelX4) can be cultured within the artificial channel, with each cell line reaching confluency within the device. Perhaps the addition of a mechanical environment would help the field better understand BMPR2's protein regulation within PAH. As seen in Chapter 2, three key molecules, SRC, DYNLT1, and LIMK1 have a direct relationship to the cell surface or cytoskeletal architecture. Since the device allows for easy imaging, trafficking and localization studies can be carried out within the platform to better understand these interactions.

The OXPHOS pathway and mitochondrial pathways may play a legitimate role in the development and progression of PAH. Going forward, the study should include all races (not just Caucasian patients). Including more races not only increases the already small cohort size, but can also elucidate if race plays a role in these findings. Ultimately, this study lacks power. In the future, more collaboration between other universities or institutions should be built in order to increase the number of patients within the study. Including other group's cohorts also introduces opportunity to validate findings through repetition. The connection between CITED2 in the RNA Seq study and PPARA's

association to increased RV function will need to be fully investigated. Using the platform from chapter 4, a BMPR2 mutant cell line could be grown in the artificial channels and then CITED2 or PPARA activity be reduced through siRNA. This study could track the number and migration of mitochondria throughout the cells as well as investigate other metabolic processes. While it is currently not possible to recreate RV health in the current platform, other experiments can be designed to secondarily assess the outcomes associated with probing the CITED2 and PPARA pathway.

Other clinically relevant uses could be exploited in the platform. For example, the platform and artificial channels could possibly be used in a personalized medicine approach. By culturing a relevant cell type from the patient, a treatment assay could be done to see how patients may respond to therapy in vitro before dosing them in vivo.

The platform could also be used for a number of experiments not relevant to the work we have completed. For example, the device could be used to investigate the effects of a number of different mechanical stimuli on the expression or function of the pulmonary vascular endothelium. Our studies only examined a certain set pressure range and shear stress, but modeling other disease stages could be possible. Increasing the shear stress and pressure could be a way to model advanced PAH, and could elucidate other genetic of phenotypic clues with regard to disease state.

The crosslinking of the gelatin was also kept consistent across all studies within the platform. Varying the stiffness of the hydrogel may serve as a valuable tool to assess disease-state changes associated with the mechanical properties of the ECM. Introducing other growth factors, cells, or signaling factors could also serve as a valuable experiment.

The perfusion environment within the platform could also be altered to study how circulating cells (e.g. macrophages) could play a role in modeling PAH. Introducing other pharmaceutical agents or disease state modeling chemicals (e.g. sugen) may provide a unique opportunity to model PAH and over pulmonary vascular diseases in vitro. To date, these techniques have not been studied within the platform, and will need to be fully investigated and engineered prior to experimentation.

Finally, it may be possible to translate our to model the blood vessels in other organ systems. Next generation models of human disease mark a strong movement into more realistic screening and understanding of complex conditions. The motivation to create our platform can likely also be used to engineer models of other vascular diseases. For example, the permeability studies could provide powerful insight into the blood brain barrier and the movement of medications and other factors into the surrounding brain tissue.

Ultimately, our platform serves as a foundation for the development of a number of experiments that could be used in several different fields in medicine. Future development, verification, and replication is needed to ensure suitable modeling of other disease states and organ systems.

REFERENCES

1. Bloodworth, N. C., et al. (2015). "Microvessel mechanobiology in pulmonary arterial hypertension: cause and effect." Hypertension 65(3): 483-489.

2. Simonneau G, G. M., Adatia I, et al (2013). "Updated Clinical Classification of Pulmonary Hypertension." J Am Coll Cardiol.

3. Newman JH, W. L., Lane KB, et al. (2001). "Mutation in the gene for bone morphogenetic protein receptor II as a cause of primary pulmonary hypertension in a large kindred." New England Jounral of Medicine.

4. Lammers, S., et al. (2012). "Mechanics and Function of the Pulmonary Vasculature: Implications for Pulmonary Vascular Disease and Right Ventricular Function." Compr Physiol 2(1): 295-319.

5. Mahapatra, S., et al. (2006). "Relationship of pulmonary arterial capacitance and mortality in idiopathic pulmonary arterial hypertension." J Am Coll Cardiol 47(4): 799-803.

6. Brittain, E. L., et al. (2013). "Shorter survival in familial versus idiopathic pulmonary arterial hypertension is associated with hemodynamic markers of impaired right ventricular function." Pulm Circ 3(3): 589-598.

7. Mahapatra, S., et al. (2006). "The prognostic value of pulmonary vascular capacitance determined by Doppler echocardiography in patients with pulmonary arterial hypertension." J Am Soc Echocardiogr 19(8): 1045-1050.

8. Austin ED, Loyd JE, Phillips JA 3rd (2009) Genetics of pulmonary arterial hypertension. Semin Respir Crit Care Med 30: 386–398.

9. Long L, MacLean MR, Jeffery TK, Morecroft I, Yang X, et al. (2006) Serotonin increases susceptibility to pulmonary hypertension in BMPR2-deficient mice. Circ Res 98: 818–827.

10. Johnson et al. Cytoskeletal defects in Bmpr2-associated pulmonary arterial hypertension. Am J Physiol Lung Cell Mol Physiol. 2011.

11. Paulin R et al. Dehydroepiandrosterone inhibits the Src/STAT3 constitutive activation in pulmonary arterial hypertension. Am J Physiol Heart Circ Physiol. 2011;301(5):H1798-809.

12. Wong WK et al. Bone morphogenetic protein receptor type II C-terminus interacts with c-Src: implication for a role in pulmonary arterial hypertension. Am J Respir Cell Mol Biol. 2005;33(5):438-46.

13. West J, et al. "Serotonin 2B receptor antagonism prevents heritable pulmonary arterial hypertension." *PloS one*11.2 (2016): e0148657.

14. Saouti, Nabil, et al. "Right ventricular oscillatory power is a constant fraction of total power irrespective of pulmonary artery pressure." American journal of respiratory and critical care medicine 182.10 (2010): 1315-1320.

15. Mitchell, Gary F. "Arterial stiffness and hypertension." Hypertension 64.1 (2014): 13-18.

16. Stenmark, Kurt R., et al. "Animal models of pulmonary arterial hypertension: the hope for etiological discovery and pharmacological cure." American Journal of Physiology-Lung Cellular and Molecular Physiology 297.6 (2009): L1013-L1032.

17. Foletta VC, Lim MA, Soosairajah J, et al. Direct signaling by the BMP type II receptor via the cytoskeletal regulator LIMK1. *J Cell Biol.* 2003; 162(6):1089-1098.

18. West, James, James E. Loyd, and Rizwan Hamid. "Potential Interventions Against BMPR2-Related Pulmonary Hypertension." *Advances in Pulmonary Hypertension* 11.1 (2012).

19. Machado RD, Rudarakanchana N, Atkinson C, et al. Functional interaction between BMPR-II and Tctex-1, a light chain of Dynein, is isoform-specific and disrupted by mutations underlying primary pulmonary hypertension. *Hum Mol Genet.* 2003;12(24): 3277-3286.

20. Fang YD, Xu X, Dang YM, et al. MAP4 mech- anism that stabilizes mitochondrial permeability transition in hypoxia: microtubule enhancement and DYNLT1 interaction with VDAC1. *PLoS One.* 2011;6(12):e28052.

21. Meiri D, Greeve MA, Brunet A, et al. Modu- lation of Rho guanine exchange factor Lfc activity by protein kinase A-mediated phosphorylation. *Mol Cell Biol.* 2009;29(21):5963-5973.

22. Lane KL, Talati M, Austin E, et al. Oxidative injury is a common consequence of BMPR2 muta- tions.*Pulm Circ.* 2011;1(1):72-83.

23. Li, Xiaohai, et al. "Characterization of dasatinib and its structural analogs as CYP3A4 mechanism-based inactivators and the proposed bioactivation pathways." *Drug Metabolism and Disposition*37.6 (2009): 1242-1250.

24. Hennequin L et al. "N-(5-Chloro-1, 3-benzodioxol-4-yl)-7-[2-(4-methylpiperazin-1-yl) ethoxy]-5-(tetrahydro-2 H-pyran-4-yloxy) quinazolin-4-amine, a novel, highly selective, orally available, dual-specific c-Src/Abl kinase inhibitor." *Journal of medicinal chemistry*49.22 (2006): 6465-6488.

25. Chung, Seok, et al. "Cell migration into scaffolds under co-culture conditions in a microfluidic platform." Lab on a Chip 9.2 (2009): 269-275.

26. Song, Jonathan W., and Lance L. Munn. "Fluid forces control endothelial sprouting." Proceedings of the National Academy of Sciences 108.37 (2011): 15342-15347.

27. Douville, Nicholas J., et al. "Fabrication of two-layered channel system with embedded electrodes to measure resistance across epithelial and endothelial barriers." Analytical chemistry 82.6 (2010): 2505-2511.

28. Shao, Jianbo, et al. "A microfluidic chip for permeability assays of endothelial monolayer." Biomedical microdevices 12.1 (2010): 81-88.

29. Wyckoff, Jeffrey B., et al. "Direct visualization of macrophage-assisted tumor cell intravasation in mammary tumors." Cancer research 67.6 (2007): 2649-2656.

30. Reinitz, Adam, et al. "Human brain microvascular endothelial cells resist elongation due to shear stress." Microvascular research 99 (2015): 8-18.

31. Shevkoplyas, Sergey S., et al. "Direct measurement of the impact of impaired erythrocyte deformability on microvascular network perfusion in a microfluidic device." Lab on a Chip 6.7 (2006): 914-920.

32. Parmar, Kush M., et al. "Integration of flow-dependent endothelial phenotypes by Kruppel-like factor 2." Journal of Clinical Investigation 116.1 (2006): 49.

33. Förstermann, Ulrich, and Thomas Münzel. "Endothelial nitric oxide synthase in vascular disease." Circulation 113.13 (2006): 1708-1714.

34. Busse, Rudi, et al. "EDHF: bringing the concepts together." Trends in pharmacological sciences 23.8 (2002): 374-380.

35. Hirase, Tetsuaki, and Koichi Node. "Endothelial dysfunction as a cellular mechanism for vascular failure." American Journal of Physiology-Heart and Circulatory Physiology 302.3 (2012): H499-H505.

36. Tsukita, Shoichiro, Mikio Furuse, and Masahiko Itoh. "Multifunctional strands in tight junctions." Nature reviews Molecular cell biology 2.4 (2001): 285-293.

37. Furuse, Mikio, and Shoichiro Tsukita. "Claudins in occluding junctions of humans and flies." Trends in cell biology 16.4 (2006): 181-188.

38. Dejana, Elisabetta, Elisabeth Tournier-Lasserve, and Brant M. Weinstein. "The control of vascular integrity by endothelial cell junctions: molecular basis and pathological implications." Developmental cell 16.2 (2009): 209-221.

39. Vittet, Daniel, et al. "Targeted null-mutation in the vascular endothelial–cadherin gene impairs the organization of vascular-like structures in embryoid bodies." Proceedings of the National Academy of Sciences 94.12 (1997): 6273-6278.

40. Bianchi, Cesario, et al. "Biochemical and structural evidence for pig myocardium adherens junction disruption by cardiopulmonary bypass." Circulation 104.suppl 1 (2001): I-319.

41. Ozaki, Masanori, et al. "Overexpression of endothelial nitric oxide synthase accelerates atherosclerotic lesion formation in apoE-deficient mice." The Journal of clinical investigation 110.3 (2002): 331.

42. Kevil, Christopher G., et al. "Role of cadherin internalization in hydrogen peroxide-mediated endothelial permeability." Free Radical Biology and Medicine 24.6 (1998): 1015-1022.

43. Kevil, Christopher G., et al. "H 2 O 2-mediated permeability: role of MAPK and occludin." American Journal of Physiology-Cell Physiology 279.1 (2000): C21-C30.

44. Bélanger, Mireille, et al. "Hyperammonemia induces transport of taurine and creatine and suppresses claudin-12 gene expression in brain capillary endothelial cells in vitro." Neurochemistry international 50.1 (2007): 95-101.

45. Kiuchi-Saishin, Yumiko, et al. "Differential expression patterns of claudins, tight junction membrane proteins, in mouse nephron segments." Journal of the American Society of Nephrology 13.4 (2002): 875-886.

46. Morita, Kazumasa, et al. "Claudin multigene family encoding four-transmembrane domain protein components of tight junction strands." Proceedings of the National Academy of Sciences 96.2 (1999): 511-516.

47. Witt, Ken A., et al. "Effects of hypoxia-reoxygenation on rat blood-brain barrier permeability and tight junctional protein expression." American Journal of Physiology-Heart and Circulatory Physiology 285.6 (2003): H2820-H2831.

48. Nitta, Takehiro, et al. "Size-selective loosening of the blood-brain barrier in claudin-5–deficient mice." The Journal of cell biology 161.3 (2003): 653-660.

49. Asaka, Machiko, et al. "Rab5a-mediated localization of claudin-1 is regulated by proteasomes in endothelial cells." American Journal of Physiology-Cell Physiology 300.1 (2011): C87-C96.

50. Lee, Tsu-Yee Joseph, and Avrum I. Gotlieb. "Microfilaments and microtubules maintain endothelial integrity." Microscopy research and technique 60.1 (2003): 115-127.

51. Wong, M. K., and Avrum I. Gotlieb. "The reorganization of microfilaments, centrosomes, and microtubules during in vitro small wound reendothelialization." The Journal of cell biology 107.5 (1988): 1777-1783.

52. Horio, Tetsuya, and Hirokazu Hotani. "Visualization of the dynamic instability of individual microtubules by dark-field microscopy." Nature 321.6070 (1986): 605-607.

53. Mitchison, Tim, and Marc Kirschner. "Dynamic instability of microtubule growth." nature 312.5991 (1984): 237-242.

54. Kristofferson, David, Tim Mitchison, and Marc Kirschner. "Direct observation of steady-state microtubule dynamics." The Journal of cell biology 102.3 (1986): 1007-1019.

55. Cheng, Jing-Jy, et al. "Cyclic strain–induced reactive oxygen species involved in ICAM-1 gene induction in endothelial cells." Hypertension 31.1 (1998): 125-130.

56. Dartsch, P. C., and E. Betz. "Response of cultured endothelial cells to mechanical stimulation." Basic research in cardiology 84.3 (1989): 268-281.

57. Pandithage, Ruwin, et al. "The regulation of SIRT2 function by cyclin-dependent kinases affects cell motility." The Journal of cell biology 180.5 (2008): 915-929.

58. Yano, Yoshiko, John Geibel, and Bauer E. Sumpio. "Cyclic strain induces reorganization of integrin α5β1 and α2β1 in human umbilical vein endothelial cells." Journal of cellular biochemistry 64.3 (1997): 505-513.

59. Gatti, Chiara Delli, et al. "Pulsatile stretch induces release of angiotensin II and oxidative stress in human endothelial cells: effects of ACE inhibition and AT1 receptor antagonism." Clinical and experimental hypertension 30.7 (2008): 616-627.

60. Hashimoto-Komatsu, Aiko, et al. "Angiotensin II induces microtubule reorganization mediated by a deacetylase SIRT2 in endothelial cells." Hypertension Research 34.8 (2011): 949-956.

61. Buchanan, Cara F., et al. "Three-dimensional microfluidic collagen hydrogels for investigating flow-mediated tumor-endothelial signaling and vascular organization." Tissue Engineering Part C: Methods 20.1 (2013): 64-75.

62. Nguyen, Duc-Huy T., et al. "Biomimetic model to reconstitute angiogenic sprouting morphogenesis in vitro." Proceedings of the National Academy of Sciences 110.17 (2013): 6712-6717.

63. Price, Gavrielle M., et al. "Effect of mechanical factors on the function of engineered human blood microvessels in microfluidic collagen gels." Biomaterials 31.24 (2010): 6182-6189.

64. Lee, Vivian K., et al. "Generation of multi-scale vascular network system within 3D hydrogel using 3D bio-printing technology." Cellular and molecular bioengineering 7.3 (2014): 460.

65. Nishiyama, Yuichi, et al. "Development of a three-dimensional bioprinter: construction of cell supporting structures using hydrogel and state-of-the-art inkjet technology." Journal of Biomechanical Engineering 131.3 (2009): 035001.

66. Topper, James N., and Michael A. Gimbrone Jr. "Blood flow and vascular gene expression: fluid shear stress as a modulator of endothelial phenotype." Molecular medicine today 5.1 (1999): 40-46.

67. Davies, Peter F. "Flow-mediated endothelial mechanotransduction." *Physiological reviews* 75.3 (1995): 519-560.

68. Blackman, Brett R., Guillermo Garcıa-Cardena, and Michael A. Gimbrone. "A new in vitro model to evaluate differential responses of endothelial cells to simulated arterial shear stress waveforms." Journal of biomechanical engineering 124.4 (2002): 397-407.

69. Simmers, Michael B., Andrew W. Pryor, and Brett R. Blackman. "Arterial shear stress regulates endothelial cell-directed migration, polarity, and morphology in confluent monolayers." American Journal of Physiology-Heart and Circulatory Physiology 293.3 (2007): H1937-H1946.

70. Pawlik, Gunter, Angelika Rackl, and Richard J. Bing. "Quantitative capillary topography and blood flow in the cerebral cortex of cats: an in vivo microscopic study." Brain research 208.1 (1981): 35-58.

71. “BioVU Characteristics.” *VICTR - BioVU & Synthetic Derivative*, victr.vanderbilt.edu/pub/biovu/?sid=217.

72. Rabinovitch M et al. Molecular pathogenesis of pulmonary arterial hypertension. J Clin Invest. 2012;122:4306–4313.

73. Adnot S et al. Serotonin transporter and serotonin receptors. Handb Exp Pharmacol 218: 365–380.

74. West J et al. Pulmonary hypertension in transgenic mice expressing a dominant-negative BMPRII gene in smooth muscle. Circ Res. 2004;94(8):1109-14.

75. Hunter KS et al. Pulmonary vascular input impedance is a combined measure of pulmonary vascular resistance and stiffness and predicts clinical outcomes better than pulmonary vascular resistance alone in pediatric patients with pulmonary hypertension. Am Heart J. 2008;155:166–174.

76. Parsons S et al. Src family kinases, key sikmregulators of signal transduction. Oncogene. 2004;23:7906–7909

77. Bromann PA et al. The interplay between Src family kinases and receptor tyrosine kinases. Oncogene. 2004;23:7957–7968.

78. Rosenkranz S et al. Src family kinases negatively regulate platelet-derived growth factor alpha receptor-dependent signaling and disease progression. J Biol Chem. 2000;275:9620–9627.

79. Chen WC et al. Right ventricular systolic pressure measurements in combination with harvest of lung and immune tissue samples in mice. J Vis Exp. 2013(71):e50023.

80. Austin ED et al. "Alterations in oestrogen metabolism: implications for higher penetrance of familial pulmonary arterial hypertension in females." *European Respiratory Journal* 34.5 (2009): 1093-1099.

81. Rasheed, Walid, Brendan Flaim, and John F. Seymour. "Reversible severe pulmonary hypertension secondary to dasatinib in a patient with chronic myeloid leukemia." *Leukemia research* 33.6 (2009): 861-864.

82. Cool CD, Stewart JS, Werahera P, et al. Three-dimensional reconstruction of pulmonary arteries in plexiform pulmonary hypertension using cell-specific markers. Evidence for a dynamic and heterogeneous process of pulmonary endothelial cell growth. Am J Pathol 1999;155:411-9.

83. Austin ED, West J, Loyd JE, Hemnes AR. Molecular Medicine of Pulmonary Arterial Hypertension: From Population Genetics to Precision Medicine and Gene Editing. American journal of respiratory and critical care medicine 2016.

84. de Jesus Perez VA. Molecular pathogenesis and current pathology of pulmonary hypertension. Heart failure reviews 2016;21:239-57.

85. Humbert M, Sitbon O, Chaouat A, et al. Survival in patients with idiopathic, familial, and anorexigen-associated pulmonary arterial hypertension in the modern management era. Circulation 2010;122:156-63.

86. Rubin LJ. Pulmonary arterial hypertension. Proceedings of the American Thoracic Society 2006;3:111-5.

87. Runo JR, Loyd JE. Primary pulmonary hypertension. Lancet 2003;361:1533-4

88. Geraci, Mark W., et al. "Gene expression patterns in the lungs of patients with primary pulmonary hypertension." Circulation research 88.6 (2001): 555-562.

89. Rajkumar, Revathi, et al. "Genomewide RNA expression profiling in lung identifies distinct signatures in idiopathic pulmonary arterial hypertension and secondary pulmonary hypertension." American Journal of Physiology-Heart and Circulatory Physiology 298.4 (2010): H1235-H1248.

90. Bayless, Kayla J., and George E. Davis. "The Cdc42 and Rac1 GTPases are required for capillary lumen formation in three-dimensional extracellular matrices." Journal of cell science 115.6 (2002): 1123-1136.

91. Connolly, John O., et al. "Rac regulates endothelial morphogenesis and capillary assembly." Molecular biology of the cell 13.7 (2002): 2474-2485.

92. Koh, Wonshill, Rachel D. Mahan, and George E. Davis. "Cdc42-and Rac1-mediated endothelial lumen formation requires Pak2, Pak4 and Par3, and PKC-dependent signaling." Journal of cell science 121.7 (2008): 989-1001.

93. Lovren, Fina, et al. "Angiotensin converting enzyme-2 confers endothelial protection and attenuates atherosclerosis." *American Journal of Physiology-Heart and Circulatory Physiology*295.4 (2008): H1377-H1384.

94. Resnick, Nitzan, and M. A. Gimbrone. "Hemodynamic forces are complex regulators of endothelial gene expression." The FASEB Journal 9.10 (1995): 874-882.

95. Chen, Benjamin PC, et al. "DNA microarray analysis of gene expression in endothelial cells in response to 24-h shear stress." Physiological genomics 7.1 (2001): 55-63.

96. Blank RH, Muller WH, Jr., Dammann JF, Jr. Changes in pulmonary vascular lesions after restoring normal pulmonary artery pressure. Surg Forum 1958;9:356-

97. Dammann JF, Jr., Mc EJ, Thompson WM, Jr., Smith R, Muller WH, Jr. The regression of pulmonary vascular disease after the creation of pulmonary stenosis. J Thorac Cardiovasc Surg 1961;42:722-34.

98. Ferguson DJ, Berkas EM, Varco RL. Process of healing in experimental pulmonary arteriosclerosis. Proc Soc Exp Biol Med 1955;89:492-4.

99. Heath D, Helmholz HF, Jr., Burchell HB, Dushane JW, Kirklin JW, Edwards JE. Relation between structural change in the small pulmonary arteries and the immediate reversibility of pulmonary hypertension following closure of ventricular and atrial septal defects. Circulation 1958;18:1167-74.

100. Geer JC, Glass BA, Albert HM. The Morphogenesis and Reversibility of Experimental Hyperkinetic Pulmonary Vascular Lesions in the Dog. Exp Mol Pathol 1965;26:399-415.

101. Bertero T, Oldham WM, Cottrill KA, et al. Vascular stiffness mechanoactivates YAP/TAZ-dependent glutaminolysis to drive pulmonary hypertension. J Clin Invest 2016;126:3313-35.

102. Scott D, Tan Y, Shandas R, Stenmark KR, Tan W. High pulsatility flow stimulates smooth muscle cell hypertrophy and contractile protein expression. Am J Physiol Lung Cell Mol Physiol 2013;304:L70-81.

103. Wedgwood S, Lakshminrusimha S, Schumacker PT, Steinhorn RH. Cyclic stretch stimulates mitochondrial reactive oxygen species and Nox4 signaling in pulmonary artery smooth muscle cells. Am J Physiol Lung Cell Mol Physiol 2015;309:L196-203.

104. Ingber, Donald E. "Mechanical signaling and the cellular response to extracellular matrix in angiogenesis and cardiovascular physiology." *Circulation research* 91.10 (2002): 877-887.

105. Intengan, Hope D., and Ernesto L. Schiffrin. "Structure and mechanical properties of resistance arteries in hypertension: role of adhesion molecules and extracellular matrix determinants." *Hypertension* 36.3 (2000): 312-318.

106. Lee, Kyung-Mi, et al. "Extracellular matrix and pulmonary hypertension: control of vascular smooth muscle cell contractility." *American Journal of Physiology-Heart and Circulatory Physiology* 274.1 (1998): H76-H82.

107. Levesque, M. J., and R. M. Nerem. "The elongation and orientation of cultured endothelial cells in response to shear stress." *Journal of biomechanical engineering* 107.4 (1985): 341-347.

108. Dewey, C. F., et al. "The dynamic response of vascular endothelial cells to fluid shear stress." *Journal of biomechanical engineering* 103.3 (1981): 177-185.

109. Tzima, Eleni, et al. "Activation of integrins in endothelial cells by fluid shear stress mediates Rho-dependent cytoskeletal alignment." *The EMBO journal* 20.17 (2001): 4639-4647.

110. Budhiraja, Rohit, Rubin M. Tuder, and Paul M. Hassoun. "Endothelial dysfunction in pulmonary hypertension." *Circulation* 109.2 (2004): 159-165.

111. Humbert, Marc, et al. "Cellular and molecular pathobiology of pulmonary arterial hypertension." *Journal of the American College of Cardiology* 43.12 Supplement (2004): S13-S24.

112. Morrell, Nicholas W., et al. "Cellular and molecular basis of pulmonary arterial hypertension." *Journal of the American College of Cardiology* 54.1 Supplement (2009): S20-S31.

113. Lo, Chun-Min, et al. "Cell movement is guided by the rigidity of the substrate." *Biophysical journal*79.1 (2000): 144-152.

114. Bellan, Leon M., et al. "A 3D interconnected microchannel network formed in gelatin by sacrificial shellac microfibers." Advanced Materials 24.38 (2012): 5187-5191.

115. Jat PS, Noble MD, Ataliotis P, Tanaka Y, Yannoutsos N, et al. (1991) Direct derivation of conditionally immortal cell lines from an H-2Kb-tsA58 transgenic mouse. Proc Natl Acad Sci U S A 88: 5096–5100. pmid:1711218

116. Pozzi A, Moberg PE, Miles LA, Wagner S, Soloway P, et al. (2000) Elevated matrix metalloprotease and angiostatin levels in integrin alpha 1 knockout mice cause reduced tumor vascularization. Proc Natl Acad Sci U S A 97: 2202–2207. pmid:10681423

117. Wang, Jing, et al. "WEB-based gene set analysis toolkit (WebGestalt): update 2013." *Nucleic acids research*41.W1 (2013): W77-W83.

118. Zhang, Bing, Stefan Kirov, and Jay Snoddy. "WebGestalt: an integrated system for exploring gene sets in various biological contexts." *Nucleic acids research*33.suppl_2 (2005): W741-W748.

119. Gimbrone, Michael A., et al. "Endothelial dysfunction, hemodynamic forces, and atherogenesis." *Annals of the New York Academy of Sciences* 902.1 (2000): 230-240.

120. Balcells, Mercedes, et al. "Cells in fluidic environments are sensitive to flow frequency." *Journal of cellular physiology*204.1 (2005): 329-335.

121. Li, Min, et al. "High pulsatility flow induces adhesion molecule and cytokine mRNA expression in distal pulmonary artery endothelial cells." *Annals of biomedical engineering* 37.6 (2009): 1082-1092.

122. Chrobak, Kenneth M., Daniel R. Potter, and Joe Tien. "Formation of perfused, functional microvascular tubes in vitro." *Microvascular research* 71.3 (2006): 185-196.

123. Wong, Andrew D., and Peter C. Searson. "Live-cell imaging of invasion and intravasation in an artificial microvessel platform." Cancer research 74.17 (2014): 4937-4945.

124. Malek, Adel M., Seth L. Alper, and Seigo Izumo. "Hemodynamic shear stress and its role in atherosclerosis." Jama 282.21 (1999): 2035-2042.

125. Gollnick PD , Saltin B .Significance of skeletal muscle oxidative enzyme enhancement with endurance training.***Clin Physiol*** 2: 1-12, 1982.

126. Holloszy JO , Coyle EF .Adaptations of skeletal muscle to endurance exercise and their metabolic consequences.***J Appl Physiol*** 56: 831-838, 1984.

127. Ahmetov II , Mozhayskaya IA , Flavell DM , Astratenkova IV , Komkova AI , Lyubaeva EV ,Tarakin PP , Shenkman BS , Vdovina AB , Netreba AI , Popov DV , Vinogradova OL , Montgomery HE , Rogozkin VA .PPARalpha gene variation and physical performance in Russian athletes.***Eur J Appl Physiol*** 97: 103-108, 2006.

128. Akhmetov II , Astranenkova IV , Rogozkin VA .[Association of PPARD gene polymorphism with human physical performance].***Mol Biol (Mosk)*** 41: 852-857, 2007.

129. Eynon N , Meckel Y , Sagiv M , Yamin C , Amir R , Sagiv M , Goldhammer E , Duarte JA , Oliveira J .Do PPARGC1A and PPARalpha polymorphisms influence sprint or endurance phenotypes?.***Scand J Med Sci Sports*** 20: e145-e150, 2011.

130. Eynon N , Sagiv M , Meckel Y , Duarte JA , Alves AJ , Yamin C , Sagiv M , Goldhammer E , Oliveira J .NRF2 intron 3 A/G polymorphism is associated with endurance athletes' status.***J Appl Physiol*** 107: 76-79, 2009.

131. Lucia A , Gomez-Gallego F , Barroso I , Rabadan M , Bandres F , San Juan AF , Chicharro JL , Ekelund U , Brage S , Earnest CP , Wareham NJ , Franks PW .PPARGC1A genotype (Gly482Ser) predicts exceptional endurance capacity in European men.***J Appl Physiol*** 99: 344-348, 2005.

132. Eynon N , Alves AJ , Sagiv M , Yamin C , Sagiv M , Meckel Y .Interaction between SNPs in the NRF2 gene and elite endurance performance.***Physiol Genomics*** 41: 78-81, 2010.

133. Akhmetov II , Popov DV , Missina SS , Vinogradova OL , Rogozkin VA .[Association of the mitochondrial transcription factor (TFAM) gene polymorphism with physical performance of athletes].***Fiziol Cheloveka*** 36: 121-125, 2010.

134. Tsianos GI , Evangelou E , Boot A , Zillikens MC , van Meurs JB , Uitterlinden AG , Ioannidis JP .Associations of polymorphisms of eight muscle- or metabolism-related genes with performance in Mount Olympus marathon runners.***J Appl Physiol*** 108: 567-574, 2010.

135. Eynon N , Ruiz JR , Meckel Y , Moran M , Lucia A .Mitochondrial biogenesis related endurance genotype score and sports performance in athletes.***Mitochondrion*** 11: 64-69, 2011.

136. Rivera MA , Wolfarth B , Dionne FT , Chagnon M , Simoneau JA , Boulay MR , Song TM , Perusse L , Gagnon J , Leon AS , Rao DC , Skinner JS , Wilmore JH , Keul J , Bouchard C .Three mitochondrial DNA restriction polymorphisms in elite endurance athletes and sedentary controls.***Med Sci Sports Exerc*** 30: 687-690, 1998.

137. Niemi AK , Majamaa K .Mitochondrial DNA and ACTN3 genotypes in Finnish elite endurance and sprint athletes.***Eur J Hum Genet*** 13: 965-969, 2005.

138. Castro MG , Terrados N , Reguero JR , Alvarez V , Coto E .Mitochondrial haplogroup T is negatively associated with the status of elite endurance athlete.***Mitochondrion*** 7: 354-357, 2007.

139. Scott RA , Wilson RH , Goodwin WH , Moran CN , Georgiades E , Wolde B , Pitsiladis YP .Mitochondrial DNA lineages of elite Ethiopian athletes.***Comp Biochem Physiol***140: 497-503, 2005.

140. Scott RA , Fuku N , Onywera VO , Boit M , Wilson RH , Tanaka M , H Goodwin W , Pitsiladis YP .Mitochondrial haplogroups associated with elite Kenyan athlete status.***Med Sci Sports Exerc*** 41: 123-128, 2009.

141. Tamura Y , Watada H , Tanaka Y , Daimaru N , Nomiyama T , Sakuraba K , Sawaki K , Kawamori R .Preliminary report: mitochondrial DNA 5178 polymorphism in male elite Japanese endurance runners.***Metabolism***59: 62-63, 2010.

142. Mikami E , Fuku N , Takahashi H , Ohiwa N , Scott RA , Pitsiladis YP , Higuchi M , Kawahara T , Tanaka M .Mitochondrial haplogroups associated with elite Japanese athlete status.***Br J Sports Med*** June152010.

143 He Z , Hu Y , Feng L , Li Y , Liu G , Xi Y , Wen L , Lucia A .NRF-1 genotypes and endurance exercise capacity in young Chinese men.***Br J Sports Med*** 42: 361-366, 2008.

144. Bo H , Zhang Y , Ji LL .Redefining the role of mitochondria in exercise: a dynamic remodeling.***Ann NY Acad Sci*** 1201: 121-128, 2010.

145. Eynon, Nir, et al. "The champions' mitochondria: is it genetically determined? A review on mitochondrial DNA and elite athletic performance." *Physiological Genomics* 43.13 (2011): 789-798.

146. Kersten, Sander. “Integrated Physiology and Systems Biology of PPARα.” *Molecular Metabolism*3.4 (2014): 354–371. *PMC*. Web. 16 May 2018.

147. Negrini, D. A. N. I. E. L. A., C. A. N. Z. I. O. Gonano, and G. I. U. S. E. P. P. E. Miserocchi. "Microvascular pressure profile in intact in situ lung." *Journal of Applied Physiology* 72.1 (1992): 332-339.

148. Lee, G. de J., and A. B. DuBois. "Pulmonary capillary blood flow in man." *The Journal of clinical investigation* 34.9 (1955): 1380-1390.

149 . Haber S, Clark A, Tawhai M. Blood Flow in Capillaries of the Human Lung. ASME. *J Biomech Eng.* 2013;135(10):101006-101006-11. doi:10.1115/1.4025092.

APPENDIX

A: Arduino Microcontroller Code:

```
int motorPin = A1;
int blinkPin = 13;

int pumptime =100
; // how long pump is on
int waittime =1000; // how long pump is off

void setup() {
  // put your setup code here, to run once:
pinMode(motorPin, OUTPUT);
  pinMode(blinkPin, OUTPUT);
}

void loop() {
  // put your main code here, to run repeatedly:
digitalWrite(motorPin, HIGH);
  digitalWrite(blinkPin, HIGH);
  delay(pumptime);
  digitalWrite(motorPin, LOW);
  digitalWrite(blinkPin, LOW);
  delay(waittime);
}
```

B: Matlab Permeability Calculation Code

```
%% Calculate permeability from confocal imaging datasets

        Dgelatin=20.9 %From FRAP Data 10k=12.6, 3k=20.9
        Distance_microns = 1120 %distance from channel edge to gel edge

        %%Import measurements from fiji macro
        Iedge = xlsread('C:\path\ GelBG.csv',1,'B2:B241');%%Average Intensity at no-
flux region
        Channel_Io = xlsread('C:\pathChannelBG.csv',1,'B2:B241'); %%Intensity within
channel
        Igel=  xlsread('C:\path\GelNearChannelBG.csv','B2:B241');%%Average intensity
of gel

        %% Convert slice/frame number to time interval
        Slice = xlsread('C:\path\Profile.csv','Profile','C1:IH1');
        Time_minute = Slice*.5;
        Time_second = Time_minute*60;

        %%Calculating C for each timepoint
        C_numerator=Iedge-Channel_Io;
        C_denominator = Igel-Channel_Io;
        C=C_numerator./C_denominator;

        %% Graphing logC versus time
        x = Time_second;
        y = C;
        plot=semilogy(x,y);

        %%Fit logC versus time to extract Lambda (slope)
        curvefit = fitlm(x,y,'poly1');
                coeff=curvefit.Coefficients.Estimate;
                Rvalue=curvefit.Rsquared.Ordinary;
                output = xlswrite('C:\path\curvefit.xlsx', coeff,1);

        %Use Lambda to calculate K (permeability) in microns/second
        Lamda = xlsread('C:\path\curvefit.xlsx',1,'A2:A2');
        K=(Dgelatin/Distance_microns)*(Lamda*tan(Lamda));
        K_cm = K*10000; %% conversion to cm/s
                outputValue = {;'K cm/s';'Lambda';'Rsquared'}
                values=[;K_cm; K;Lamda;Rvalue];
                result= table(outputValue, values);
                %Save results in excel file
                writetable(result,'C:\path\Results.xlsx','Sheet',1,'Range','A1:B3')
```

C: Parts List for Circuit of Peristaltic Pump

A. Arduino UNO rev3
B. USB Cable (Arduino fitted)
C. 1N4001 diode
D. PN2222A transistor
E. 12V 1000mA DC Power Supply
F. Peristaltic Pump
G. Resistor (300 ohm)
H. Alligator clip or wire

D: Immortomouse Endothelial Cell Culture

A. Grow at 33C for propagation
B. Media from Lonza, cat #CC-3202 with cat #CC-4147 soliquot additives
C. Add M-INF gamma to the media at 33C (concentration 10ng/mL). Note: 37°C media is identical except for M-INF gamma
D. Cells are lifted with 0.05% trypsin for three minutes (washing with PBS without calcium and magnesium)
E. Once ready, transition cells to 37°C incubator. Use 37°C media and add 300ng/mL doxycycline

Gene Symbol	WT static	WT static 2	WT perfused	WT perfused 2	R899X static	R899X static 2	R899X perfused 2	R899X perfused
1010001N08Rik	1.5	1.5	1.3	0.8	2.0	1.9	1.5	1.1
1700123I01Rik	1.1	1.5	0.7	0.7	1.8	1.1	1.4	0.6
2610044O15Rik8	3.6	3.7	3.7	4.0	2.8	2.9	3.4	3.3
2900097C17Rik	1.1	1.4	1.9	2.3	3.4	3.8	4.3	3.6
3110001I22Rik	1.8	2.0	2.5	2.3	1.6	1.5	2.3	2.9
4930581F22Rik	0.3	0.8	0.2	-0.6	0.4	0.7	0.1	0.0
5830415F09Rik	3.1	3.2	4.1	3.7	2.4	2.9	3.6	3.4
9330179D12Rik	0.2	-0.6	0.3	0.3	-0.4	-0.2	0.5	0.2
A130014A01Rik	1.4	1.7	0.9	1.2	0.8	0.7	-0.1	-0.1
Adamts1	6.1	5.5	5.6	7.5	5.7	6.0	8.0	7.7
Ankrd1	5.4	5.9	6.6	7.0	5.1	5.2	6.3	7.7
Anks1b	1.1	0.6	-1.3	-0.6	1.2	0.8	0.1	0.6
Ankzf1	4.1	3.6	3.4	3.7	4.2	4.1	3.8	3.5
Apoe	0.2	-0.1	-0.4	-0.4	4.9	3.9	3.8	3.5
Arhgef4	0.8	0.9	-0.6	0.1	1.6	1.4	1.1	0.8

Arid5a	5.4	4.9	5.7	5.9	6.1	5.7	6.6	6.8
Armc5	3.8	4.0	4.2	4.2	3.7	4.2	4.3	4.6
Arrdc3	3.4	3.9	4.4	4.5	3.7	4.3	4.9	3.8
Atp5sl	4.2	4.1	3.7	3.7	3.9	3.8	3.6	3.8
Atxn7l2	2.5	2.3	2.9	3.1	2.4	2.4	2.9	2.5
Bbs10	2.2	2.0	1.1	1.2	2.2	2.3	1.5	0.5
Bhlhe40	7.0	7.2	8.2	8.2	6.8	6.8	8.2	7.5
Bora	4.6	4.6	5.0	5.3	4.9	4.6	5.1	5.2
Brd1	4.5	4.6	3.1	3.2	2.7	4.3	3.0	2.5
Btg2	5.2	5.0	6.7	6.5	6.6	4.5	8.8	8.3
C1qtnf6	3.5	3.5	2.3	2.8	2.8	3.7	3.3	2.1
Cacnb3	3.8	3.7	3.1	3.3	3.4	4.1	3.6	3.4
Ccdc64	3.9	3.7	3.4	3.3	3.5	3.6	2.9	3.0
Ccsap	3.5	3.5	2.9	2.7	3.5	3.2	2.8	2.9
Cdc34-ps	1.2	1.4	0.8	0.9	1.2	0.8	0.5	0.8
Cdkn2aip	5.6	5.0	5.8	6.1	5.3	5.2	5.8	5.6
Cenpv	3.8	4.1	3.6	3.5	3.4	3.8	3.2	3.4
Cep85l	0.1	-0.7	1.2	0.8	-0.5	-0.5	0.9	0.5
Ces2e	4.0	4.4	3.4	2.9	3.8	3.5	3.1	3.3
Cfap43	5.4	4.9	5.0	6.3	5.6	6.0	6.8	6.7
Chsy1	2.9	3.5	2.0	2.4	2.5	3.5	2.1	1.9
Cmtr2	4.7	4.5	4.9	5.3	4.5	4.8	5.4	5.4
Commd5	4.3	4.5	4.3	3.9	4.5	4.3	3.6	3.9
Coq10b	5.5	5.7	6.2	6.0	6.1	5.5	6.2	6.4

Cpz	0.7	0.6	0.0	-0.4	2.3	2.4	2.2	1.8
Crabp2	1.1	1.3	0.8	0.7	-0.2	-0.1	-1.2	-0.5
Csn3	1.1	1.3	0.4	0.5	-0.2	0.3	-0.5	-1.2
Csnk2a2	4.4	4.6	2.7	2.8	2.4	4.0	2.4	1.6
Cspp1	2.7	2.7	3.1	3.2	2.9	2.7	3.3	2.9
Csrnp1	4.7	4.6	6.2	6.7	5.7	4.2	7.4	6.9
Cul3	6.4	6.4	4.5	4.8	4.1	6.5	4.7	4.4
Cxx1a	3.5	3.5	3.0	3.2	3.2	3.2	3.0	2.9
Cxx1b	3.6	3.9	3.3	3.3	3.1	3.5	3.0	3.1
Cyhr1	6.8	6.4	4.2	5.2	4.1	6.3	5.2	3.8
Cyr61	7.3	7.4	10.6	10.7	8.1	7.4	10.2	11.3
Ddit4l	4.1	3.9	3.5	3.5	3.8	3.4	3.4	3.4
Dhrs3	2.5	2.7	1.9	2.0	2.5	3.0	2.4	2.5
Dnajc18	5.4	5.1	4.8	4.9	4.4	4.7	4.5	4.2
Dnhd1	1.0	0.4	0.0	-0.1	0.7	0.7	0.5	0.3
Dok1	5.6	5.3	5.2	5.2	6.1	5.9	5.5	5.4
Dtwd2	2.3	2.4	2.9	2.7	1.8	2.0	2.2	2.1
Dus4l	3.6	3.5	4.0	4.1	3.2	3.6	4.0	3.6
Dusp5	3.4	3.7	4.9	6.3	5.5	4.5	6.9	6.9
Dusp6	5.5	5.9	6.8	7.5	7.0	7.4	8.3	8.4
E130102H24Rik	0.5	0.7	-0.3	-0.4	0.5	0.5	0.1	0.2
Eda2r	4.7	5.0	4.9	5.2	4.3	4.7	5.1	5.1
Edn1	2.1	2.8	4.4	3.6	2.7	3.1	4.0	3.2
Egln1	4.9	5.1	3.2	3.1	2.6	4.3	2.3	2.2

Egr1	6.3	6.1	7.8	8.7	6.9	5.4	9.4	9.5
Egr2	-2.0	-2.0	0.6	3.2	-2.0	-1.0	4.9	5.5
Eid2b	3.4	2.8	3.0	2.7	3.1	3.2	2.6	2.7
Epha2	5.6	6.2	5.8	6.9	5.4	6.0	6.9	6.5
Errfi1	4.9	4.8	5.5	6.5	6.3	5.9	8.5	8.5
Exog	4.4	4.0	3.9	4.0	4.4	4.5	4.0	4.0
F3	3.6	3.8	4.5	4.5	5.6	5.2	6.2	7.4
Fam110c	0.7	0.6	1.3	0.8	4.3	4.5	4.8	5.0
Fam120a	6.5	7.2	5.6	5.8	5.9	6.7	5.8	5.4
Fam98c	3.8	3.5	3.7	3.3	3.7	3.6	3.1	3.4
Fblim1	2.4	2.3	1.6	1.9	4.0	4.4	3.8	4.0
Fbxo30	5.7	5.5	5.7	6.2	5.9	5.9	6.4	6.6
Fbxo44	2.6	2.4	1.8	1.6	3.1	2.9	2.9	2.5
Filip1l	4.0	4.0	4.4	4.5	3.3	3.7	4.3	4.6
Flt3l	2.4	2.4	1.9	2.0	2.7	2.2	2.4	2.2
Fos	4.2	4.5	8.0	6.3	5.8	3.9	8.0	7.7
Fosb	-1.6	-1.1	2.0	2.1	-1.0	-2.0	4.0	2.3
G2e3	4.6	4.5	5.0	5.2	4.6	5.0	5.0	5.0
Gadd45g	4.6	4.9	7.4	6.3	3.8	3.7	5.5	6.7
Gid8	3.3	3.3	2.7	3.0	3.1	3.5	3.2	2.8
Git1	6.1	5.9	4.0	4.7	4.3	6.1	5.0	3.7
Glrb	3.5	3.2	3.2	3.1	1.3	1.3	0.6	0.9
Gm10254	5.1	5.1	5.3	5.6	5.0	5.1	5.6	5.6
Gm12565	1.9	1.7	1.6	1.2	1.3	1.3	0.9	0.9

Gm12715	7.3	8.2	8.2	8.3	7.7	7.7	8.3	8.7
Gm12966	5.3	5.4	5.9	5.4	5.0	5.2	5.5	5.7
Gm14295	2.1	2.3	2.9	2.9	2.4	2.8	2.5	3.1
Gm15270	-0.2	-0.4	0.7	0.3	-0.3	-0.8	1.0	1.4
Gm17501	1.3	1.2	2.3	2.0	-1.1	-0.6	-0.1	1.2
Gm20541	1.7	1.6	2.2	2.2	-0.4	0.8	2.0	1.7
Gm26648	2.0	1.9	1.2	0.9	1.4	1.3	1.6	0.4
Gm42547	1.2	0.9	-0.5	-1.0	0.0	1.4	0.0	-1.2
Gm43579	1.3	1.6	0.6	0.7	1.0	0.7	0.2	0.2
Gm6685	0.2	0.0	0.6	0.8	-0.8	0.0	1.1	0.8
Gm6710	2.5	2.7	3.3	3.2	1.2	2.2	2.8	2.5
Gm7436	1.2	0.7	0.9	0.1	0.6	0.4	-0.3	-0.2
Gm8185	2.2	2.4	2.4	1.7	2.3	2.0	1.7	1.6
Gm8261	0.2	0.1	0.2	0.7	-0.2	0.3	1.0	0.9
Gm8752	2.4	2.7	2.6	2.9	1.9	2.3	2.7	2.9
Gm9726	2.3	2.2	1.4	1.5	1.6	2.3	1.6	1.0
Gpr137	3.3	3.1	2.8	2.6	3.1	3.3	3.0	2.6
Gpsm3	2.2	1.7	1.3	1.3	2.3	2.4	2.2	1.8
Guca1a	1.5	1.0	1.1	0.5	1.5	1.1	0.6	0.5
H2-Q2	4.8	4.7	4.8	4.3	2.8	3.1	2.6	2.5
Hbegf	3.2	3.4	4.4	4.9	3.3	2.9	4.1	4.1
Heca	4.1	3.6	0.9	1.8	1.6	3.7	1.8	0.2
Hes1	3.2	3.8	5.9	5.6	4.0	3.1	5.8	5.5
Hilpda	4.8	4.8	6.2	5.5	6.0	4.7	6.1	5.8

Hint3	3.7	3.8	3.6	3.1	3.5	3.7	3.4	3.3
Hlx	0.6	1.1	0.3	0.7	1.5	1.8	0.8	0.9
Hoxa9	2.8	2.7	2.6	2.3	2.4	1.8	1.3	1.2
Hoxb2	3.3	3.3	2.9	2.6	4.1	3.0	1.9	2.4
Hyal1	2.8	3.0	1.9	2.4	2.0	2.4	1.6	1.6
Iba57	1.5	1.9	2.1	2.7	1.4	1.6	2.6	2.5
Id1	4.0	4.7	6.6	6.4	6.5	4.8	6.6	6.1
Id2	3.8	3.8	5.5	5.0	4.2	2.8	4.1	4.2
Id3	7.2	7.3	9.0	8.5	8.5	7.5	8.7	8.7
Ier2	6.0	5.9	7.2	7.5	6.7	5.5	7.9	8.2
Ier5	4.6	4.2	5.1	5.5	5.7	4.6	6.5	6.6
Ifrd1	7.8	7.6	8.1	8.2	8.2	7.7	8.6	8.4
Irak2	5.7	5.6	6.0	6.0	6.1	6.1	6.4	6.6
Itgb2	2.8	2.9	1.9	2.3	2.2	2.3	1.8	2.0
Itgb7	5.5	5.1	4.5	4.5	4.0	4.3	4.0	3.7
Jun	5.9	5.7	7.5	6.8	7.7	5.3	8.7	7.8
Junb	7.2	7.2	8.1	7.8	7.9	6.7	8.5	8.6
Klf10	6.1	5.9	7.2	7.8	6.8	6.3	7.8	7.3
Klf11	5.3	4.7	5.2	6.1	4.9	4.8	5.6	5.3
Klf13	5.8	5.8	5.0	5.4	5.2	5.6	5.5	4.6
Lmnb1	4.8	4.4	4.8	5.8	4.0	3.9	4.7	4.3
Lpar1	-0.4	0.0	1.8	1.9	1.0	2.1	2.2	2.4
Luc7l3	4.8	5.0	4.3	4.6	4.4	4.3	3.9	4.2
Lypd1	0.0	-0.1	-0.8	-1.1	2.9	1.6	0.9	0.7

Lysmd3	4.6	4.4	4.9	5.5	4.5	4.7	5.3	5.0
Mafk	6.6	6.5	6.7	7.2	6.3	6.2	7.1	7.1
Mapk3	6.7	6.5	6.2	6.3	6.3	6.6	6.4	6.0
Mars2	4.0	4.0	4.1	4.6	3.7	3.9	4.3	4.2
Mbd2	6.6	6.5	3.6	4.6	3.7	6.7	4.3	2.8
Mex3d	5.0	5.1	2.6	3.8	3.1	5.0	3.6	2.3
Mir99ahg	1.7	1.8	2.4	2.6	1.8	1.5	2.5	2.1
Mms22l	5.0	5.2	5.1	5.3	4.6	4.8	5.1	5.2
Mri1	5.7	5.6	5.6	5.3	6.0	5.9	5.5	5.6
Mta1	5.0	5.0	2.9	4.0	3.3	4.9	3.7	2.6
Mxd4	4.4	4.4	3.8	3.7	3.9	3.3	3.7	3.2
Myc	6.9	7.0	8.1	7.8	8.1	7.7	8.7	8.4
Nabp1	4.3	4.4	4.5	5.4	5.2	4.7	6.0	5.8
Nfil3	5.7	5.4	6.1	6.1	6.1	5.4	6.2	6.2
Nfix	5.5	5.7	4.0	4.1	4.0	5.0	4.3	3.4
Nfkb1	4.4	4.7	3.8	3.7	3.5	4.4	4.0	3.2
Nfkbid	1.9	1.6	0.3	0.9	2.4	1.7	0.6	1.3
Nop58	6.1	6.4	6.6	7.0	6.4	6.4	6.9	6.7
Nppb	1.4	2.2	3.4	4.0	0.1	0.2	2.4	3.0
Nr4a1	2.5	2.5	5.7	6.0	5.0	2.2	8.4	8.6
Nudt16	4.3	4.2	4.2	3.5	4.7	4.5	3.9	4.0
Nufip2	6.0	6.0	5.8	7.0	6.2	5.9	7.4	6.8
Osbp	5.8	5.6	3.5	4.3	3.5	5.7	4.6	2.9
Oxld1	2.2	2.3	1.5	1.6	2.7	2.4	1.8	1.7

Palm3	1.3	1.4	1.9	1.4	0.1	0.4	1.0	0.9
Pcdhb22	1.6	1.3	1.8	1.4	1.0	1.2	1.6	1.4
Pcdhga8	3.8	4.6	4.2	2.8	3.8	3.6	1.4	2.4
Pdgfa	3.8	4.0	3.6	3.2	3.5	3.4	2.7	2.9
Pgam1-ps1	0.5	0.1	0.9	0.9	0.1	-0.1	0.5	0.4
Pgpep1	4.8	4.8	4.5	4.2	4.2	4.4	4.0	3.9
Phc3	2.8	3.1	3.2	3.7	2.5	2.9	3.9	3.4
Phf13	5.8	5.5	4.7	4.9	5.6	5.7	5.1	5.3
Platr16	1.3	1.3	1.7	1.8	0.9	1.3	1.4	1.5
Plk2	7.3	7.1	8.6	8.4	8.4	7.8	9.3	9.5
Ppt2	4.3	4.1	3.6	3.8	4.1	3.9	3.5	3.4
Pramef8	5.4	5.1	5.7	5.5	5.2	5.2	5.6	5.6
Prps1l3	5.4	5.2	5.6	5.8	5.7	5.5	5.7	5.8
Ptbp2	3.4	3.7	4.2	4.0	2.5	3.5	3.7	3.6
Ptp4a3	3.9	4.1	3.4	3.0	4.7	4.2	3.7	4.4
Pus7l	2.4	2.5	2.9	3.2	2.3	3.1	3.1	3.1
Qk	6.5	6.6	4.9	5.1	4.8	6.7	4.9	4.2
Rab30	1.8	2.0	2.6	2.5	1.3	1.6	1.8	1.9
Ranbp9	4.8	5.1	3.3	3.5	3.2	4.8	3.3	3.2
Rasl11b	2.1	1.8	3.0	3.2	2.5	2.3	3.2	3.7
Rdh10	2.9	2.8	3.0	3.2	2.5	2.7	3.2	3.0
Rgs2	-0.2	-0.5	2.4	1.2	0.6	-1.0	4.7	3.4
Rnd3	7.4	7.1	7.9	8.0	7.8	8.1	8.6	8.6
Rnf113a1	3.0	2.9	2.6	2.6	2.9	2.7	2.0	2.1

Rnf126	5.4	5.4	4.8	5.1	5.0	5.4	5.0	4.6
Rnf145	5.5	5.4	4.2	4.6	4.7	5.4	4.3	5.1
Rom1	2.3	1.7	1.7	1.1	1.2	1.6	0.7	0.2
RP23-325D10.4	0.9	0.8	-0.3	0.3	0.5	0.6	0.3	0.0
Rps12-ps19	0.3	0.9	0.2	0.1	0.1	0.4	-0.4	-0.3
Rrnad1	3.7	3.3	2.9	2.9	3.0	3.1	3.0	2.7
Rundc3a	0.6	0.7	0.1	-0.5	0.1	0.2	-0.5	0.1
Rxra	4.7	4.7	3.2	3.2	3.6	5.2	3.7	3.2
Samd1	2.4	3.0	1.6	1.7	1.5	1.8	1.2	0.4
Scrn2	2.7	2.6	2.2	2.2	3.2	3.2	2.8	3.2
Sertad1	5.4	5.5	6.3	6.4	6.1	5.1	6.7	7.0
Sertad3	3.9	3.5	2.6	3.3	4.4	4.0	3.1	3.3
Shisa4	3.2	3.3	2.8	2.7	2.5	2.5	2.3	2.3
Slc25a25	4.9	4.5	5.4	5.8	4.7	4.6	6.5	6.6
Slc25a32	4.3	4.5	4.9	5.0	4.6	4.6	4.8	4.9
Slc33a1	4.8	5.0	5.2	5.2	4.5	5.1	5.2	5.3
Slc38a2	7.1	7.2	7.0	8.5	6.7	7.5	8.7	8.2
Slc4a11	3.7	3.8	2.9	3.0	2.6	2.3	1.7	2.4
Snhg20	3.7	3.9	3.4	3.4	3.5	3.4	2.9	3.1
Snx21	4.9	4.5	4.5	4.0	4.5	4.6	4.3	4.1
Srrm4	0.5	0.9	1.5	1.6	-1.0	0.3	2.2	1.2
Srsf5	7.3	7.4	7.6	7.6	7.2	7.2	7.6	7.7
Steap3	3.1	2.7	2.3	2.1	3.0	3.8	3.3	2.7
Tada2b	4.6	4.6	2.4	3.1	1.7	4.0	2.3	1.7

Tcfl5	4.5	4.5	1.9	2.5	0.3	3.5	1.3	0.2
Thap11	5.7	5.5	5.4	5.0	5.5	5.5	5.0	5.1
Thbd	4.2	4.3	4.0	5.3	5.5	5.8	7.1	6.6
Tmbim6	8.3	8.2	7.3	7.8	7.2	8.2	7.9	7.0
Tmem185b	4.5	4.8	5.3	5.2	4.8	4.7	5.3	5.2
Tmem265	1.9	1.7	1.3	1.2	1.7	1.7	0.8	0.4
Tmem69	3.0	3.2	3.6	3.5	2.6	2.6	3.5	3.5
Tra2b	7.0	7.2	7.3	7.6	6.9	7.1	7.6	7.5
Trib1	2.0	2.5	3.4	5.0	2.1	3.3	5.5	5.4
Trim11	5.0	4.9	4.5	4.6	4.7	4.6	4.1	4.5
Trim16	4.8	4.8	5.2	5.8	5.0	4.9	5.1	5.3
Trim6	2.2	2.0	2.5	2.6	2.0	2.2	2.6	2.1
Trmt5	3.6	3.7	4.0	4.1	3.5	3.7	3.7	3.8
Tshz1	3.2	3.3	2.7	2.8	2.6	3.2	2.9	2.4
Tst	1.3	1.2	0.8	0.6	2.3	2.8	2.3	2.0
Ufsp1	3.0	2.9	2.7	2.3	2.9	2.8	2.4	2.6
Uprt	1.6	1.4	1.7	2.0	1.9	2.0	2.4	2.4
Usp49	2.0	3.0	1.7	1.8	2.1	2.0	1.6	1.2
Vgll3	5.3	5.6	5.9	6.0	5.3	5.6	6.1	6.2
Wsb1	6.9	7.0	7.6	7.9	6.9	7.0	8.1	8.2
Wtip	4.9	4.7	1.2	2.6	1.8	4.6	2.4	1.0
Xkr8	3.6	3.5	3.2	3.3	4.4	3.9	3.5	3.6
Zbtb7b	4.1	4.2	3.4	3.7	4.3	4.0	4.1	3.3
Zc2hc1c	1.8	1.1	1.3	0.4	2.2	2.0	1.0	0.9

Zfand5	6.8	6.6	6.9	7.2	6.8	6.9	7.3	7.3
Zfp119a	2.5	2.7	3.4	3.5	2.3	3.0	3.8	3.6
Zfp236	2.8	3.1	1.7	2.8	2.6	2.7	1.9	1.9
Zfp296	3.1	2.9	2.9	2.5	3.8	3.4	2.7	2.7
Zfp30	2.2	1.7	1.9	1.2	2.0	1.6	1.1	1.1
Zfp36	5.1	5.0	6.1	6.1	7.3	4.8	8.2	7.7
Zfp433	3.1	3.1	3.9	3.9	3.2	3.3	4.0	3.6
Zfp668	3.6	3.5	3.0	3.0	3.1	3.4	3.1	2.9
Zfp688	4.6	4.1	4.4	3.7	4.6	4.1	3.6	3.5
Zfp747	2.9	2.7	3.0	3.2	2.4	2.8	3.5	3.3
Zfp947	1.2	1.0	2.0	2.2	0.5	1.6	2.4	1.6
Zfp958	4.7	4.2	4.2	4.3	4.6	4.3	4.0	3.7
Zfp959	3.4	3.2	3.8	4.0	2.6	3.2	3.8	4.0
Zfpm1	4.7	4.5	1.7	3.0	1.8	4.7	2.1	1.2
Zmym1	4.2	4.1	4.3	4.9	4.4	4.6	4.8	4.9
Znrf2	4.6	4.7	1.8	2.6	2.4	4.5	2.7	1.8
Zrsr1	1.3	1.0	0.7	-0.2	1.6	1.2	0.5	0.8

Table A.1 Congruent Genes in the Heatmap. WT devices represented in green and R899X represented in red.

Gene Symbol	WT static	WT static 2	WT perfused	WT perfused 2	R899X static	R899X static 2	R899X perfused 2	R899X perfused
1500004A13Rik	0.8	1.3	0.2	1.1	0.6	0.9	1.9	1.3
1700030J22Rik	0.4	0.6	-0.3	0.3	-0.3	0.0	0.4	0.7
1810010H24Rik	2.6	2.3	1.4	1.5	0.5	1.6	2.2	1.7
5031425E22Rik	3.2	3.2	3.1	3.1	2.3	2.3	2.9	2.8
6330408A02Rik	2.4	2.4	2.0	2.1	1.5	2.4	2.8	2.6
A630052C17Rik	2.2	2.1	1.7	1.5	0.9	1.6	1.7	1.6
A830082K12Rik	2.0	2.0	2.5	2.5	2.3	2.4	2.1	1.8
A930005H10Rik	2.7	2.6	2.1	1.8	2.0	1.8	2.2	1.5
Abcb9	0.9	0.8	0.2	-0.3	0.4	0.1	0.7	0.3
AC158396.1	3.2	3.3	3.5	3.2	3.3	3.0	2.4	2.7
Acss2	2.0	1.8	1.8	2.0	2.3	2.3	1.8	2.0
Adck4	4.7	4.4	4.7	4.5	5.0	5.0	4.5	4.7
Adm	-0.5	-0.9	0.9	0.8	1.7	-0.2	0.5	1.3
Adrb2	2.4	2.6	2.9	2.6	1.9	1.6	2.8	2.9
Aipl1	1.7	1.7	0.9	0.8	0.9	0.8	1.0	0.7

Alkbh4	4.4	4.3	4.5	4.0	3.9	4.0	3.1	3.2
Ank3	3.0	2.4	1.7	2.8	-1.5	-1.4	-0.2	-0.2
Ap1s2	3.9	4.2	4.5	4.6	3.7	3.7	4.0	3.7
Arc	1.9	1.4	2.4	3.4	0.9	-0.4	3.8	5.2
Arhgef6	2.1	1.7	1.6	2.1	0.9	1.4	2.3	1.9
Armcx5	3.6	3.7	3.4	3.5	3.1	3.6	3.8	4.0
Arsj	1.3	1.4	2.0	2.0	2.4	2.2	1.3	1.9
Asic3	3.8	3.1	3.8	3.5	1.3	1.2	0.4	0.4
Asna1	6.6	6.6	6.1	6.1	5.5	6.0	5.9	5.4
Ass1	3.2	3.6	2.4	2.6	2.5	3.3	3.4	2.4
Atp6v0d1	7.2	7.2	6.4	6.5	5.9	6.6	6.6	6.0
B3galnt1	-0.3	-0.2	-2.0	-2.0	4.7	4.6	4.4	4.7
B4galnt2	1.1	0.7	0.3	0.0	-0.8	0.2	0.0	-0.6
BC023105	4.3	3.7	4.2	3.8	3.8	3.8	4.7	4.3
Bcam	2.9	2.7	2.0	1.3	3.3	3.6	3.5	3.1
Bcas3	5.1	5.0	4.7	4.8	3.5	4.5	4.9	4.6
Bcdin3d	2.8	2.5	2.9	2.3	3.0	2.9	2.5	2.1
Brd3	5.8	5.8	5.2	5.5	5.1	5.7	5.4	5.5
Btg3	4.1	4.2	4.6	4.9	4.6	4.5	4.2	4.2
C630043F03Rik	0.5	1.1	1.2	0.8	1.4	1.2	0.9	0.9
C920006O11Rik	0.7	0.3	-0.3	-0.2	0.4	0.5	0.4	0.2
Cacnb1	0.8	0.4	0.7	0.4	1.1	0.7	-0.1	-0.3
Calr3	1.8	1.6	2.3	1.9	2.1	2.3	1.5	1.8

Ccdc163	1.9	1.7	2.2	2.1	2.6	2.1	1.6	1.9
Cers4	3.4	3.3	3.0	2.6	4.0	4.2	3.7	4.3
Ces2g	4.7	4.9	4.4	4.3	5.8	5.9	5.8	5.9
Cited2	6.0	5.9	6.5	6.0	5.6	6.2	7.1	7.1
Coq10a	5.0	4.8	4.4	4.5	4.7	4.7	4.5	4.7
Csrp1	7.3	7.4	7.2	7.2	6.4	6.5	7.0	6.8
Cyb5d2	2.8	2.8	2.2	2.3	2.4	2.5	2.7	2.6
D130017N08Rik	2.3	2.6	1.9	1.8	1.2	1.4	1.5	1.4
Def6	2.8	2.5	1.8	1.5	3.1	4.0	3.8	3.8
Dlx2	2.3	2.8	3.6	3.9	3.1	3.0	3.2	3.4
E230001N04Rik	1.4	1.7	0.7	0.3	-0.1	1.2	1.0	0.6
Eif3s6-ps4	1.1	0.8	1.2	0.9	-0.1	0.1	0.7	0.8
Eva1b	3.4	3.3	3.3	3.0	4.3	4.0	3.6	3.7
Exoc3l4	4.2	4.2	4.7	4.0	4.4	4.5	3.9	3.7
Fam213a	2.5	2.5	1.6	1.7	3.9	4.1	4.0	4.1
Fam43a	0.7	0.4	-0.2	1.7	-0.2	-0.8	1.3	0.9
Fam53c	6.5	6.2	5.8	6.8	5.3	5.7	6.5	6.2
Fcor	1.6	2.2	2.3	1.7	0.4	0.6	-0.1	0.1
Flot2	7.7	7.5	7.3	7.1	6.9	7.5	7.2	7.2
Fmo5	0.5	0.7	0.0	-0.6	0.5	1.2	1.7	1.4
Fnbp1	3.9	3.8	3.3	3.4	3.4	3.9	3.6	3.5
Fpgt	4.0	4.0	4.5	4.8	4.2	4.3	4.6	4.3
Gadd45a	6.3	6.1	6.6	6.8	6.8	6.2	6.5	5.9

Gadd45b	4.9	5.2	6.0	5.9	5.4	4.7	4.8	5.1
Gale	4.4	4.3	4.7	4.7	4.4	4.0	3.5	3.9
Gata2	3.4	2.9	3.1	3.4	0.9	1.0	1.4	1.4
Gfra4	0.8	1.2	0.4	0.5	1.6	2.1	1.8	1.7
Gimap9	2.2	2.5	2.8	2.4	3.4	3.4	2.6	3.0
Gm10224	1.2	1.2	1.8	1.0	2.0	1.9	1.2	1.4
Gm10335	4.2	4.4	4.5	4.1	4.7	4.5	3.8	4.1
Gm11821	0.6	0.7	0.3	1.0	0.4	0.5	1.0	0.9
Gm11847	-0.6	-0.4	0.4	0.7	0.8	0.9	0.5	0.2
Gm12094	0.4	0.4	0.7	0.5	0.7	0.0	-0.8	-0.5
Gm12185	4.8	4.4	4.7	4.9	4.1	4.7	5.3	5.6
Gm12430	1.4	1.2	1.5	1.5	1.3	1.3	1.7	1.9
Gm12502	0.5	0.1	0.7	0.0	0.5	0.3	-0.6	-0.6
Gm12758	0.2	-0.1	1.0	0.8	-0.6	0.0	-0.6	0.5
Gm12791	0.9	0.7	0.5	0.4	0.2	0.3	0.9	0.6
Gm13147	0.2	0.2	1.0	0.4	0.8	0.6	0.1	0.3
Gm13331	1.9	2.0	2.5	1.9	2.8	2.5	2.0	2.3
Gm13408	2.1	1.8	2.5	2.3	2.9	2.4	2.3	2.3
Gm13743	0.3	0.3	1.0	0.9	0.6	0.5	-0.2	0.3
Gm14434	2.0	2.5	2.4	2.1	1.2	1.5	0.5	0.1
Gm15710	5.8	5.9	6.3	5.5	5.9	5.6	5.0	5.2
Gm18180	1.0	0.8	0.9	1.2	0.1	0.3	0.8	0.8
Gm18853	1.9	2.6	2.2	2.7	2.6	3.4	4.2	4.1
Gm20707	0.8	0.8	1.4	1.3	0.9	1.5	1.4	1.2

Gm28437	8.5	8.7	9.1	9.4	9.4	8.6	9.2	8.7
Gm43110	2.7	2.7	2.9	2.4	2.3	2.2	1.8	1.8
Gm4841	5.6	5.5	5.6	5.5	5.7	5.5	6.1	6.3
Gm5145	0.4	0.4	0.7	0.7	1.0	0.6	-0.2	0.4
Gm5385	-0.3	-0.4	-0.3	-0.1	0.9	1.0	-0.4	0.1
Gm5424	4.8	5.2	4.0	4.1	4.4	5.1	4.8	4.2
Gm6065	1.5	1.5	1.6	1.3	1.7	1.6	0.8	1.1
Gm6576	2.2	2.4	2.7	2.3	2.9	2.6	2.0	2.0
Gm8210	4.4	4.4	4.8	4.2	4.8	4.5	3.7	4.0
Gm8623	0.6	1.3	1.5	0.6	1.6	1.2	0.6	0.7
Gm9795	0.2	0.2	-0.6	-1.3	0.7	1.1	1.6	0.5
Gm9826	0.7	0.5	1.3	1.1	2.9	2.9	2.6	2.5
Gpr176	-1.0	-1.2	-1.8	-2.0	3.5	4.5	4.7	4.7
Gpt	2.2	1.8	1.4	1.2	1.3	1.5	2.0	1.3
Gstcd	2.4	2.9	2.4	2.5	3.2	3.2	2.3	2.3
Hacl1	3.9	3.8	3.4	3.2	3.1	3.5	3.6	3.4
Hcn2	1.5	1.7	-1.2	0.2	-0.9	0.5	0.2	-1.4
Hist1h1b	0.6	0.5	1.6	1.7	1.7	0.3	1.1	0.5
Hist1h2ad	4.6	5.0	5.1	5.0	3.5	3.3	2.7	2.8
Hist1h2ap	6.9	7.3	7.5	7.3	7.7	7.2	6.6	6.8
Hmgb1-ps1	1.6	1.7	2.2	1.0	1.7	1.7	0.5	1.0
Hpdl	0.8	0.8	1.5	1.3	1.4	0.8	-0.4	0.5
Itga7	1.3	1.2	1.3	1.6	3.2	3.2	2.9	2.8
Katnbl1	5.7	5.7	6.1	6.2	6.5	6.1	6.3	6.4

Kazn	2.0	2.2	1.5	1.4	3.0	3.8	4.2	3.5
Krt19	7.0	7.1	7.1	6.9	6.9	6.6	6.2	6.1
Lama5	3.4	3.8	2.6	2.5	3.5	4.6	4.8	3.5
Lims2	4.2	3.9	3.9	3.0	1.5	1.4	1.8	1.7
Lppr2	2.4	2.5	1.9	1.7	1.9	2.4	2.6	2.1
Lyrm4	3.1	3.4	2.2	2.7	3.4	3.7	3.5	3.4
Lzts2	6.4	6.1	5.8	5.8	6.0	6.5	6.2	6.1
Map9	0.4	1.3	0.1	0.4	-1.3	-0.6	0.7	0.3
Mdm2	7.8	7.5	7.4	7.8	7.2	7.2	7.7	7.7
Mettl23	3.3	3.4	3.0	2.8	3.1	3.5	3.4	3.2
Mfsd2a	-0.9	-0.1	1.4	1.5	1.5	-0.6	0.7	0.9
Mir17hg	0.2	0.5	0.5	0.4	-1.0	-0.1	0.9	1.0
Mme	2.8	2.6	2.2	3.0	1.9	1.9	3.0	2.7
Mpv17l	1.7	1.5	2.1	2.3	2.1	1.5	2.0	1.6
Mtfp1	1.4	1.3	1.3	1.2	0.4	0.4	0.0	-0.2
Mum1l1	3.9	4.0	3.8	4.4	3.4	3.8	4.2	4.5
Mzf1	0.9	0.9	0.1	0.3	0.3	0.3	0.3	0.1
Nat14	1.6	1.3	1.4	1.1	2.1	2.0	1.4	1.1
Neurl4	2.2	2.6	1.2	1.6	1.6	2.1	2.3	1.3
Noxo1	1.8	1.2	0.7	0.8	-0.3	0.7	0.7	1.3
Nqo1	7.2	7.2	7.8	7.5	8.9	8.4	8.2	8.7
Nr1h4	3.8	3.4	3.8	3.2	3.1	3.4	3.9	3.8
Nr4a2	-0.6	0.0	0.8	1.5	-1.2	-0.9	4.2	3.7
Nrg1	1.3	1.5	1.6	1.1	2.2	2.0	2.6	2.5

Nudt17	1.6	1.8	1.8	1.2	2.9	2.9	2.1	2.2
P2ry2	3.4	3.1	3.0	3.6	3.1	3.0	3.7	3.6
Paqr7	3.6	3.9	3.0	3.0	3.3	3.9	3.4	3.5
Pcdhgc5	1.2	1.6	0.2	0.0	0.5	1.1	0.9	1.3
Pcsk4	2.3	1.6	2.6	2.2	3.1	2.8	2.3	2.2
Phtf1os	1.6	1.5	0.4	-0.2	0.6	0.9	1.1	1.0
Plekha7	2.2	2.0	0.3	1.0	1.8	2.6	2.8	2.7
Ppm1m	4.6	4.6	4.1	4.2	3.8	4.3	4.2	4.0
Ppp1r10	5.0	4.9	4.4	4.9	4.4	4.6	5.7	5.6
Prdm16	2.7	2.6	2.2	2.4	2.3	2.8	2.9	2.7
Ptms	4.4	4.7	4.0	3.9	3.8	3.9	4.0	3.4
Ralgds	1.0	1.1	-0.2	0.3	1.5	2.0	2.3	2.3
Rasa4	2.0	1.3	1.4	1.7	1.6	2.0	1.0	1.2
Rbm12b1	2.6	2.4	2.3	2.8	2.6	2.6	3.0	3.1
Rbm5	5.9	5.8	5.8	6.0	5.7	6.0	6.5	6.3
Rgl1	0.6	0.1	0.7	0.1	1.1	0.8	0.3	0.5
Ribc1	1.7	1.0	1.5	1.1	1.8	1.6	1.3	1.1
Rnf130	3.4	3.3	2.6	2.1	3.7	4.6	4.5	4.2
Rorc	2.0	1.7	0.9	1.1	1.4	1.9	2.3	1.2
Rpgrip1l	1.4	2.2	1.5	2.0	0.1	1.1	2.2	2.0
Rpl28-ps3	1.2	1.6	1.9	1.5	1.6	1.4	0.7	1.1
Rpl31-ps10	0.9	1.2	1.3	0.5	1.7	1.5	0.9	1.0
Rpl31-ps16	1.2	1.3	1.4	0.7	1.6	1.2	0.4	0.8
Rragd	3.1	3.1	2.1	2.5	2.5	2.7	3.2	3.1

Rsad2	8.6	7.8	7.8	8.4	7.3	7.0	7.8	8.0
Rsbn1	3.3	3.1	3.6	3.9	3.7	3.7	4.0	3.4
Sass6	3.4	3.0	3.1	3.6	2.2	2.5	3.2	3.0
Scn1b	1.7	1.5	0.2	0.1	0.7	1.1	0.5	1.0
Sco2	2.6	2.7	3.5	3.2	3.1	2.5	2.9	2.9
Sdsl	2.5	2.6	1.9	1.7	0.5	0.4	0.8	0.0
Sema3b	3.6	3.5	2.9	2.6	1.0	2.0	2.3	1.3
Serpina3g	0.5	0.0	-1.8	-1.6	5.0	5.3	5.7	4.9
Serpina3n	1.8	1.6	1.0	0.7	4.7	4.9	5.2	4.6
Slc25a42	4.4	4.0	3.3	3.5	3.2	3.4	3.5	3.1
Slc37a4	4.1	3.5	3.8	3.5	4.4	4.1	3.5	3.5
Slc41a3	4.3	4.1	3.9	3.7	3.4	3.3	3.5	3.3
Slc44a3	0.0	-0.5	-1.6	-1.2	2.9	2.5	2.5	2.5
Smim19	5.6	5.7	4.9	5.0	4.9	5.1	5.0	4.9
Snai2	5.9	5.8	6.3	6.5	6.3	6.1	6.2	6.0
Snhg17	4.0	4.1	5.1	4.6	5.0	4.0	5.0	4.2
Sord	5.1	4.7	4.2	4.3	5.1	4.9	5.0	5.0
Speer3	-1.2	-2.0	0.2	-0.1	0.7	1.3	1.1	1.4
St3gal3	2.2	2.4	2.0	1.7	2.0	2.3	2.0	2.1
Syt12	3.4	3.6	3.7	3.6	2.5	2.5	2.0	2.1
Sytl1	3.2	3.2	2.5	2.0	2.6	3.0	2.9	2.7
Tab1	4.9	4.3	4.6	4.7	4.7	4.8	4.3	4.0
Taf1c	3.7	3.8	3.8	3.9	3.6	3.6	4.0	4.1
Taf5	4.4	4.0	4.1	4.4	4.3	4.1	3.8	3.9

Tec	0.0	0.3	-0.7	-0.8	1.2	1.8	1.5	2.0
Tmem121	3.6	3.4	3.6	2.9	4.3	3.9	3.1	3.3
Tmem170	1.0	0.8	0.4	1.0	0.5	0.3	1.5	1.2
Tmem25	1.0	0.3	0.4	0.1	0.2	0.9	1.9	1.7
Tmem86a	1.3	1.3	0.4	0.4	0.8	0.3	0.2	0.8
Tnip1	5.2	4.9	4.4	4.7	4.5	4.9	5.1	4.5
Tprn	4.2	3.6	4.0	3.7	4.1	3.9	3.5	3.5
Trim12a	5.1	4.9	5.0	5.1	4.3	4.5	4.8	4.9
Trim34b	-1.4	-1.3	-1.1	-0.6	2.0	2.1	1.7	1.8
Trim56	3.3	4.0	3.3	4.0	2.8	2.6	3.7	3.3
Trim7	1.5	1.6	0.9	0.9	-0.1	0.6	0.6	0.6
Ttc12	0.0	0.6	0.3	0.0	-0.5	0.1	0.6	0.7
Ttpa	1.7	1.7	2.3	2.2	0.3	0.8	0.8	0.4
Tuft1	6.6	6.8	6.8	6.6	5.7	5.9	6.2	6.3
Ube2e2	6.0	5.9	5.4	5.2	4.9	5.4	5.1	5.1
Usp2	1.7	2.2	2.3	2.0	1.7	1.5	3.5	2.8
Vsig10l	0.8	0.8	0.6	0.4	1.1	1.3	1.8	1.5
Wars2	3.9	3.9	4.3	4.4	4.3	4.2	4.1	4.1
Wsb2	8.0	8.1	7.8	7.7	6.8	7.3	7.4	7.6
Ypel2	0.6	0.3	-0.8	-0.9	-0.9	0.9	1.6	0.5
Zcwpw1	1.5	1.1	0.3	0.4	-0.6	0.6	0.8	0.8
Zfp362	2.9	3.2	2.0	1.9	1.5	3.0	2.3	2.1
Zfp472	3.1	3.2	3.7	3.6	3.0	3.3	3.3	3.1
Zfp566	3.5	3.2	3.9	3.7	3.9	3.5	3.8	3.7

Zfp763	3.1	3.0	2.4	3.3	2.9	3.3	2.2	2.1
Zfp772	3.2	3.0	3.0	3.3	3.1	2.8	2.6	2.4
Zfp775	4.1	3.7	3.9	3.7	4.1	4.0	3.7	3.3
Zfp81	2.9	2.8	3.6	3.6	4.0	3.2	3.4	3.4

Table A.2 Incongruent Genes in the Heatmap. WT devices represented in green and R899X represented in red.